ABSTRACT

Title of Dissertation:	EFFECTS OF MINERAL COMPOSITION ON DYNAMIC PROPERTIES OF DRY SANDS
	Ricardo E. Rodriguez, Doctor of Philosophy, 2020
Dissertation directed by:	Professor M. Sherif Aggour, Department of Civil and Environmental Engineering.

The effects of mineral composition on the dynamic properties of dry sands, mainly the shear modulus and damping, are not well determined. Due to the vast geologic diversity, knowledge of the effects of mineral composition on dynamic properties can be very beneficial since it can have a direct effect on the site's seismic response analysis. To understand these effects, a series of dynamic tests using a Drnevich Resonant Column device were performed on various sand samples with different mineral compositions. Sands were selected and classified based on their respective ranking in the Mohs scale of hardness. All sand samples were engineered to have the same gradation properties. Resonant column tests were performed at various confining pressures in order to assess each sand's shear modulus and damping ratio as a function of strain. Tests results show that the mineral composition has a large effect on both the shear modulus and damping. It was concluded that testing soils during the site characterization process should be emphasized.

EFFECTS OF MINERAL COMPOSITION ON DYNAMIC PROPERTIES OF DRY SANDS

by

Ricardo Enrique Rodriguez

Dissertation submitted to the Faculty of the Graduate School of the
University of Maryland, College Park, in partial fulfillment
of the requirements for the degree of
Doctor of Philosophy
2020

Advisory Committee:
Dr. M.S. Aggour, Chair
Dr. A.M. Amde
Dr. D. Goulias
Dr. Chung C. Fu
Dr. Sung W. Lee, Dean Representative

Dedication

To my advisor, Dr. Aggour, for his patience and guidance.

To my wife, Lymari, for supporting me.

To my son, Daniel, for bringing me joy.

Acknowledgements

The author wished to express his thanks to the following people who helped him achieve his research's tasks:

- The chairman of his doctoral committee, Professor M. Sherif Aggour, for his continued guidance, generosity, and constant support, and for the time he generously shared with the author. His objective and invaluable criticism of the manuscript was of great assistance in the preparation of this dissertation. It has been an extreme pleasure learning from and working with him. He always believed in me!
- Member of his doctoral committee, Professors Amde M. Amde, Dimitrios G. Goulias, Chung C. Fu and Sung Lee, for accepting to be part of his dissertation committee.
- The technical personnel at the Civil and Environmental Engineering Laboratory, University of Maryland, especially Mr. Alfred Bituin, for assisting in connecting water and air pipes to the test apparatus and aiding during the experimental stage of the work.

Table of Contents

List of Tables

List of Figures

CHAPTER 1

RESEARCH BACKGROUND

1.1 Introduction

A well-conceived plan for site exploration, starting from literature research to detailed site investigation should include a clear basis of what is needed for the geotechnical work and subsequent foundation design. This is especially true for critical structures, such as Nuclear Power Plants (NPPs) and the like. These types of structures require ample knowledge of subsurface conditions in order to obtain pertinent soil and rock properties that are needed for designing foundations. Special interest is given to the response of soil and rock to dynamic loading in order to properly address potentially undesirable responses to seismic events. An actual site investigation program for an NPP will require it to be site specific and involve various in-situ and laboratory investigations. Such a program is usually tailored to the specific conditions of the site using sound professional judgment.

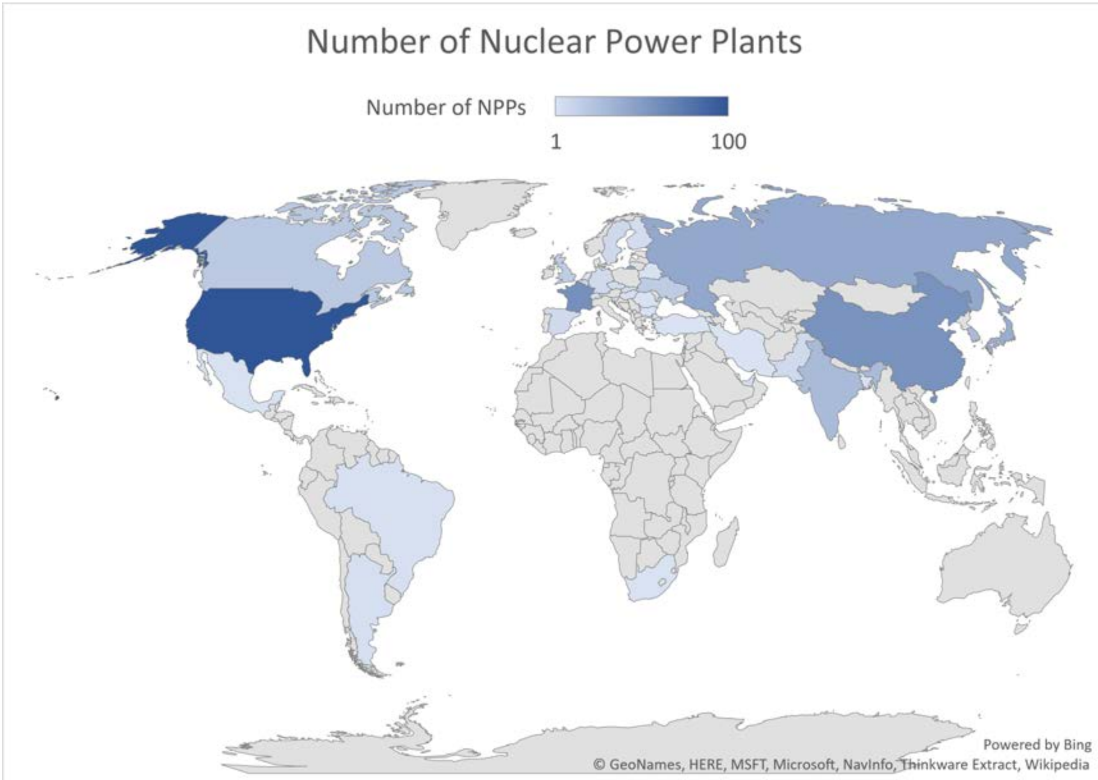

Figure 1.1 Number of Nuclear Power Plants in the World

Current NPPs are sited in many places around the world. (see Figure 1.1). Given the diversity in location, it is very likely that site specific conditions will vary immensely among them. It is common that soils, especially sands, deposits contain particles from numerous sources and mineralogical compounds at various degrees. Every mineral has a particulate range of characteristics that distinguish it from other minerals. Many of these properties are physical, including its hardness, its density and the way it bends or breaks. There are multiple naturally occurring minerals throughout the world. This research was undertaken to investigate the dynamic behavior of dry sands from different mineralogical compositions.

1.1 Motivation

Nuclear Power Plants (NPPs) are considered critical infrastructure. A lot of rigor is involved in the siting of these plants. In order to properly assess the subsurface properties needed for site response analysis, engineers need to consider numerous factors, including the geological nature of the in-situ soils. Given that NPPs are currently sited in multiple places around the world, it is common that soil deposits, especially sands, are comprised of numerous sources and mineralogical compounds at various degrees. There is not a lot of research that discusses the effects mineralogical composition on the dynamic properties of sands, mainly shear modulus (G) and damping (D). This research was undertaken to investigate the dynamic behavior of dry sands from different mineralogical compositions.

1.2 Research Objectives

The main objective of this research project is to study the effects of mineral composition on dynamic properties of dry sands. More specific objectives include:

1. Obtaining sand samples from diverse naturally occurring minerals. These minerals should represent a wide variety of minerals.
2. Perform geotechnical characterizations of all sands. Geotechnical characterization includes determination of index properties, etc.
3. Create engineered sand samples for all sands with different mineralogical composition. These sand samples will have similar uniformity coefficient (C_u) and gradation. This approach will aid in isolating the effect of mineral composition, which is the variable of interest.

4. Determine the dynamic properties of all sands with different mineral composition using Drnevich resonant column apparatus. This includes derivation of the small strain shear modulus (G_{max}), damping (D) and variation of the shear modulus values and damping ratios with shear strain levels.
5. Study the effects of mineral composition on a site's natural frequency. This will aid in understanding the effect of mineral composition on a site's seismic responses analysis.
6. Compare values of shear modulus and damping against current design curves.

1.3 Organization

This dissertation is organized into seven chapters and two appendixes.

Chapter 2, "Literature Review" provides additional background and definitions related to the dynamic geotechnical behavior of sands. It discusses pertinent information related to factors that influence shear modulus and damping.

Chapter 3, "Test Equipment" discusses the equipment used for this research. Dynamic properties of each sand were measured using the Drnevich Resonant Column from the Soil Dynamics Laboratory at the University of Maryland.

Chapter 4, "Material Selection" discusses the selection process for the different types of sands tested. It provides the methodology behind the selection, descriptions and brief literature review.

Chapter 5, "Dynamic Testing Program", provides additional information on the testing apparatus and how variables were treated.

Chapter 6, “Analysis and Results”, presents the Drnevich resonant column results for the determination of the dynamic properties of the sands tested and their comparison with the design curve. The results are mostly presented in terms of shear modulus, damping ratio and their variations with shear strain.

Chapter 7, “Conclusions and Recommendations”, provides the insights and lessons learned from this research.

Appendix A provides additional shear modulus results performed in support of this research.

Appendix B provides additional damping ratio results performed in support of this research.

CHAPTER 2

LITERATURE REVIEW

2.1 Introduction

This chapter provides a brief review of concepts related to soil dynamic properties. It discusses in situ and laboratory investigations techniques. In addition, it emphasizes on factors that affect the determination of shear modulus and damping specifically for sands.

2.2 Determination of Shear Modulus and Damping

The measurement of dynamic soil properties is a vital task in the solution of geotechnical earthquake engineering problems. Analysis of dynamic engineering problems requires the determination of the shear modulus (G) and damping ratio (D). These parameters can be determined using laboratory or field methods. Methods used to measure dynamic soil properties requires thorough understanding of the problem in question.

The shear modulus (G) and damping ratio (D) are the two variable properties in the dynamic response analysis of soils. They are the reason that soils are not considered a linear-elastic material (Amir Faryar, 2012). The shear modulus and damping of soils are strain dependent.

When a soil or rock element is subjected to vibratory motions, these motions cause shear strains. If we were to plot these motions on a typical stress-strain curve (Figure 2.1) a hysteresis loop can be made.

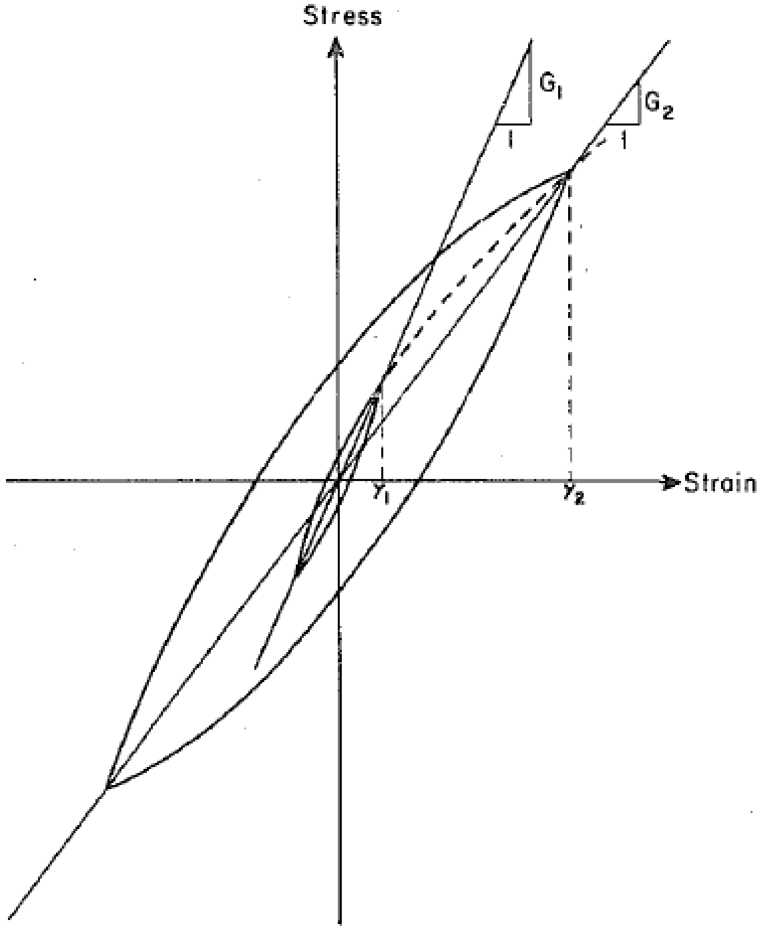

Figure 2. 1 Hysteresis Stress-Strain Relationships at Different Strain Amplitudes (Seed, et al. 1986)

Based on the figure above, shear modulus, G, can be calculated as the slope of the line passing through the end points of the hysteresis loop of the stress vs strain diagram.

$$G = \frac{\tau_c}{\gamma_c} \tag{1}$$

Where:

G = Shear Modulus

τ_c = applied shear stress

γ_c = corresponding shear strain

On the other hand, damping ratio, D, can be estimated based on the area inside the hysteresis loop.

$$D = \frac{1}{2\pi}\frac{\Delta E}{G{\gamma_c}^2} \tag{2}$$

Where:

ΔE = energy dissipated per cycle per unit volume

G = Shear Modulus

γ_c = corresponding shear strain

These variables can be obtained both in the laboratory and field. Each selection technique has an associated strain range in which the test is conducted. For examples, field testing usually have larger strains than laboratory testing. A summary of the laboratory and field tests for soil dynamics, along with the advantages and disadvantages of the testing methods are tabulated in Figure 2-2 (Tawfiq et.al, 1986).

Laboratory Techniques
1 – Cyclic Triaxial
2 – Cyclic Simple Shear
3 – Cyclic Torsional Shear
4 – Resonant Column
5 – Ultrasonic
6 – Shaking Table

Advantages
1 – Better control of boundary conditions
2 – Evaluate different parameters of soil behavior
3 – Provide wide ranges of strain amplitudes
4 – Evaluate damping characteristics

Disadvantages
1 – Sample disturbance
2 – In general, the advantages and disadvantages of laboratory testing methods depend on the minimum criteria for obtaining adequate values of soil behavior

Field Techniques
1 – In-Hole Methods
- Cross Hole
- Down Hole
- Up Hole

2 – Surface Wave Methods

Advantages
1 – Measure large masses
2 – Less soil disturbance
3 – Measurements under actual field conditions

Disadvantages
1 – Low strain amplitude
2 – Damping characteristics cannot be measured

Figure 2.2 Advantages and Disadvantages of laboratory and field-testing methods (Tawfiq, 1986)

More information on the laboratory and field techniques used are given by Woods, 1978; Hoadley, 1985; Kramer, 1996; Towhata, 2008.

2.3 Effect of Strain

When plotted at the same scale as shown in Figure 2.3, the stress – strain loops at very small strains collapse to a straight line with a slope equal to the maximum shear modulus, G_{max}, which closely approximates the initial tangent modulus on first loading (Ishihara, 1986). As the amplitude of the cyclic shear strain increases, the equivalent shear modulus decreases, and the damping ratio increases (see Figure 2.3)

It is frequently convenient to normalize the shear modulus at a given strain level by dividing it by G_{max} and if the resulting quantity G/G_{max} and the damping ratio are plotted against cyclic shear strain, curves such as those shown in Figure 2.3 are obtained. These are commonly referred to as modulus reduction and damping curves (Kramer, 1986).

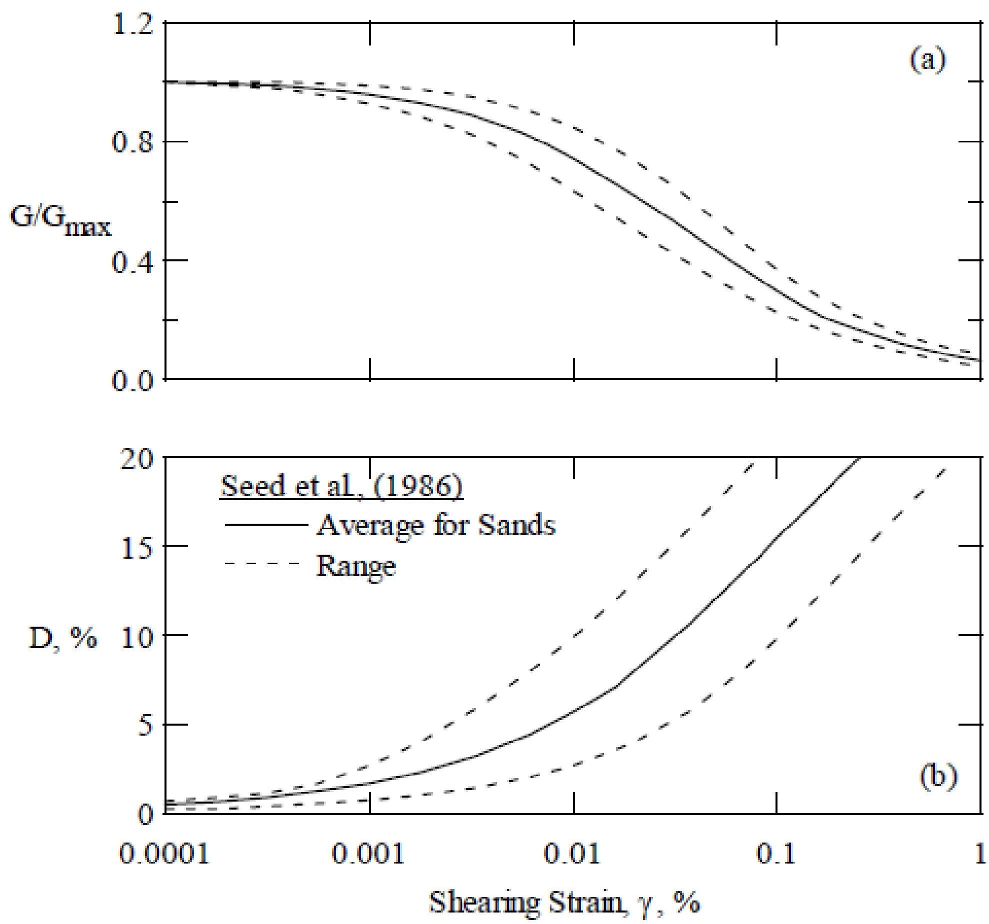

Figure 2.3 Normalized Shear Modulus Reduction and Damping Curves by Seed et al. (1986) (from Darendeli, 2001)

The force of inertia plays an increasingly significant role as the time interval at which deformation occurs become short (Ishihara, 1996). Therefore, even if the level of strain is infinitesimal, the inertia force could become significantly great with increasing rapidity in motion and reach a point where its influence can no longer be disregarded in engineering practice. For this reason, it becomes necessary in soil dynamics to draw attention to the behavior of soils subjected to a strain level as small as 10^{-6} (Ishihara, 1996).

2.4 Laboratory Methods

A wide variety of laboratory techniques are available, each with different advantages and limitations with respect to different problems. Many are oriented toward measurement of low-strain properties and many others toward properties mobilized at larger strains. The following section discusses some of the more common methods:

2.4.1 Resonant Column Test

The resonant column (RC) test is the most commonly used laboratory test for measuring the low-strain properties of soils (Kramer, 1996). The results of these project were used this type of device and it is further discussed in later sections.

The RC method subjects solid or hollow cylindrical specimens to torsional or axial loading by an electromagnetic loading system. The loading systems usually apply sinusoidal loads to samples. Frequency and amplitude can be controlled, but random noise loading (Al-Sanad and Aggour, 1984) and impulse loading (Tawfiq et al., 1988) have also been used. Figure 2.4 depicts a common resonant column apparatus.

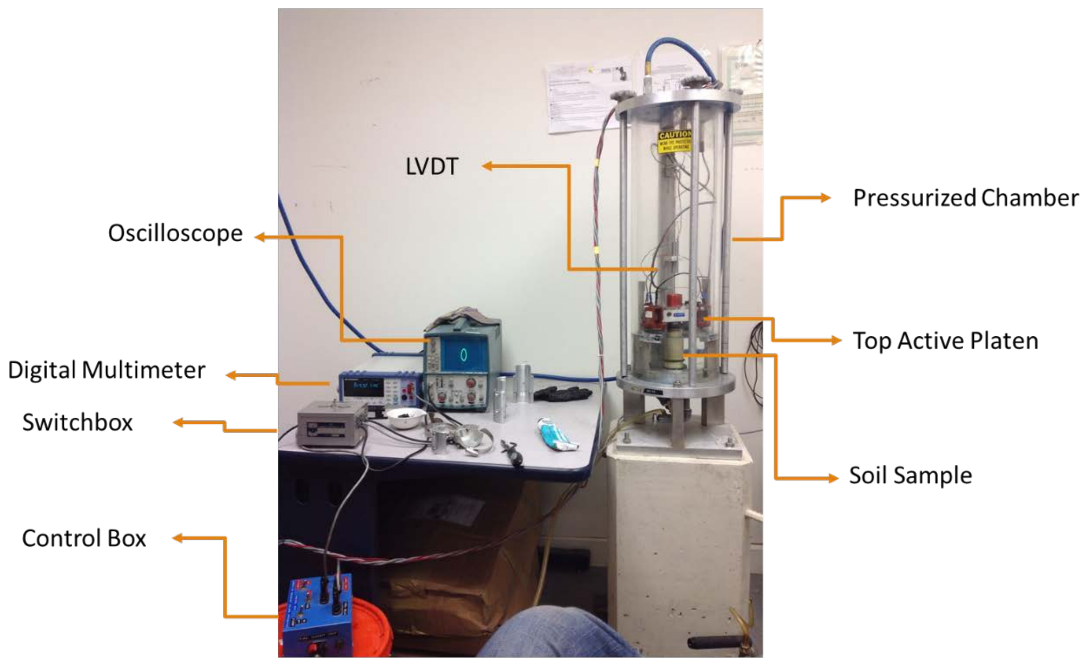

Figure 2.3 Typical Drnevich Resonant Column Apparatus Set Up

Figure 2.4 shows a typical resonant column apparatus. Cyclic loading is applied at the top of a soil specimen by way of a drive coil located in the top active platen. The loading frequency is initially set at a low value and is then gradually increased until the response (strain amplitude) reaches a maximum. The lowest frequency at which the response is locally maximized is the fundamental frequency of the specimen (Drnevich, 1975).

The fundamental frequency is a function of the low-strain stiffness of the soil. the geometry of the specimen, and certain characteristics of the resonant column apparatus (Kramer, 1996). Based on this, Shear Modulus (G) can then be obtained as follows:

$$G = \rho(2\pi L)^2 \left(\frac{f_T}{F_T}\right)^2 \qquad (1)$$

Where:

ρ = specimen mass density

L = specimen length

f_T = system resonant frequency

F_T = dimensionless frequency factor specific to RC apparatus

Damping can be determined by switching off the driving power at resonance and recording the decaying vibration (Drnevich, 1975). The logarithmic decrement is calculated using the following relationship:

$$\delta_s = \frac{1}{n} ln\left(\frac{A_1}{A_{n+1}}\right) \qquad (2)$$

Where:

δ_s = logarithmic decrement

n = number of oscillations

A_1 = initial amplitude value

A_{n+1} = amplitude at n oscillations

Damping Ratio (D) is then obtained by calculating, the following:

$$D = \frac{1}{2\pi}\lfloor \delta_s(1+S) - \delta_a \rfloor \tag{3}$$

Where:

D = Damping ratio

δ_s = logarithmic decrement

S = System Energy Ration

δ_a = logarithmic decrement of the RC apparatus without specimen

2.4.2 Ultrasonic Pulse Test

The Ultrasonic Pulse test is another low strain test to measure dynamic properties (Lawrence, 1963; Nacci and Taylor, J 967). Transmitters and receivers are attached to platens that can be placed at each end of a soil specimen (see Figure 2.5)

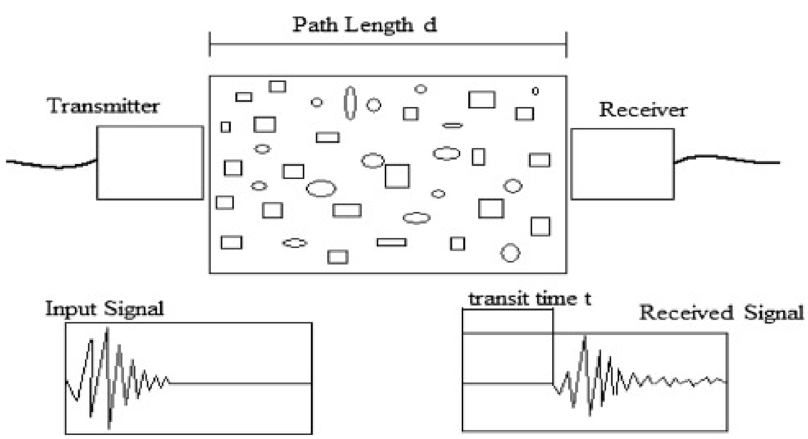

Figure 2.4 Schematic of Ultrasonic Pulse Test

They are made of piezoelectric materials which exhibit changes in dimensions when subjected to a voltage across their faces. A high-frequency stress wave is created that travels through the specimen toward the receiver. When the stress wave reaches the receiver, it generates a voltage pulse that is the measured. The distance between the transmitter and receiver is divided by the time difference between the voltage pulses to obtain the wave propagation velocity (Kramer, 1996). Shear modulus, G, can be obtained by the classical formula:

$$G = \rho V_s^{\ 2} \tag{4}$$

Where:

G = Shear Modulus

ρ = specimen mass density

V_s = shear Wave Velocity

Logarithmic decrement is then measured by:

$$\delta = \frac{2.302}{n} log\left(\frac{A_0}{A_n}\right) \tag{5}$$

Where:

δ_s = logarithmic decrement

n = number of oscillations

A_0 = initial amplitude value

A_n = amplitude at n oscillations

2.4.3 Piezoelectric Bender Element Test

Similarly, to the previous test, this test relies on measurement of shear wave velocity (V_s) on a soil specimen using bender elements (Shirley and Anderson, 1975;

De Alba et al., 1984;). Bender elements are constructed by bonding two piezoelectric materials together in such a way that a voltage applied to their faces causes one to expand while the other contracts, causing the entire element to bend as shown in Figure 2.6 (Kramer, 1996).

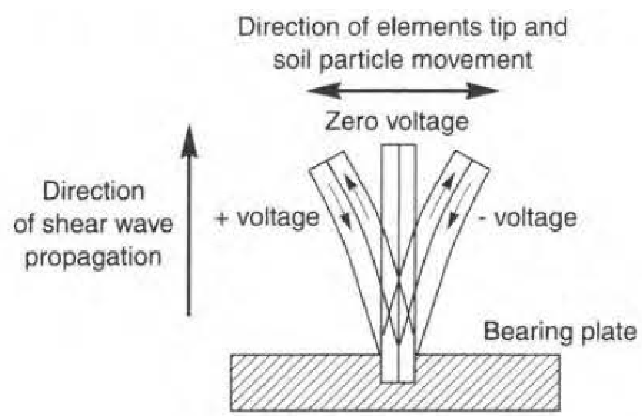

Figure 2.5 Piezoelectric Bender Element Schematic (Kramer 1996)

Similarly, a lateral disturbance of the bender element will produce a voltage, so the bender elements can be used as both s-wave transmitters and receivers (Kramer, 1996). These bender elements have been incorporated into numerous conventional soil dynamic devices. The time difference between the two voltage pulses is measured with an oscilloscope and divided into the distance between the tips of the bender elements to give the s-wave velocity of the specimen (Kramer, 1996). Shear modulus, G, is calculated in a similar manner as in Equation (6).

2.4.4 Cyclic Triaxial Test

In the cyclic triaxial test, a cylindrical soil sample is placed between top and bottom loading platens. It is then surrounded by a rubber membrane. The soil specimen is subjected to a radial stress and an axial stress (see Figure 2.7). A deviatoric stress is applied cyclically (Kramer, 1996).

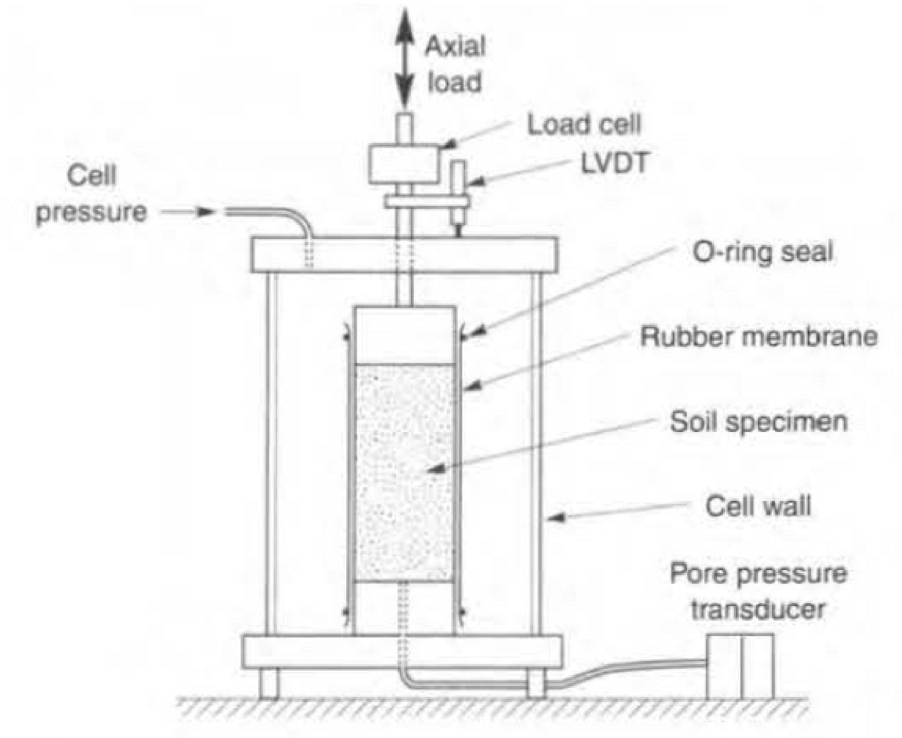

Figure 2.6 Cyclic Triaxial Test Schematic

The sample is first consolidated under a confining and all-around pressure, σ_3, and subsequently a vertical predetermined cyclic stress (stress controlled) or strain (strain controlled) is applied (Amir Faryar, 2012). A hysteresis loop is obtained and the elastic modulus, E, is then calculated through the slope of the straight line connecting the two extreme points of the hysteresis loop as follows:

$$E = \frac{\Delta\sigma_d}{\varepsilon_a} \tag{6}$$

Where:

$\Delta\sigma_d$ = Deviatoric axial stress

ε_a = Maximum Axial Strain

The Shear modulus can then be calculated as follows:

$$G = \frac{E}{2(1+\mu)} \qquad (7)$$

Where:

E = Elastic Modulus from (8)

μ = Poisson's ratio

The damping ratio can be determined from the hysteresis stress-strain graph as follows:

$$D = \frac{1}{4}\frac{\text{Area of loop}}{Area\ of\ Triangle} \qquad (8)$$

2.4.5 Cyclic Torsional Shear Test

Cyclic torsional shear tests allow isotropic or anisotropic initial stress condition and can impose cyclic shear stresses on horizontal plane with continuous rotation of principal stresses (Kramer, 1996). They are most commonly used to measure stiffness and damping characteristics over a wide range of strain levels (Kramer, 1996). Solid (Ishihara and Li, 1972) and hollow specimens can be used. Hollow cylinders seem to provide better results as they have the advantage of having more uniform shear strains (Amir Faryar, 2012). For dry sands, the only disadvantage is that the soil specimen formation is very hard to create. Solid cylindrical specimens are still very commonly used especially for dry sands as they are cohesionless.

Solid cylindrical samples are twisted at one free end and then released to vibrate freely with a heavy weight placed on the free end. This creates a single degree of freedom system (Kramer, 1996). Shear Modulus, G, can then be calculated, as follows:

$$G = \frac{W_{nc}^2 K}{1 - \frac{W_{nc}^2}{W_{ni}}} \tag{9}$$

Where:

W_{nc} = natural frequency of the system

W_{ni} = natural frequency of the apparatus.

K = constant characteristic dependent upon the geometry and apparatus

Damping Ratio, D, can be obtained in the same manner as in equation (10).

2.5 Field Methods

The advantage of field tests is that they do not require sampling. Sampling alters the stress and structural conditions of the soil specimen. Therefore, they can provide measurements of the in-situ conditions (Kramer, 1996). On the other hand, precisely because of the aforementioned, only in-situ conditions can be assessed and the effects of other variables cannot be discerned.

Some field tests can be performed from the ground surface, while others require the drilling of boreholes or the advancement of a probe into the soil. Surface tests are often less expensive and can be performed relatively quickly. They are particularly useful for materials in which drilling, and sampling or penetration is difficult

(Kramer, 1996). The following are examples of common field techniques to measure dynamic properties.

2.5.1 Seismic Reflection Test

The seismic reflection test allows the wave propagation velocity and thickness of surficial layers to be determined from the ground surface (Kramer, 1996). It is advantageous because boreholes are not needed in order to perform the test. Figure 2.8 shows an idealistic setup. A compressional wave is created at the source (S) which then radiates hemispherically until it reaches a receiver (R) (Kramer, 1996).

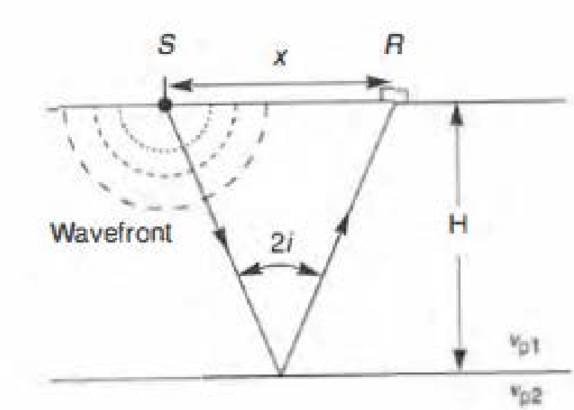

Figure 2.7 Typical Seismic Reflection Test configuration (Kramer, 1996)

The time from wave initiation and arrival is then recorded. Compressional wave velocity (V_p) is the calculated as follows.

$$GV_p = \frac{X}{t_d} \tag{10}$$

Where:

X = distance from source and receiver

T_d = time from wave to travel from source to receiver.

Shear modulus (G) can then be calculated from the following relationship:

$$G = \frac{V_p^2 \rho (1 - 2\mu)}{2(1 - \mu)} \tag{11}$$

Where:

V_p = compressional wave velocity

ρ = soil density

μ = Poisson's ratio

2.5.2 Suspension Logging Test

The suspension logging test consist of an instrumented probe that is inserted and lowered into an uncased borehole filled with water or drilling fluid (Kramer, 1996). The probe is mainly composed of two parts. A horizontal reversible polarity solenoid that acts as the source (S) located near the base of the probe and a pair of biaxial geophones, that act as receivers (R), located near the top of the probe. Figure 2.9 shows a typical schematic of how this test is performed.

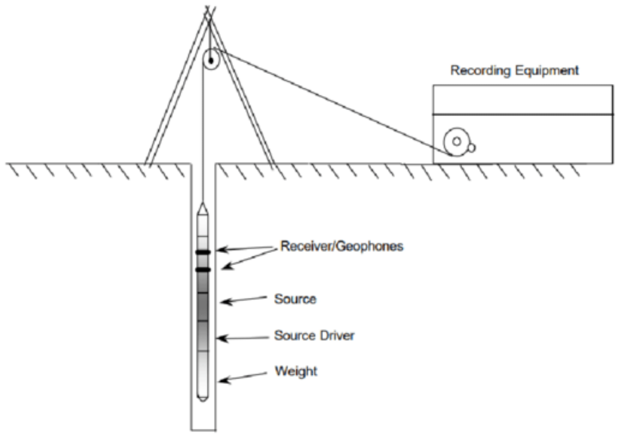

Figure 2. 8 Schematic of suspension logging setup (Luna and Jadi 2000)

The source creates an impulse wave in the drilling fluid. Upon reaching the borehole wall, the pressure wave produces compressional (V_p) and shear (V_s) waves in the surrounding soil (Kramer, 1996) which then transmit energy back to the receivers. The differences in arrival times are used to compute the average V_p and V_s. The probe is then moved up and down the borehole at known depths. Shear Modulus, G, can be obtained using the same relationship found in Equation (6).

2.5.3 Seismic Crosshole Test

The seismic cross-hole test relies on boreholes. It uses two (2) or more boreholes to measure wave propagation velocities along horizontal paths (Kramer, 1996). An input energy source, S, is placed in one borehole while the other one contains a receiver. See figure 2.10. By having both the source and the receiver at the same elevation in each borehole the wave propagation velocity at that depth is measured. A velocity profile is obtained by recording data at multiple elevations. The use of more than two boreholes is desirable (Kramer, 1996). Compression, V_p, and shear, V_s, velocities can then be calculated from differences in arrival time in a similar manner as previous tests (see Equation 6).

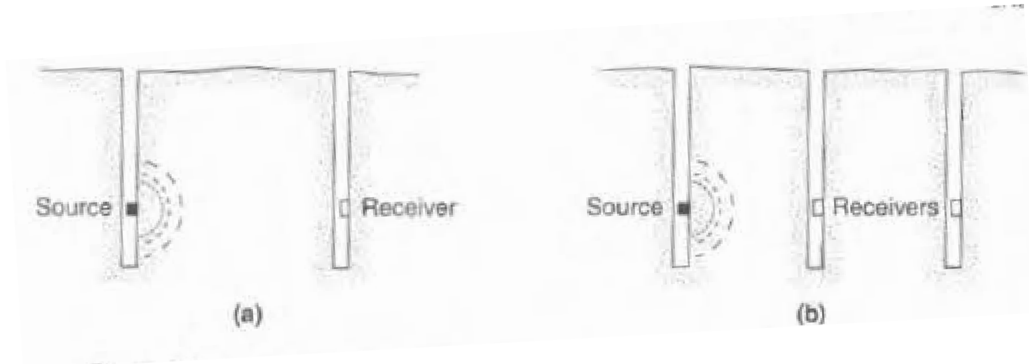

Figure 2.9 Typical seismic crosshole setup with 2 and 3 boreholes, a and b, respectively (Kramer, 1996)

2.6 Factors that affect Shear Modulus and Damping

Hardin and Richart (1963) performed one of the first laboratory investigations of variables affecting shear wave velocity (V_s) in soils. The applied cyclic loads with a resonant column testing device to engineered samples of Ottawa sand, crushed quartz sand, and crushed quartz silt (Sykora, DW, 1987). Variables considered were:

- confining pressure,
- void ratio,
- moisture content,
- grain size distribution, and
- grain characteristics

Hardin and Richart (1963) concluded that confining pressure and void ratio were the variables that had the greater effect on dynamic properties. It needs to be stated, that they only tested samples of Ottawa (Silica) sand in their experiment.

Shear wave velocity (Vs) was found to be inversely proportional to the amount of void ratio. In addition, Hardin and Richart (1963) found Vs to be independent of relative grain size, gradation and relative density. They further concluded that the shear wave velocity of at the same relative density and confining pressure may be quite different, but that different soils at the same void ratio should have the same shear wave velocity. The following empirical equations were developed:

For effective confinement pressure, σ'_o, less than 2000 pounds per square feet (psf):

$$V_s = (119 - 56.0e)\sigma'^{0.30}_o \quad (12)$$

For effective confinement pressure, σ'_o, greater than 2000 pounds per square feet (psf):

$$V_s = (170 - 78.2e)\sigma'^{0.25}_o \quad (13)$$

Where:

e = void ratio

σ'_o = effective confining pressure (psf)

Later, Hardin and Drnevich (1972), conducted one of the first comprehensive investigation of parameters affecting the stress-strain relations in soils in the strain range of 0.1 percent or less using results of resonant column and simple shear testing (Sykora, DW, 1987). The authors calculated shear modulus and damping ration for both cohesionless (clean sands) and cohesive soils. For both types of soils, Hardin and Drnevich concluded that strain amplitude, effective mean principal stress, and void ratio were the most important variables that affect the dynamic properties (Sykora, DW, 1987). In contrast, the authors also showed that for clean sands, the number of low-amplitude cycles of loading, degree of saturation, overconsolidation ratio, frequency of loading, thixotropy, soil structure, and grain characteristics (size, shape, gradation, and mineralogy) have relatively little influence on shear modulus (Sykora, DW, 1987). Figure 2.11 shows the factors that affect G and D, per Hardin and Drnevich, 1972.

	Importance To*			
	Modulus		Damping	
	Clean Sands	Cohesive Soils	Clean Sands	Cohesive Soils
Strain amplitude	V	V	V	V
Effective mean principal stress	V	V	V	V
Void ratio	V	V	V	V
Number of cycles of loading	R**	R	V	V
Degree of saturation	R	V	L	U
Overconsolidation ratio	R	L	R	L
Effective strength envelope	L	L	L	L
Octahedral shear stress	L	L	L	L
Frequency of loading (above 0.1 cycle/sec)	R	R	R	L
Other time effects (thixotropy)	R	L	R	L
Grain characteristics, size, shape, gradation, mineralogy	R	R	R	R
Soil structure	R	R	R	R
Volume change due to shear strain (for strains less than 0.5 percent)	U	R	U	R

* V means very important, L means less important, and R means relatively unimportant except that it may affect another parameter; U means relative importance is not clearly known at this time.
** Except for saturated clean sand where the number of cycles of loading is a less important parameter.

Figure 2.10 Factors affecting Shear Modulus and Damping (Hardin and Drnevich (1972) obtained from Sykora, DW, (1987))

Hardin and Drnevich developed a relationship with G_{max} for an isotropic state of stress for soils:

$$G_{max} = 1230 \frac{(2.973 - e)^2}{1 + e} OCR^k \sigma'^{0.5}_m \qquad (14)$$

Where:

e = void ratio

σ'_m = mean effective stress (psi)

OCR = Overconsolidation ratio

K = dimensionless quantity which is a function of plasticity index (PI). For sands PI equals zero. Table 2.1 shows the additional factors.

Table 2.1 Empirical Values of Exponential Parameter (k) (Hardin and Drnevich (1972) obtained from Sykora, DW, (1987))

Plasticity Index (PI)	**Dimensionless Factor, K**
0 (sands)	0
20	0.18
40	0.30
60	0.41
80	0.48
>100	0.50

Later, Vucetic and Dobry (1991) performed a study on the influence of plasticity index (PI) on the cyclic stress-strain parameters of saturated soils needed for site-response evaluations. They compiled and created charts and tables based on data obtained from multiple publications and many soil types. Vucetic and Dobry (1991) work includes relationships for dynamic properties for both cohesive soils and cohesionless soils. In particular, Figures 2.12 and 2.13 show the results of their work. For this research, the focus will be on the curves with a PI = 0 which correspond to cohesionless soils or clean sands. Of note, Vucetic and Dobry stated that saturated cohesionless nonplastic soils, like gravels and sands, for which PI = 0, are the most nonlinear, as they start to behave nonlinearly at the smallest strain levels (Sykora, DW, (1987)). Accordingly, the cohesionless soils also have the largest damping values. It should be noticed that the curves for PI = 0 in Fig. 6 are fully consistent with those published by Seed and Idriss 1970 and Seed et al. 1986 for saturated cohesionless soil.

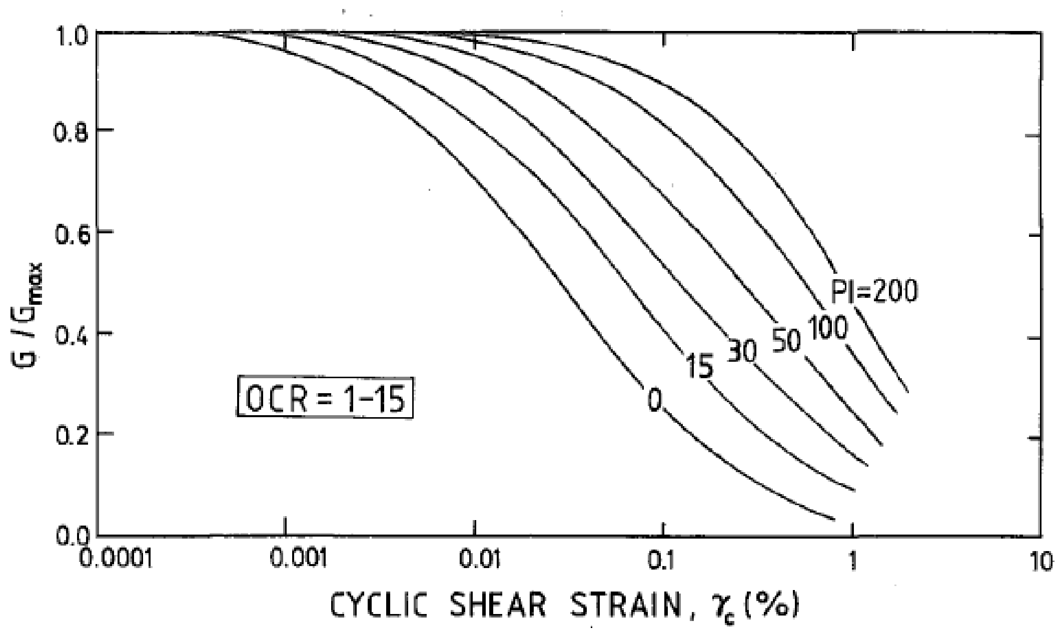

Figure 2.11 Relations between G/ G_{max} versus γ (Vucetic and Dobry, 1991)

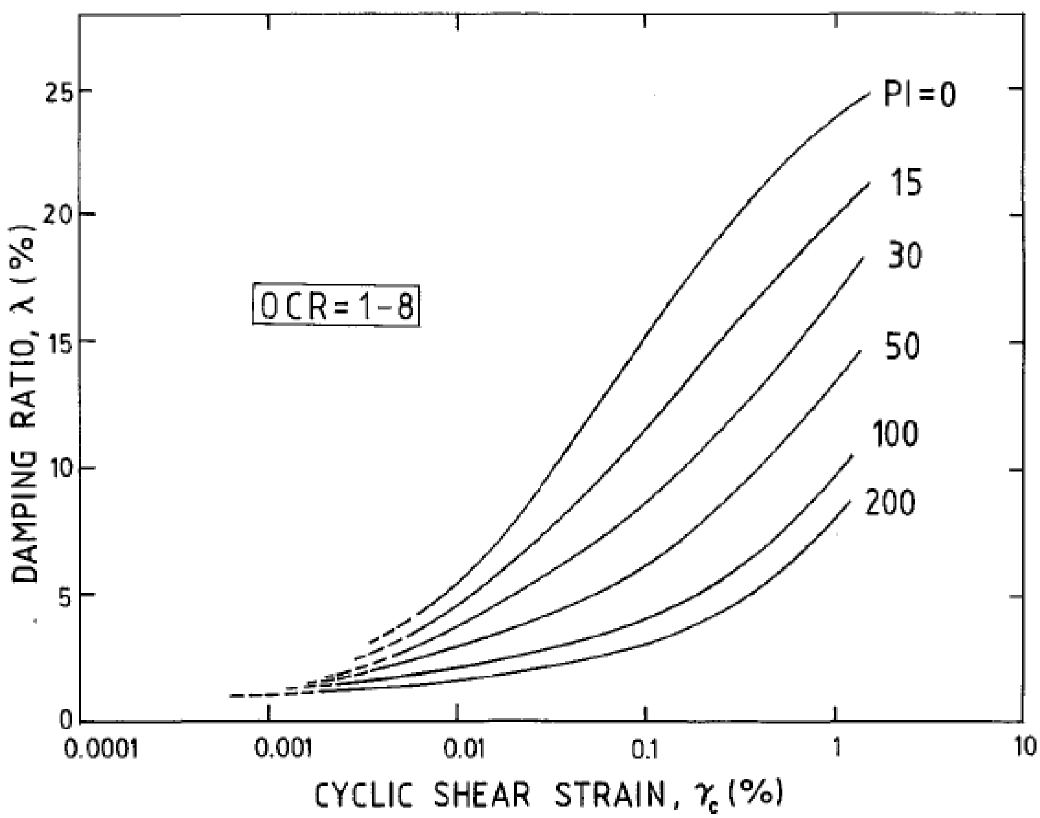

Figure 2.12 Relations between Damping versus γ (Vucetic and Dobry, 1991)

2.7 *Effects of Gradation and Particle Shape*

Median grain size, D_{50}, and uniformity coefficient, C_u, are usually the two most important variables when studying the effects of gradation (Menq, 2003). Particle shape can be further subdivided into rounded and angular particles. In order to study the effects of grain-size distribution characteristics on dynamic properties of sandy soils, researchers such as Chang and Ko (1986) used a Drnevich-type, free-free resonant column device. They engineered specimens with median grain size, D_{50}, ranging from 0.149 to 1.68 mm and a uniformity coefficient, C_u, ranging from 2 to 16. Menq (2003) further analyzed Chang and Ko's (1986) work and created trend lines to better visualize the behavior. Figures 2.14 and 2.15 show the relationship between G_{max} and C_u and D_{50} of various samples per Menq (2003) and Chang and Ko (1986).

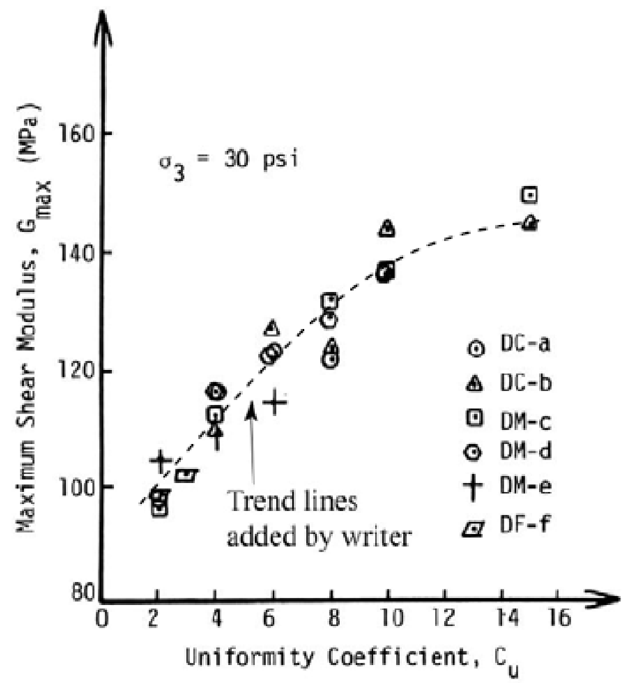

Figure 2.13 Small Strain Shear Modulus vs Uniformity Coefficient at a mean effective confining pressure of 30 psi (From Menq, 2003, after Chang and Ko, 1986)

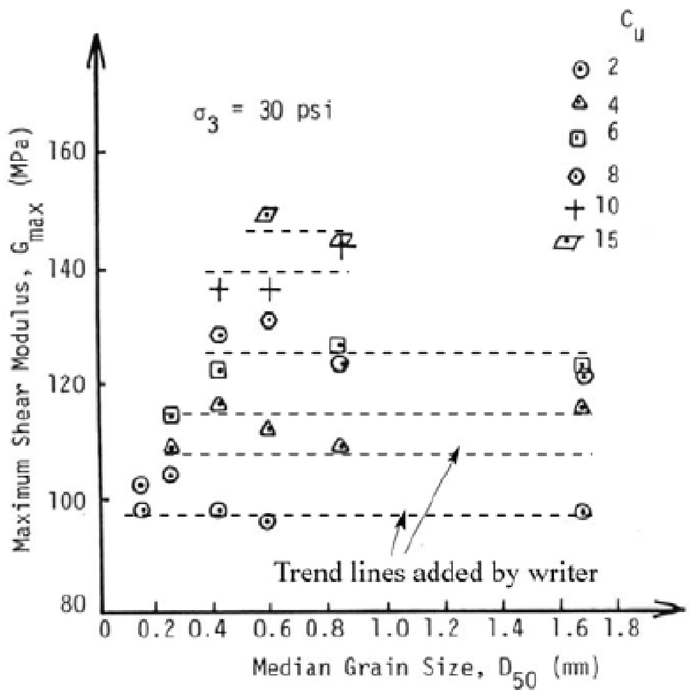

Figure 2.14 Small Strain Shear Modulus vs Median Grain Size, D_{50}, at a median effective confining pressure of 20 psi (From Menq 2003, after Chang and Ko, 1986)

Based on the figures, Menq (2003) concluded the G_{max} of medium loose specimens are mostly function of C_u, with very little effect of D_{50}.

Another pair of researchers, T. Wichtman and T. Triantafyllidis (2009), studied the effects of C_u and D_{50} on G_{max} of well graded sands. They demonstrated that the small strain shear modulus does not depend on the mean grain size. In contrary to what Menq (2003) found, they were able to find that the small strain shear modulus significantly decreases with increasing coefficient of uniformity (see Figure 2.16). Other researchers have found similar observed similar downward trending behavior in their respective research, such Iwasaki and Tatsuoka (1977) and Kokusho et. Al. (2004).

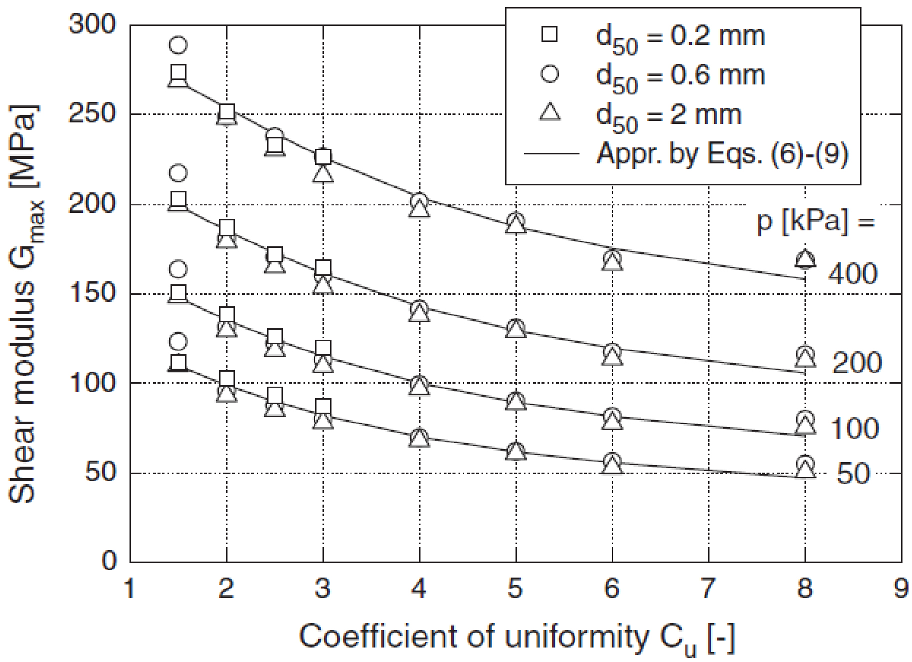

Figure 2.15 Low strain shear modulus at e = 0.55 as a function of C_u for different pressures (T. Wichtman and T. Triantafyllidis, 2009)

The same researchers also studied the effects of C_u and D_{50} on the normalized shear modulus and damping ratio of sands. In their research, they mostly studied well graded quartz sands. Based on their data, they demonstrated that the shear modulus degradation is larger for higher values of the uniformity coefficient (see Figure 2.17). They also concluded that the curves of damping ratio, D, were found to be almost independent of the grain size distribution curve.

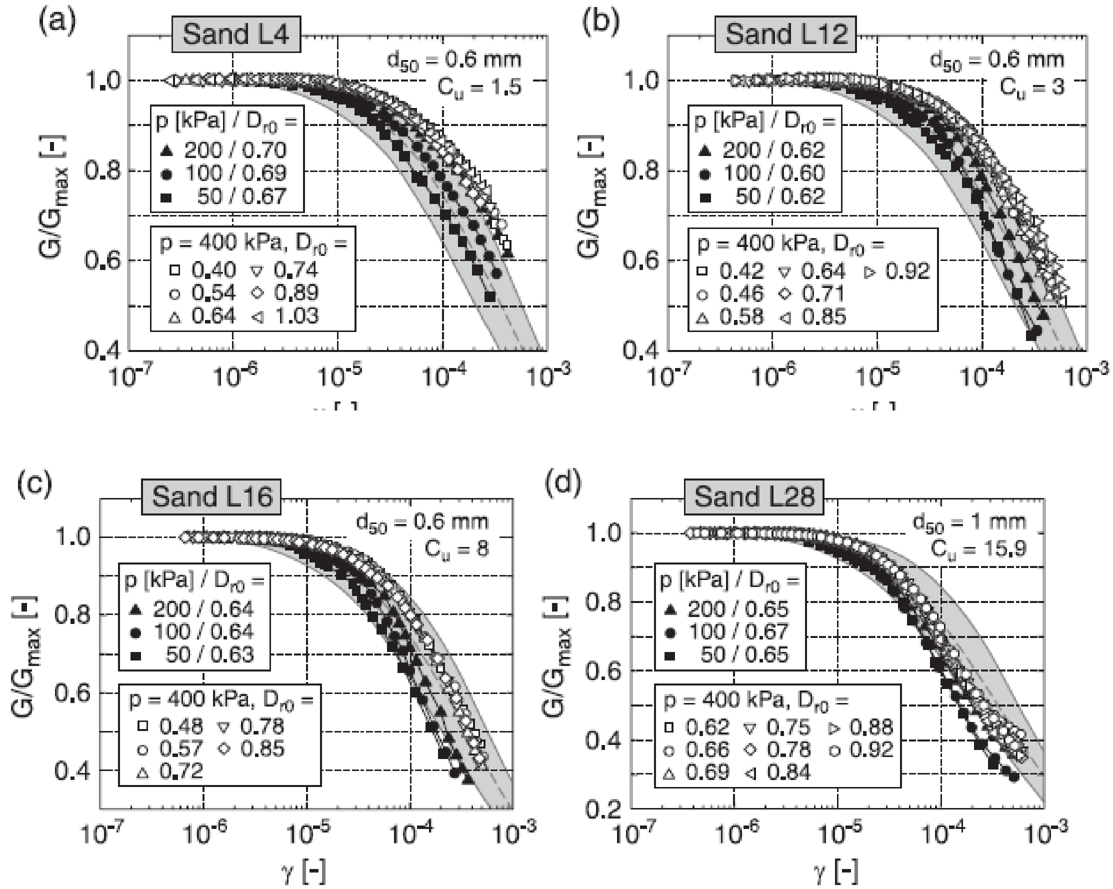

Figure 2.16 Modulus Degradation curves measured for various materials, pressures and densities. Gray shading represents Seed et al. (1986) (From T. Wichtmann and T. Traintafyllidis, 2013)

2.8 <u>Speed of Loading</u>

The time of loading is defined as the length of time at which a certain level of stress or strain is attained in soils. Shorter time of loading is related to phenomena with shorter periods or higher frequencies. In contrast, longer time of loading is related to longer periods or lower frequencies. Dynamic problems correspond to those that have a shorter time of load application. Static problems correspond to those that have longer time of load applications (more than tens of seconds). The

Drnevich resonant column device used in this research corresponds to the former as cyclical torsional loading is applied in short amount of time.

2.9 *Effects of Load Repetition*

Repetitiveness in loading is another prime attribute used to classify dynamic problems. Main shaking during earthquakes involves multiple repetition of loads with differing amplitudes and frequencies. While the seismic loading is irregular in time history, the period of each impulse, is within the range between 0.1 and 3.0 seconds, giving the corresponding time of loading on the order of 0.02 to 1.0 seconds. Seismic loading is a prime example of what is termed vibration or wave propagation.

2.10 *Summary*

Published literature discussing variables that affect the dynamic properties of soils in the are presented in this chapter. The effects of effective confining stress, effective void ratio, particle shape, and gradation on small-strain dynamic properties were discussed.

CHAPTER 3

TEST EQUIPMENT

3.1 Introduction

The properties of soils under dynamic loading, mainly shear modulus, G, and damping ratio, D, need to be well understood in order to properly assess the characteristics of the site in question. Due to its nature, soils do not behave in an elastic manner, nonetheless, because of constraints in the way engineers test materials, they need to be tested in accordance with concepts of elasticity.

The main objective of this research is to study the effect of mineral composition in dry sands using the resonant column test. The resonant column testing technique is popular among researchers since its inception as an ASTM standard testing method in 1978. This chapter describes the test equipment used in this research. The information in the following subsections is compiled from the Drnevich Resonant Column Manual (Drnevich, et al., 1978) at the University of Maryland (UMD) apparatus. In addition, previous researchers, such as Amir Faryar (2012) performed various calibration activities as part of his research. The same calibration techniques were followed by the current researcher when appropriate.

3.2 The Drnevich Resonant Column Apparatus

The Drnevich resonant column apparatus located in the Soil Dynamics Laboratory at the University of Maryland (UMD) is a nondestructive testing equipment. The apparatus consists mainly of a chamber having a lower (static) and a top platen (active platen). A column of soil, in our case a combination of dry sands, is placed between the aforementioned plates. The chamber has the means to provide water and compressed air in order to subject the column of soil to the desired conditions (in situ, engineered, etc.). Figure 2.1 shows a sketch of the Drnevich resonant column apparatus.

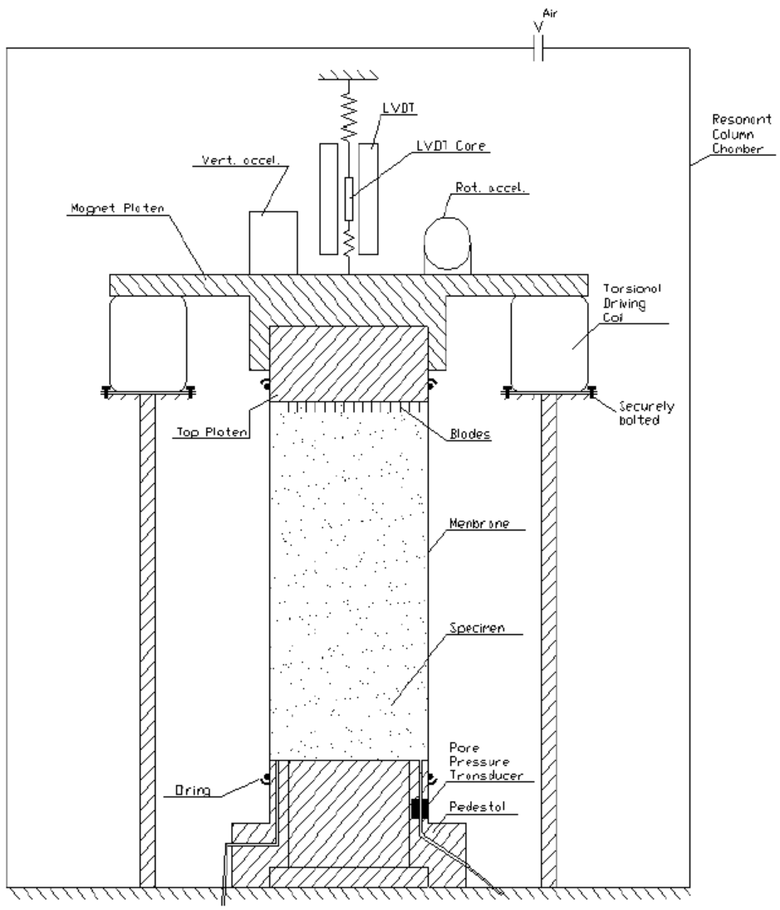

Figure 3.1 Schematic of Drnevich Resonant Column Apparatus (Drnevich, 1975)

Torsional vibration is applied to the soil columns through a magnet plate supporting torsional and longitudinal accelerometers. Fixed coils are connected with an electrical circuit to the aforementioned platen. When a current passes through the coils, a torsional vibration is applied to the soil column. The Drnevich RC can also apply longitudinal vibrations through a centrally placed coil on the torsional magnet plate in conjunction with a vertically adjustable magnet. In this arrangement, longitudinal vibration is applied to the soil column. In addition to the coils, a length measuring transducer (LVDT) attached to the upper platen serves to give constant readings of the length changes of the soil column resulting from the compaction of that column (Drnevich, 1975). For this research, a combined LVDT readout and condition unit (Digital Panel Meters Model PML-1000) was used as a conditioning module to excite and read the response received from the LVDT.

The excitation system of the resonant column device is an electromagnetic system comprising of a permanent magnet and coil that can move in the gap between the North and South Poles of the permanent magnet (Drnevich, 1975). The Drnevich resonant column apparatus has two excitation modes: longitudinal and torsional. This research was solely based on torsional mode as it is adequate to calculate the necessary dynamic properties. For the torsional mode, the assembly comprises of four rectangular coils and horseshoe-shaped magnets. The coils are connected to the brackets and the magnets to the top active platen. When activated a magnetic field is generated, which in turn develops torsional forces on the top of the soil column.

3.3 The Drnevich Resonant Column Apparatus Ancillary Equipment

As previously mentioned, the Drnevich resonant column apparatus is comprised of the main pressure chamber and several ancillary equipment. Figure 3.1 shows a schematic diagram of all devices used in this research. Additionally, Table 3.1 shows the related equipment along with its respective function.

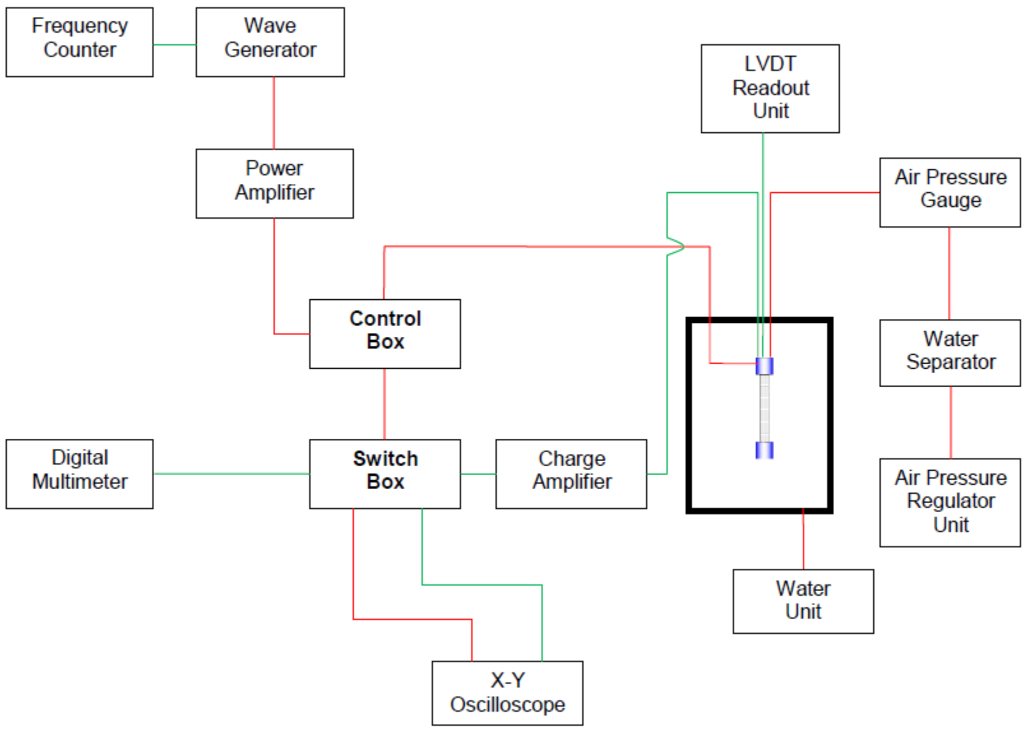

Figure 3.2 Schematic diagram of the Drnevich Resonant Column Apparatus (red lines = input; green lines = output) (Amir Faryar, 2012)

Table 3.1Drnevich Resonant Column Apparatus Ancillary Equipment (Amir Faryar, 2012)

Equipment	**Model**	**Function**
Frequency Counter	TUV - VC 2000	Measure frequency of input signal
Sine Wave Generator	GW – Instek	Provides sinusoidal input voltage for driving coils
Power Amplifier	Bogen Model MT125B	Amplifies input signal
Oscilloscope	Tektronix model T912)	Displays output signal from accelerometers
Charge Amplifier	Columbia Model 4102	Excites transducer and conditions output voltage from accelerometer
Digital Multimeter & Frequency Counter	BK Precision	Measure the input and output voltage to/from transducer through charge amplifier.
LVDT	Measurement Specialties	Measures output from LVDT

3.4 Equipment Calibration

3.4.1 Resonant Column Apparatus Calibration

The calibration of the Drnevich Resonant Column Apparatus (RC Apparatus), was performed using the process described in the device manual. It requires a calibrating rod of known torsional stiffens. This calibrating rod (see Figure 3.3) is placed with one end rigidly fixed to the base and the other end rigidly fixed to the top magnet platen (Drnevich, et al., 1978). This configuration assimilates a single degree of freedom system.

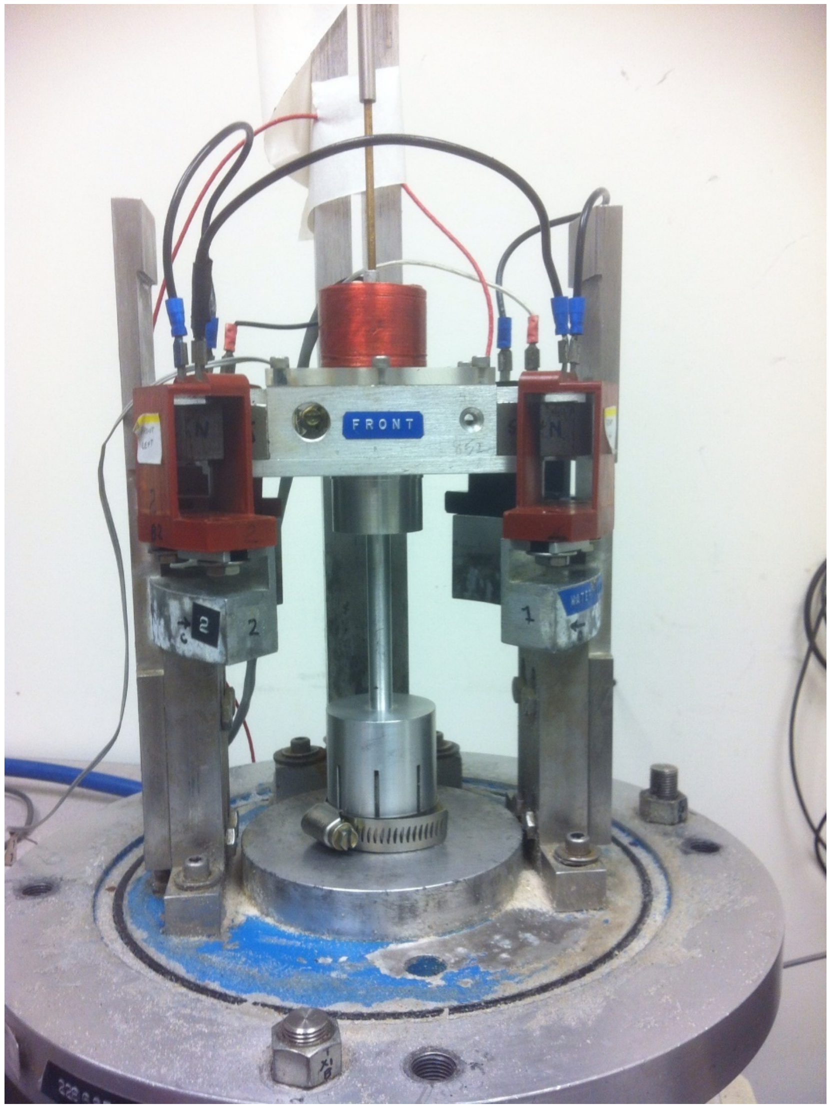

Figure 3.3 Resonant Column with Calibration Rod

Per the RC manual, \with the torsional calibration rod in place, a small current (0.05 V_{rms}) is sent to the torsional coils. The loading frequency is then adjusted to obtain resonance. The resonant frequency (f_t) is recorded and the value of $\sqrt{2}/2\ f_t$ and $\sqrt{2}\ f_t$ is calculated. A large current (1.0 V_{rms}) is applied while the frequency of oscillation is set to the frequencies one at a time. The corresponding output of the torsional accelerometer is recorded at both frequencies. Two calibration factors, C_1 and C_2, can be calculated as follows:

$$C_1 = \frac{\left(\frac{4.43}{f_1^2}\right) TO_1}{2CR_1} \tag{15}$$

$$C_2 = \frac{\left(\frac{4.43}{f_2^2}\right) TO_2}{2CR_2} \tag{16}$$

Where:

C_1,C_2 = calibration coefficients

CR_1,CR_2 = excitation voltages at $\sqrt{2}/2\ f_t$ and $\sqrt{2}\ f_t$, respectively

TO_1,TO_2 = response voltages at $\sqrt{2}/2\ f_t$ and $\sqrt{2}\ f_t$, respectively

The values of C1 and C2 should agree within 10 percent otherwise the calibration should be repeated (ASTM D4015-07). A Torque Calibration Factor (TCF) can then be calculated as follows:

$$TCF = 0.5(C_1 + C_2)K_{cr} \tag{17}$$

Where:

TCF = torsional calibration factor

K_{cr} = is spring constant of the calibration rod and is equal to 265.4 $\frac{N-M}{rad}$

The torsional calibration factor was calculated to be 7.05 x 10^{-2} $\frac{N-M}{V_{rms}}$ for the RC apparatus.

3.4.2 Polarity of Torsional Wiring System Calibration

Similarly, to the previous section, the calibration of the torsional wiring system was performed according to Drnevich Resonant Column apparatus manual. Per the manual, the polarity of the torsional wiring system needs to be checked in order to ensure that a torsional moment is created in the same direction of motion. In order to check the polarity, test leads or other convenient temporary connections were used to short out coils 2, 3 and 4. A known 6-volt DC current was then connected to the main lead for the torsional coils from the Control Box instead of the AC voltage provided by the power amplifier. This action creates a current of less than one amp through the remaining coil 1 which should be enough to cause the magnet and top platen system to rotate in a clockwise or counterclockwise manner. The operator should make note of the rotation of direction. The same procedure is performed for coil 2 with coils 1, 3, and 4 in the shorted-out configuration. After applying the current, the system should experience a motion in the same direction as previously identified. If it is not, the leads to coil 2 should be reversed. This procedure was performed for the remaining coils 3 and 4. This calibration ensures that the connections to each coil produce the same rotation of motion of the magnet-top platen system for the same voltage applied. Figure 3-4 shows the voltage test set up.

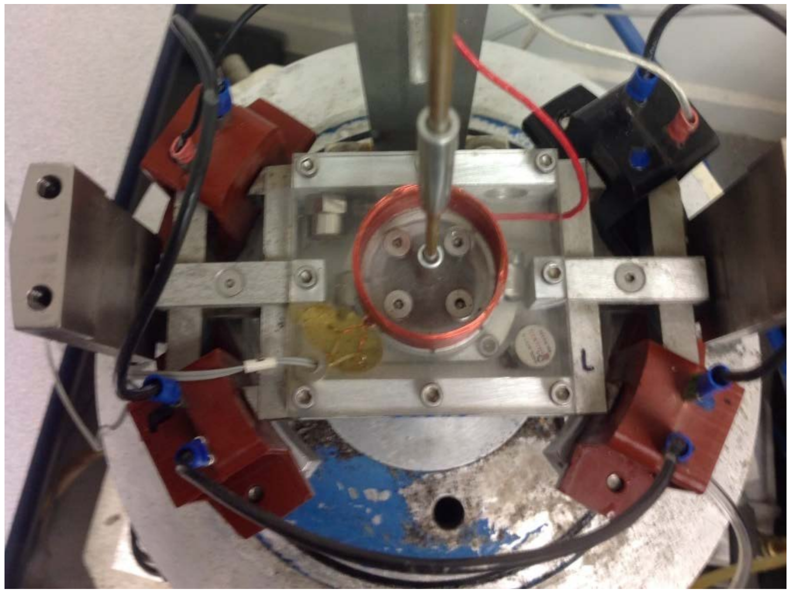

Figure 3.4 Top view of torsional coils under calibration

3.4.3 Acceleration Transducers and Charge Amplifiers Calibration

Before starting this project, the acceleration transducer and charge amplifier were recently sent to be calibrated by previous researchers (Amir Faryar, 2012). The current researcher ensured that the calibration was still applicable. A relative calibration was performed where a standard transducer (a recently calibrated transducer) and the to-be-calibrated acceleration transducer were fixed together with wax and were glued onto the plate of a shaking table. Responses up to 10 times the highest frequency of interest were compared.

In Amir Faryar, (2012) research project, an absolute calibration was performed. Both the charge amplifier and transducer (model 200-1-H serial no. 858) were sent to Columbia Research Labs, Inc. A charge sensitivity of 36.3 $\frac{pk*pcmb}{pk-g}$ for the frequency ranges between 2 Hz to 5 kHz was determined for the transducer. The calibration record was checked to ensure compliance.

3.4.4 *Coupling between Soil Specimen and Top Platen*

At very low strains, coupling can exist but as the strain amplitude increases, shear stresses increase, and incomplete coupling may occur (Drnevich, et al., 1978). To ensure a complete coupling, razor blade vanes are placed in top platen (see Figure 3.5). The protrusion of the blades should be greater than or equal to 1.5 mm (Drnevich, 1978).

Figure 3.5 Top and bottom platens with razors

3.5 *Drnevich Resonant column Data Reduction Calculations*

In this research, the Drnevich resonant column was used for studying the shear modulus and damping ratio properties of dry sands. In the following section the equations used to calculate shear modulus, damping, and shear strain from resonant column testing are presented.

3.6 Calculation of Shear Modulus

In the resonant column tests where soil specimens are subjected to torsional vibration with fixed-free conditions, the wave propagation is expressed as follows:

$$\frac{\Delta^2\Theta}{\Delta t^2} = V_s^2 \frac{\Delta^2\Theta}{\Delta x^2} \tag{18}$$

Where:

$\Delta\Theta$= angle of twist (rad),

I_s = polar moment inertia of the soil specimen (m^4)

JT = polar mass moment of inertia of the top platen (kg-m2),

Vs = shear wave velocity in soil specimen (m/s).

The solution to the wave equations for short bars or soil column vibrating in a natural mode can be written in the general form as follows:

$$U(x,t) = U(x)(A_1 + A_2 \cos\omega_n t) \tag{19}$$

$$U(x) = B_1 \sin\left(\frac{\omega_n}{V_c} x\right) + B_2 \cos\left(\frac{\omega_n}{V_c} x\right) \tag{20}$$

Where:

ω_n = undamped natural frequency

A1, A2 = constants

U(x) = amplitude of displacement along the length of soil column

B1, B2 = constants

Using the boundary conditions for the fixed-free case, at x=0 (fixed end), U(x) = 0 and X = L (free end), $\frac{dU(x)}{dx} = 0$ and U(x) is:

$$U(x) = B_2 \cos\left(\frac{w_n}{V_c}x\right) \tag{21}$$

The inertia force (F) on the soil column under torsion can be expressed in terms of polar mass moment of inertia (JT) and the shear strain at x = L.

$$F = -J_T \frac{\Delta^2 \theta}{\Delta t^2} \tag{22}$$

It can also be rephrased in terms of polar moment of inertia as follows:

$$F = GI_s \frac{\Delta \theta}{\Delta x} \tag{23}$$

The following can be obtained by substituting second derivatives of combined equations 18 and 20 in equations 21 and 22.

$$F = J_t \omega_n^2 B_1 \sin\left(\frac{\omega_s}{V_s}L\right)\left(A_1 sin\omega_n t + A_2 \cos\omega_n t\right) \tag{24}$$

$$F = GI_s \frac{\omega_n B_1}{V_s} \cos\left(\frac{\omega_s}{V_s}L\right)\left(A_1 sin\omega_n t + A_2 \cos\omega_n t\right) \tag{25}$$

Equating equations 23 and 24 and expressing G in terms of mass density and shear wave velocity the following solutions can be obtained:

$$\frac{\omega_n L}{V_s} \tan\left(\frac{\omega_n L}{V_s}\right) = \frac{J_s}{J_T} \tag{26}$$

$$F_T \tan F_T = \frac{1}{T_T} \tag{27}$$

Where:

$F_T = \frac{1}{\sqrt{(0.405 + T_T)}}$ = dimensionless frequency factor

$T_T = \frac{J_T}{J_s}$ = ratio of polar inertias

Js = $\frac{M_s d^2}{8}$ = polar mass moment of inertia of soil specimen (kg*m^2). Where M_s and d equals the specimen mass and diameter.

With the value of F_T, shear modulus (G) of the soil specimen can be determined from:

$$G = \rho(2\pi L)^2 \left(\frac{f_{nT}}{F_T}\right)^2 \tag{28}$$

Where:

f_{nT} = resonant frequency in torsional vibration (Hz)

3.7 *Calculation of Damping Ratio*

The Resonant Response Method was used to calculate the damping ratio using the following equation (Drnevich, 1978):

$$D = \frac{100\%}{(A\ X\ MMF)} \tag{29}$$

Where:

A = 2(T_L + 0.405) and;

$$MMF = \frac{RCF\ RTO}{TCF\ INP} J(2\pi f_{nt})^2 \tag{30}$$

Where:

RCF = rotational calibration factor (rad/V),

TCF = torque calibration factor (N-m/V),

INP = input reading of torsional coil (V),

RTO = response or output reading of torsional coil (V),

J = total polar mass moment of inertia including the top platen and soil column (Kg-m2),

f_{nt} = resonant frequency of the system in the torsional direction.

3.8 Calculation of Shear Strain

The moduli and damping ration of soil depend upon the magnitude of the strain. For sinusoidal torsional excitation, the shear strain amplitude can be obtained using Drnevich's approach as follows:

$$\gamma = RCF\ RTO\ \frac{d}{3L} \tag{33}$$

Where:

RCF = Rotation calibration factor (rad/V_{rms})

RTO = Rotational transduce output (V_{rms})

d = diameter of specimen

L = Length of specimen

CHAPTER 4

MATERIAL SELECTION

4.1 Introduction

The purpose of this research is to ascertain the effects of mineral composition on the dynamic properties of sands. Every mineral has a particulate range of characteristics that distinguish it from other minerals. Many of these properties are physical, including its hardness, its density and the way it bends or breaks. There are multiple naturally occurring minerals throughout the world. It is common for soils, especially sand deposits, to contain particles from numerous sources and mineralogical compounds at various degrees. It is necessary to note that not all minerals are widespread. Most naturally occurring forms of minerals located in sands are quarzitic or silica-based sands, such as Ottawa sands which are used extensively in laboratory environments. The following sections will discuss how sands of different mineralogical backgrounds were selected for this research.

4.2 Mineral hardness and Mohs scale

Like, all substances, minerals have a wide range of physical properties, from their melting points to their ability to conduct heat. The focus of this research was based on the classification of minerals based on easily attainable physical properties.

The two (2) most useful properties for a scientist to differentiate between minerals is hardness and density (Farndon, 2006). Hardness can be established very easily in the field and gives an instant clue to a mineral’s identity. Friedrich Mohs first devised a system to measure the relative hardness of minerals in 1812. Consequently, it was named the Mohs Scale. He selected ten standard minerals and arranged them on a scale of 1 to 10, with each one slightly harder than the preceding one. The softest of the scale is talc with a score of 1. The hardest is diamond with a score of 10. All other minerals can be rated on this scale. Table 4.1 and Figure 4.1 show tabular and graphical representations of the Mohs Scale.

Table 4.1 Mohs Scale

Mineral	**Hardness (Mohs)**
Diamond	10
Corundum	9
Topaz	8
Quartz	7
Orthoclase	6
Apatite	5
Fluorite	4
Calcite	3
Gypsum	2
Talc	1

Figure 4.1 Graphical Representation of Mohs Scale (Obtained from www.shopic.com/education/gemstone-mohs-ranking)

The criteria for selecting sands for this research was performed as follows:

1. Sands selected had to represent the wide range of hardness established in the Mohs Scale. This was the most important selection criterion.
2. Sands had to be from naturally occurring environments.
3. Sands had to be available and accessible. During the research it was found that a lot of sands were exotic and not readily available. This was more of a constraint.

Based on the criteria described above, Table 4.2 shows the types of sand selected for this research. The following sections provide additional details.

Table 4.2 Types of Sand used for this research

Mineralogical Composition	**Mohs Scale**
Carbonate Sand	3
Silica Sand	7
Olivine Sand	7
Corundum Sand	9

4.3 <u>Carbonate Sand (Mohs = 3)</u>

A significant part of coast lines around the world are overlain by deposits of carbonate sands (sometimes they are referred to in literature as calcareous sands). Marine deposits exist in areas of the United States such as Florida, Hawaii, Puerto Rico and Guam Islands (Morioka, 1999). They may also exist in inland ancient marine environments, such as Pierre Shale North Dakota and Alabama (Demars and Chaney 1982).

Carbonate sands predominantly consist of skeletal remains of marine organisms and typically have high carbonate (C_aCO_3) content (Olgun, et.al., 2009). This carbonate content is usually found in the form of calcite or aragonite. Carbonate sands have unique features that distinguish them from other common sands (silica sands). Carbonate sands have a wide variety of particle types which can differ in nature, shape, and form, and exist in both cemented and uncemented states. Due to the diversity in particle characteristics, these sands are more susceptible to crushing than terrigenous sands. Table 4.3 shows some of the pertinent properties of carbonate sands.

Table 4.3 Properties of Carbonate Sands (from Farndon, 2006)

Grain Size	Varies from clay sized to gravel sized
Texture	Highly variable, from very fine grained, porcelain like to aggregate of large fossils.
Color	White, grey, cream plus red, brown, black
Mohs Hardness	3 (mainly from the calcite)
Composition	Skeletal remains; algae and microbes; foraminfera; corals; sponges; molluscs; echinoderms; arthropods; carbonate grains; aggregates; wood; pollen; cement (calcite, aragonite, dolomite)
Formation	Forms as carbonates form, mainly on the sea floor, either from skeletal remains of sea creatures or by the precipitation of calcite.
Notable locations	Ireland, England, Slovenia, Italy, South Africa, Sri Lanka, Thailand, China, Australia, New Zealand, USA (New Mexico, Kentucky, Texas, South Dakota, Indiana, New York, Puerto Rico, Guam)

Researchers such as Hyodo et al. 1996; Lo Presti et al. 1993; and Morioka 1999; have studied the behaviors of these sands, including dynamic behaviour, in the past. More research is needed to ascertain their dynamic properties especially under cyclic loading. (Olgun, et.al., 2009). Figure 4.2 shows a sample of the carbonate sand used in this research.

Figure 4.2 Carbonate Sand Used in Research

4.4 *<u>Silica Sand (Mohs = 7)</u>*

Silica sands or quarzitic sands as otherwise known in literature are widely distributed throughout the world. In fact, they are the second most common mineral found comprising more than 10% by mass of the Earth's crust (Florke, et.al, 2008). and is the most common type of naturally occurring sand there is (Berslien, 2012). Silica sands are mostly composed of silicon dioxide (SiO2) which is an oxide of silicon. It is most commonly found in nature as quartz (Iler, 1979). In many parts of the world, silica is the major constituent of sand. Table

Table 4.4 Properties of Silica Sand (from Fardon, 2006)

Color	Widely available but clear is most common, followed by cloudy or milky quartz, purple amethyst, pink agate, brown smoky quartz
Mohs Hardness	7
Cleavage	Poor
Crystal Habit	Widely variable but most common is hexagonal prisms
Specific Gravity	2.7
Notable locations	Second most common mineral in the world. It is widely available. Rock crystal: Switzerland, Germany, Austria, South Africa, Brazil, USA (Arkansas), Canada (Ontario) Smoky quartz: Scotland, Switzerland, Brazil, USA (Colorado) Amethyst: Hungary, Russia, Zambia, South Africa, Mexico, Brazil, Uruguay, Canada, USA (Maine, Pennsylvania)

Silica is one of the most complex and most abundant families of materials, existing as a compound of several minerals and as synthetic product. Notable examples include fused quartz, fumed silica, silica gel, and aerogels. It is used in structural materials, microelectronics (as an electrical insulator), and as components in the food and pharmaceutical industries.

Due to its abundance, researchers such as Seed et al. (1966), Iwasaki, T., and Tatsuoka, F. (1977), among others, have used silica-based sands in numerous experiments. Of note, Ottawa sand, a natural silica sand, has been popularly used in geotechnical engineering applications for a very long time. Figure 4.3 shows a sample of silica sand used in this research.

Figure 4.3 Silica Sand Used in Research

4.5 <u>Olivine Sand (Mohs = 7)</u>

Olivines are minerals rich in iron and magnesium that for at high temperatures. They are named for their olive-green color. Olivine is common in mafic rocks such as basalt and gabbro, while ultramafic rocks such as peridotite and dunite are almost pure olivine. Peridotites are what the Earth's mantle is made from, therefore olivines are among Earth's most common minerals (Farndon, 2006). Table 4.5 shows some of the more pertinent properties of olivine sand.

Table 4.5 Properties of Olivine Sand (from Fardon, 2006)

Color	Olive green; redder when weathered
Mohs Hardness	7
Cleavage	Indistinct
Crystal Habit	Short prisms
Specific Gravity	3.2
Notable locations	Norway, Germany, Italy, Egypt, Burma, Ireland, Azores Islands, USA (Arizona, Wyoming)

Figure 4.4 shows a sample of olivine sand used in this research.

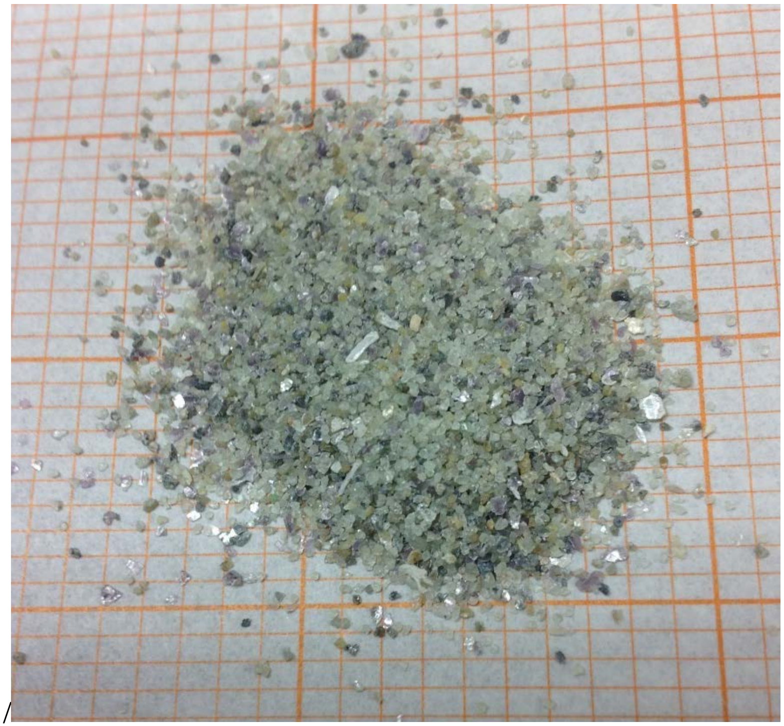

Figure 4.4 Olivine Sand Used for this Research

4.6 Corundum Sand (Mohs = 9)

Corundum, sometimes referred to as Emery, is one of the world's hardest minerals. Powdered corundum is used to make sandpaper and blocks of it are used for knife sharpening. When exposed to the atmosphere it erodes and crumbles into a powder called black sand which derives its color from traces or iron. (Ferndon, 2008). Table 4.6 shows some of the more pertinent properties of olivine sand.

Table 4.6 Properties of Olivine Sand (from Farndon, 2006)

Color	It can vary from brown to brownish white to black
Mohs Hardness	9
Cleavage	None but splits basally and in two other ways
Crystal Habit	Typically, double pyramid hexagons or flat hexagons. Also occurs as grains and masses.

Specific Gravity	4.0
Notable locations	Myanmar, Thailand, Sri Lanka, multiple locations in Africa, USA (North Carolina, Montana)

Figure 4-5 shows a sample of Corundum Sand used in this research.

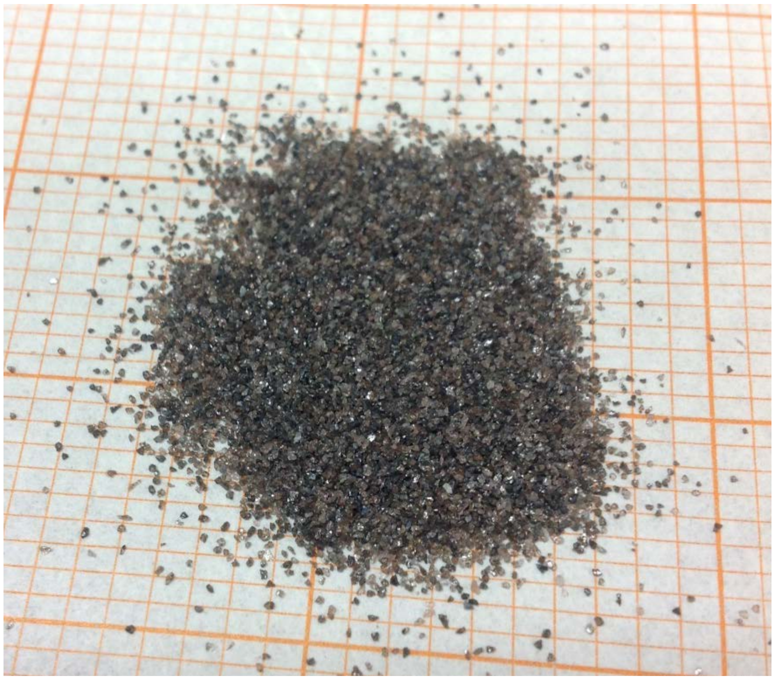

Figure 4.5 Corundum Sand Used for this Research

4.7 Index Properties of Sands used in this study

Gradations can play a very important role on how a sand behaves. Since the purpose of this research is to determine if the mineral composition of each sand influences its respective dynamic properties, it is important that all sands have similar gradations. The distribution of particles has a direct effect on very particular index properties such as: maximum void ratio (e_{max}), minimum void ration (e_{min}), density (ρ), relative density (Dr), among many others. Based on the amount of sand we had to work with, it was decided that the sands will be engineered with three (3) different uniformity coefficients (C_u) and one (1) mean particle size (D_{50}). Therefore, each type of sand studied will share three (3) similar gradations. Index properties will then be established from each gradation and each sand. Gradations were performed consisted with the requirements of ASTM D422-63. Figure 4.6 shows the average gradation for the sands tested. Each curve on the graph depicts the average of all curves for that respective uniformity coefficient.

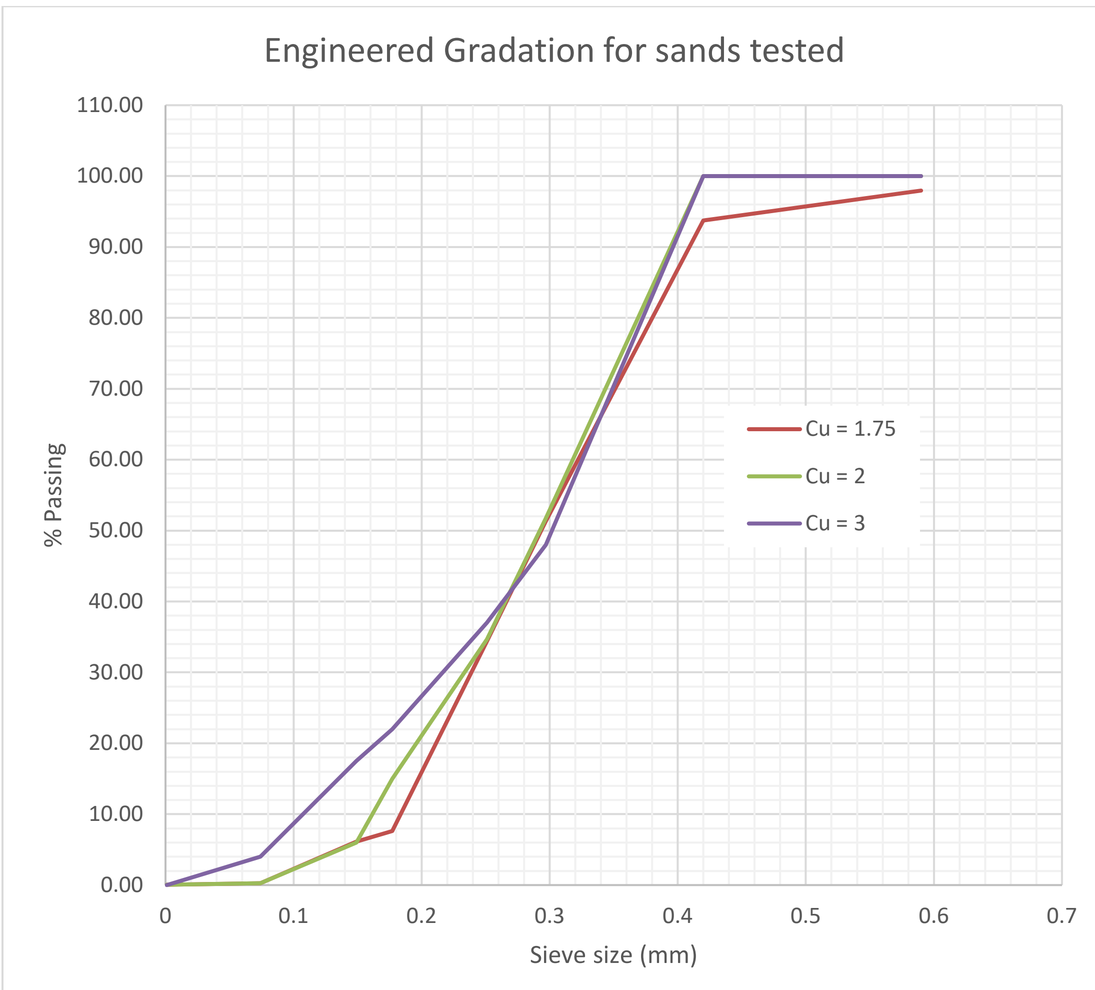

Figure 4.6 Engineered Gradations for Sands Tested

For each sand gradation the following index properties were calculated:

- Specific Gravity, G_s = obtained from literature (Farndon, 2006)
- Uniformity Coefficient, $C_u = \frac{D_{60}}{D_{10}}$

$$C_u = \frac{D_{60}}{D_{10}} \tag{31}$$

Where:

D_{60} = Particle size corresponding to 60% percentile

D_{10} = Particle size corresponding to 10% percentile

- Mean Particle Size, D_{50} = Particle size corresponding to 50% percentile
- Maximum void ratio, e_{max} = Obtained from ASTM D4254.
- Minimum void ratio, e_{min} = Consistent with the requirement of ASTM D4253, a special mold was used as specified in Figure 3 of the standard.
- Angle of Friction, φ' = Obtained from ASTM D3080. Direct shear tests were performed to determine the internal friction angles for the different sands. Displacement controlled direct shear tests with a 63.5 mm square shear box were performed. All tests were carried out at a horizontal displacement rate of 2 mm/min. Specimens were prepared using air pluviation of dry sand which was carefully poured through a funnel and then carefully tamped.

Table 4.7 shows a summary of Index Properties of all sands tested.

Table 4.7 Index Properties for Sands Tested

	G_s (1)	C_u	D_{50}	e_{max} (2)	e_{min} (3)	φ' (4)
Carbonate Sand	2.67	1.74	0.29	1.19	0.75	44
		1.97	0.29	1.13	0.75	43.5
		3.08	0.33	1.05	0.73	42.8
Silica Sand	2.65	1.75	0.29	0.98	0.59	32.2
		1.98	0.30	0.96	0.56	32.1
		3.03	0.31	0.93	0.54	32.1
Olivine Sand	3.30	1.75	0.29	0.99	0.60	32
		1.96	0.29	0.97	0.59	32.1
		3.00	0.31	0.95	0.57	31.8
Corundum Sand	3.70	1.78	0.30	1.05	0.66	32.6
		1.97	0.29	1.03	0.65	32.8
		3.0	0.31	1.00	0.62	32.5

1. From Literature (Farndon, 2006)
2. From ASTM D4254
3. From ASTM D4253
4. From ASTM D3080

CHAPTER 5

DYNAMIC TESTING PROGRAM

5.1 Introduction

The properties of soils under dynamic loading, mainly shear modulus, G, and damping ratio, D, need to be well understood in order to properly assess the characteristics of the site in question. Due to its nature, soils do not behave in an elastic manner, nonetheless, because of constraints in the way engineers test materials, they need to be tested in accordance with concepts of elasticity. The main objective of this research is to study the effects of mineral composition on the dynamic properties of dry sands using the resonant column test. The resonant column testing technique was accepted by ASTM as a standard testing method in 1978. This chapter describes in detail the test equipment used in this research.

5.2 Testing Apparatus

The Drnevich resonant column apparatus located in the Soil Dynamics Laboratory at the University of Maryland (UMD) is a nondestructive testing equipment. The apparatus consists mainly of a chamber having a lower (static) and a top platen (active platen). A column of soil, in our case a combination of dry sands, is placed between the aforementioned plates. The chamber has the means to provide water and compressed air in order to subject the column of soil to the desired conditions (in situ, engineered, etc.).

A magnetic plate supporting torsional and longitudinal accelerometers, in association with fixed coils connected with an electrical circuit, provides for torsional vibration of the soil column. A centrally placed coil on the torsional magnet plate provides for torsional vibration of the soil column and a length measuring transducer (LVDT) in the upper platen serves to give constant readings of the length changes of the soil column.

The excitation system of the resonant column device is an electromagnetic system comprising of a permanent magnet and coil that can move in the gap between the North and South Poles of the permanent magnet (Drnevich, 1975). The Drnevich resonant column apparatus has two excitation modes: longitudinal and torsional. This research was solely based on torsional mode as it is adequate to calculate the necessary dynamic properties. For the torsional mode, the assembly comprises of four rectangular coils and horseshoe-shaped magnets. The coils are connected to the brackets and the magnets to the top active platen. When activated a magnetic field is generated, which in turn develops torsional forces on the top of the soil column.

During each test, a power amplifier amplifies signals coming from a wave oscillator. The amplified signals enter a power resistor located in the control box and then continuer to the drive coils located in the active platen. The pick-up system is comprised of a piezoelectric meter (Columbia Model 200-1-H) placed in the active-end platen. The transducer is mounted at 0.0316 meters from the axes of rotation. Information coming back from these devices is read by a digital multimeter and an oscilloscope. The digital multimeter records or displays the resulting acceleration coming from the soil sample. This information is later converted to shear strains. On the other hand, the oscilloscope monitors the frequency response of the soil sample. This serves as a visual representation of when a sample reaches resonance.

In summary, soil specimens vibrate torsionally under a sinusoidal excitation by adjusting the frequency of the signal generator until a vertical ellipse is observed on the oscilloscope. The shear modulus and damping ratio are then calculated using the measured resonant frequency and response.

5.3 *Sample Preparation*

As specified in an earlier section, four (4) types of sand were used in this research. Details of the sands can be seen in Chapter 4. Three (3) engineered gradations were created with varying Coefficients of Uniformity (C_u) from 1.75 to 3. D_{50} was maintained constant at 0.29 for all gradations in order to minimize the number of variables. The following sets of instructions were performed in order to prepare the sample.

5.3.1 Preliminary Sample Setup

The purpose of this part is to ensure the correct construction of the sample. This researcher followed methodology suggested in Drnevich, et al., (1978). Since we are dealing with dry cohesionless material, extra care is needed in order to obtain specimens that are uniform, stable and can provide trustworthy results:

1. A waterproof membrane was placed onto the 3.57 mm base and safely attached with two O-rings to ensure water not entering the sample.

2. Split vacuum mold was placed onto the base and safely attached to avoid gaps. Top of the membrane was rolled onto to the top part of the mold (see Figure 5.1).

Figure 5.1 Split Mold Assembly with Membrane Attached

3. A vacuum connection was attached to the sample through the supplied connection on the split mold.
4. A predetermined amount of sand for each gradation and for each type of sand was weighed and divided into four equal parts. The amount needed to fully fill the inside of the vacuum mold was calculated by a trial and error method performed before each test.

5. Using the dry pluviation technique, sand was poured into the mold using a graduated funnel. The height of drop was equal for all four layers. This method best models the natural deposition in aeolian environments.
6. After each layer was poured, the dry sand was tamped with a wooden rod up to a specified thickness. In most occasions, forty (40) taps per layer was just enough the obtain the necessary thickness.
7. After obtaining the necessary height, the top porous stone with the razor blades was placed on top of the sand column and the membrane was rolled onto the top cap with porous stone and secured with two O-rings. A bulb leveler was used to guarantee a leveled surface (see Figure 5.2).

Figure 5.2 Bulb leveler on top of sand column during preparation of the sample

8. Vacuum supply was switched from the side of the mold to the bottom of the RC apparatus through a supplied connection.
9. The split top collar was placed on top of the assembly. The collar screws were tightened accordingly as to provide a leveled and stable array to place the top platen on. A level check was performed again (see Figure 5.3).

Figure 5.3 Split mold assembly with split top collar

5.3.2 Placement of torsional excitation system

The torsional driving mechanism for the Drnevich Resonant Column Apparatus consists of four rectangular coils and horseshoe-shaped magnets. The coils are connected to the support brackets and the magnets are connected to the top active platen. The assembly of the top platen driving mechanism and other peripherals is as follows

5.3.3 Split mold disassembly and pressurization of chamber

Before disassembling the split mold and pressurizing the chamber the following steps were taken:

1. The split top collar and split mold were carefully removed (see Figure 5.4 and 5.5)

Figure 5.4 Removal of Split Top Collar

Figure 5.5 Removal of Split Mold

2. After removing the split molds, specimen measurements of length and width were made using a digital caliper. Extra care was taken while taken measurements as to not disrupt the sand column (see Figure 5.6).

Figure 5.6 Sand Column before testing

3. A reinspection of the torsional drive coils at this time was performed to verify proper clearance between the magnets and the coils. If not, the procedure described earlier to realign them was followed.

4. Wires were brought to the top of the apparatus and draped over the support bracket of the taring spring. The wires were positioned in such a manner as to not interfere with the movement of the top platen system. In addition, the red wires coming from the accelerometers onto the top platen system were

realigned so they wouldn't touch anything for at least 10 cm (4 inches) from the top platen system.

5. The bottom O ring groove of the apparatus was dutifully cleaned of any sand residue or debris and layer of high vacuum grease was applied to ensure proper seal. The cast acrylic tube was gently lowered into place and all electrical connection to the chamber lid were made.
6. Like the bottom O ring, the chamber lids top O ring was cleaned, greased clean and seated properly on top of the chamber. The chamber rods were securely fastened.
7. The apparatus water valve was slowly opened, and the chamber was filled up to the water level mark. Extra care was taken to ensure the coils never got wet during this process.
8. The air pressure supply line was connected to the lid. With the help of a Triflex panel and an air pressure regulator, the desired confinement pressure was slowly applied to the chamber.
9. When pressurization happened, the test could commence.

5.3.4 <u>Initiation of Test</u>

After performing the numerous steps already described, the following needs to take place:

1. The initial reading of the LVDT was recorded.
2. The sample was torsionally excited with sinusoidal waves in small increments.

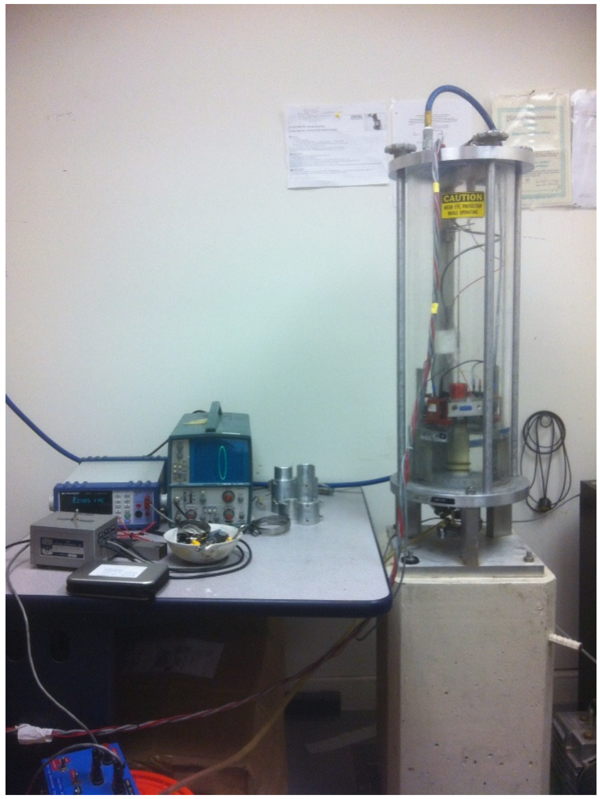

Figure 5.7 RC setup after test commenced

3. The resonance condition of the system at each strain amplitude was established by adjusting the frequency of the excitation until a Lissajous figure was observed as shown in Figure 5.8. A Lissajous figure is a vertical ellipse that corresponds to a 90-degree phase angle between the acceleration response and the excitation. The resonant frequency of the system was measured with a digital frequency counter and the excitation and response accelerations were measured by a digital multimeter in millivolt (rms).

Figure 5.8 Close up of Lissajous figure

CHAPTER 6

ANALYSIS AND RESULTS

6.1 Introduction

A total of 72 different resonant column tests were performed with various uniformity coefficients, confining pressures and, more importantly, different mineral compositions. For this discussion results from tests pertaining to a uniformity coefficient, C_u, of 1.75 are discussed. Information for the other tests are shown in Appendix A and B of this document.

6.2 Drnevich Resonant Column Testing Results

Resonant column tests were performed on dry sand samples with various uniformity coefficients, confining pressures and, more importantly, different mineral compositions. Two (2) series of tests were performed to account for repeatability. Main results, specifically maximum shear modulus (G_{max}) and minimum damping ratio (D_{min}), from these tests are shown in Tables 6.1 through 6.4.

The nominal C_u = 1.75 series corresponds to samples engineered to have a uniformity coefficient like the target. Tables 6.1 through 6.4 shows the actual C_u values with for all sand gradations tested.

Table 6.1 Main Results for Carbonate Sand Series

Carbonate Sand						
C_u	D_{50}	Series	σ' con		G_{max}	D_{min}
			psi	kPa	MPa	%
1.74	0.29	1	10	69	138.25	1.05
			15	103.4	164.14	0.55
			20	137.9	181.89	0.42
		2	10	69	137.47	1.05
			15	103.4	163.97	0.61
			20	137.9	181.94	0.50
1.97	0.29	1	10	69	139.36	1.05
			15	103.4	165.11	0.67
			20	137.9	183.25	0.48
		2	10	69	139.93	1.04
			15	103.4	166.01	0.63
			20	137.9	182.98	0.47
3.08	0.33	1	10	69	133.58	1.16
			15	103.4	159.09	0.63
			20	137.9	176.89	0.51
		2	10	69	134.58	1.08
			15	103.4	158.09	0.62
			20	137.9	176.89	0.50

Table 6.2 Main Results for Olivine Sand Series

Olivine Sand						
C_u	D_{50}	Series	σ' con		G_{max}	D_{min}
			psi	kPa	MPa	%
1.75	0.29	1	10	69	98.94	0.70
			15	103.4	121.89	0.74
			20	137.9	145.55	0.48
		2	10	69	98.94	0.70
			15	103.4	121.89	0.74
			20	137.9	145.55	0.48
0.96	0.29	1	10	69	98.91	0.81
			15	103.4	123.62	0.90
			20	137.9	146.86	0.58
		2	10	69	101.38	0.87
			15	103.4	123.05	0.89
			20	137.9	146.44	0.57
3	0.31	1	10	69	95.87	0.80
			15	103.4	116.09	0.93
			20	137.9	140.38	0.59
		2	10	69	93.87	0.84
			15	103.4	118.09	0.94
			20	137.9	139.38	0.60

Table 6.3 Main Results for Silica Sand

Silica Sand						
C_u	**D_{50}**	**Series**	**σ' con**		**G_{max}**	**D_{min}**
			psi	**kPa**	**MPa**	**%**
1.75	0.29	1	10	69	100.88	1.37
			15	103.4	122.29	1.18
			20	137.9	147.88	0.79
		2	10	69	102.28	1.55
			15	103.4	122.16	1.37
			20	137.9	147.65	0.96
1.98	0.3	1	10	69	101.32	1.68
			15	103.4	123.74	1.44
			20	137.9	148.08	0.94
		2	10	69	103.32	1.67
			15	103.4	122.71	1.39
			20	137.9	150.07	0.92
3.03	0.31	1	10	69	101.32	1.58
			15	103.4	119.85	1.41
			20	137.9	142.71	1.03
		2	10	69	102.32	1.54
			15	103.4	119.85	1.33
			20	137.9	141.71	0.89

Table 6.4 Main Results for Corundum Sand Series

Corundum Sand						
C_u	D_{50}	Series	σ' con		G_{max}	D_{min}
			psi	kPa	MPa	%
1.78	0.3	1	10	69	95.50	0.78
			15	103.4	111.72	0.94
			20	137.9	150.50	0.34
		2	10	69	95.50	0.78
			15	103.4	111.72	0.94
			20	137.9	150.50	0.34
1.97	0.29	1	10	69	98.17	0.95
			15	103.4	113.10	1.16
			20	137.9	152.84	0.39
		2	10	69	95.99	0.96
			15	103.4	113.29	1.17
			20	137.9	152.26	0.40
3	0.31	1	10	69	90.38	1.01
			15	103.4	106.76	1.07
			20	137.9	144.53	0.40
		2	10	69	91.38	0.89
			15	103.4	105.76	1.09
			20	137.9	144.53	0.41

6.3 Repeatability

In order to assess the accuracy of the results, maximum shear modulus (G_{max}) and minimum damping ratios (D_{min}) results where compared between respective series of tests. Based on the overall results shown, as shown on Tables 6.1 through 6.4, there is a good agreement between both series of tests for each of the gradations as all samples fall within a 95% mean interval level (Varde, et.al, 1996). Figure 6.1 and 6.2 show sample results for the Silica sand series. These results show that the obtained data is within the acceptable confidence level and is consistent.

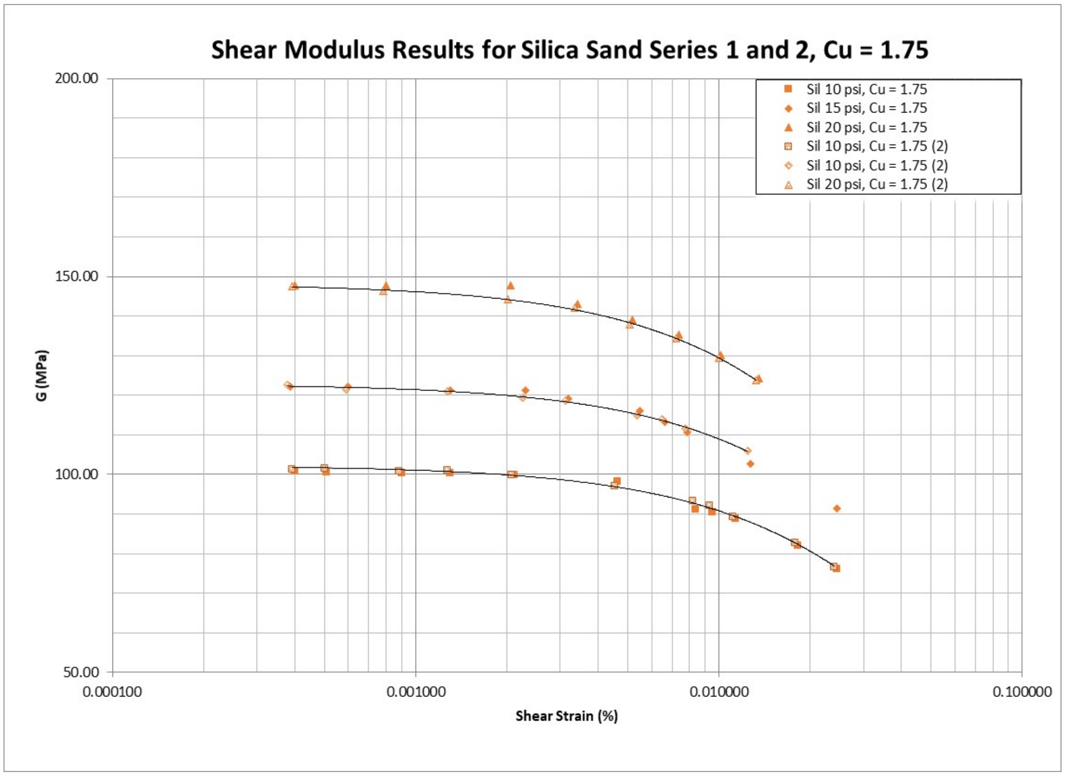

Figure 6.1 Shear Modulus Results for Silica Sand Series 1 and 2, C_u = 1.75

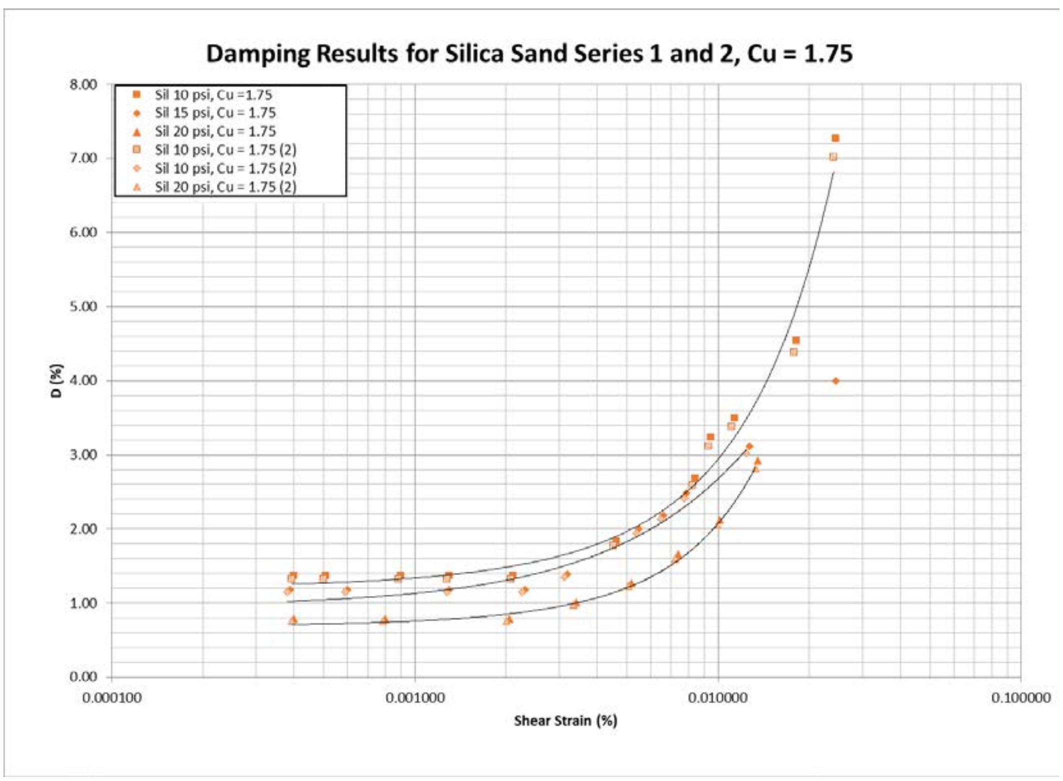

Figure 6.2 Damping Results for Silica Sand Series 1 and 2, C_u = 1.75

6.4 Shear Modulus Results

As previously mentioned, the following sections will discuss the results of sand gradations corresponding to a uniformity coefficient, C_u , of 1.75. The results for sands corresponding to C_u of 2 and 3 follow the same trends. Appendix A shows applicable graphs and charts.

The effects of confinement, mineral composition, and its effects on site response are further discussed.

6.4.1 Effects of Confinement on Shear Modulus Results

As discussed in Section 5.3, all sands were tested under three confinement pressures, 10 psi (69 kPa), 15 psi (103.4 kPa), and 20 psi (137.0 kPa). Figures 6.3 through 6.6 show the shear modulus results for all sands tested. It is clearly seen that as the confinement pressure is increased, the shear modulus increases proportionally. This behavior is observed in all sands tested and is consistent with the conclusions arrived by Hardin and Richart (1963) and Vucetic and Dobry (1991). In general, the authors confirmed that variations in confining pressure were found to have the greatest effect on shear modulus.

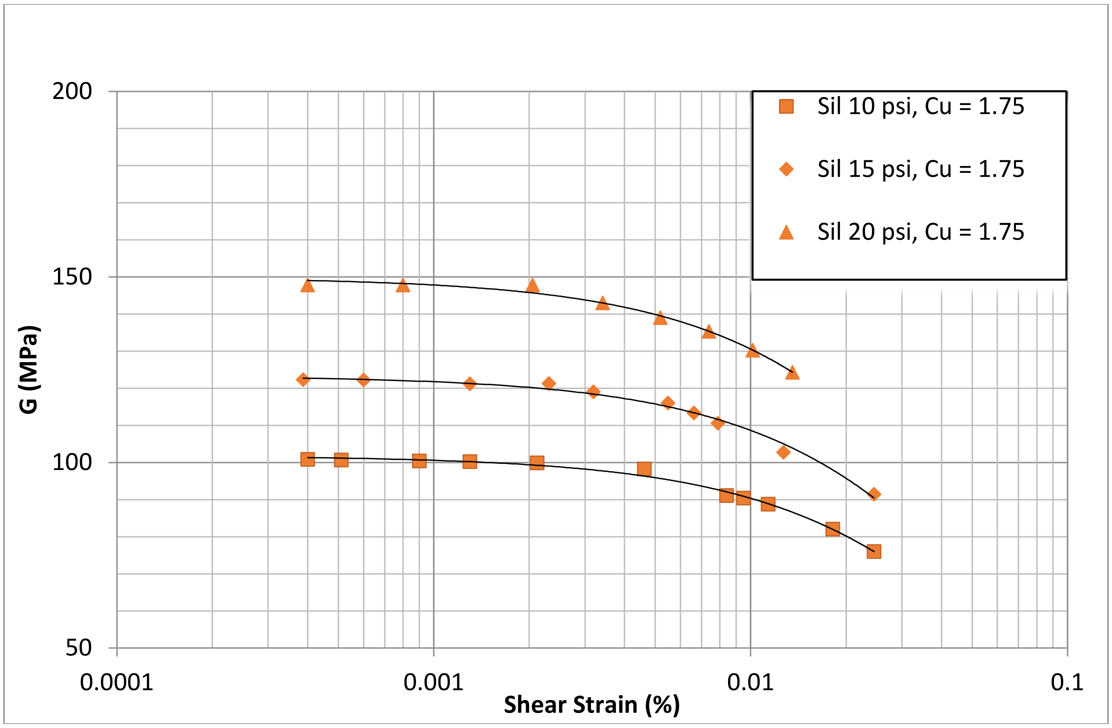

Figure 6.3 Effects on Confinement on Shear Modulus (G) for Silica Sand

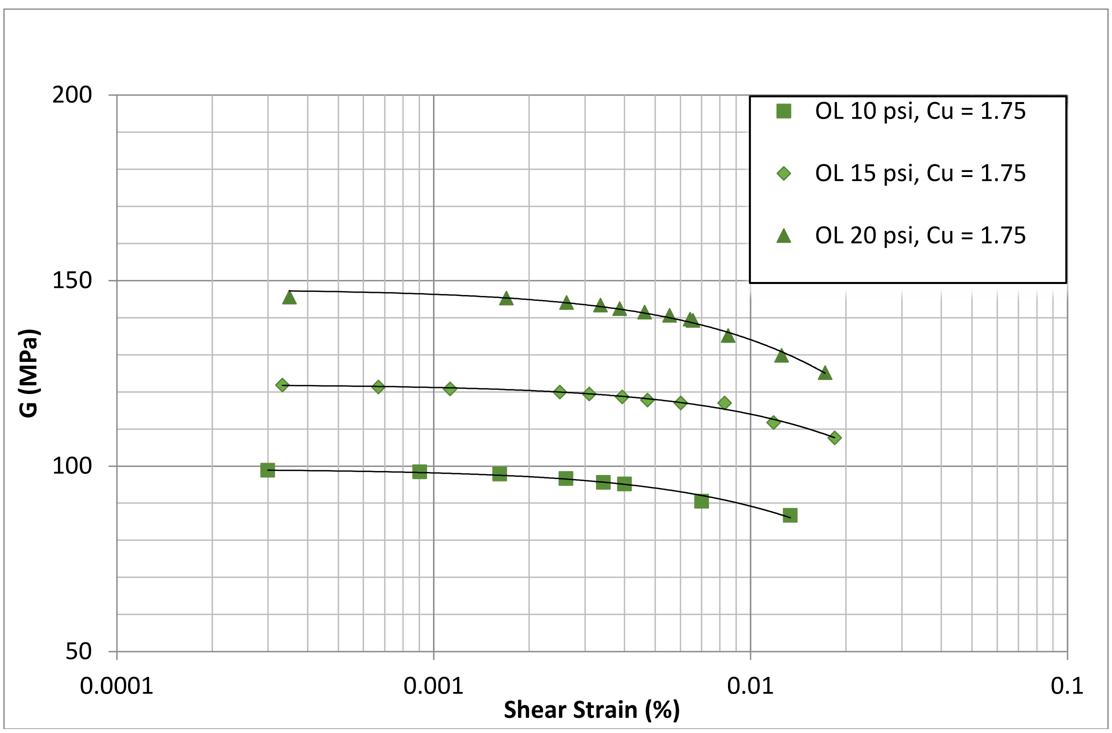

Figure 6.4 Effects on Confinement on Shear Modulus (G) for Olivine Sand

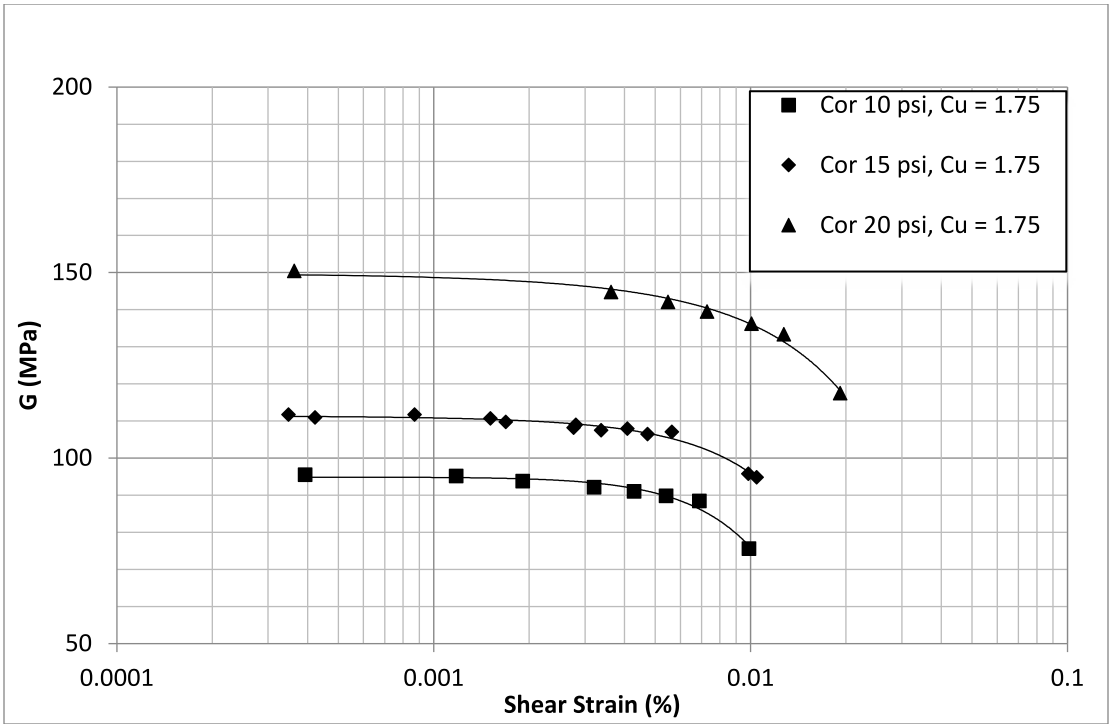

Figure 6.5 Effects of Confinement on Shear Modulus (G) on Corundum Sand

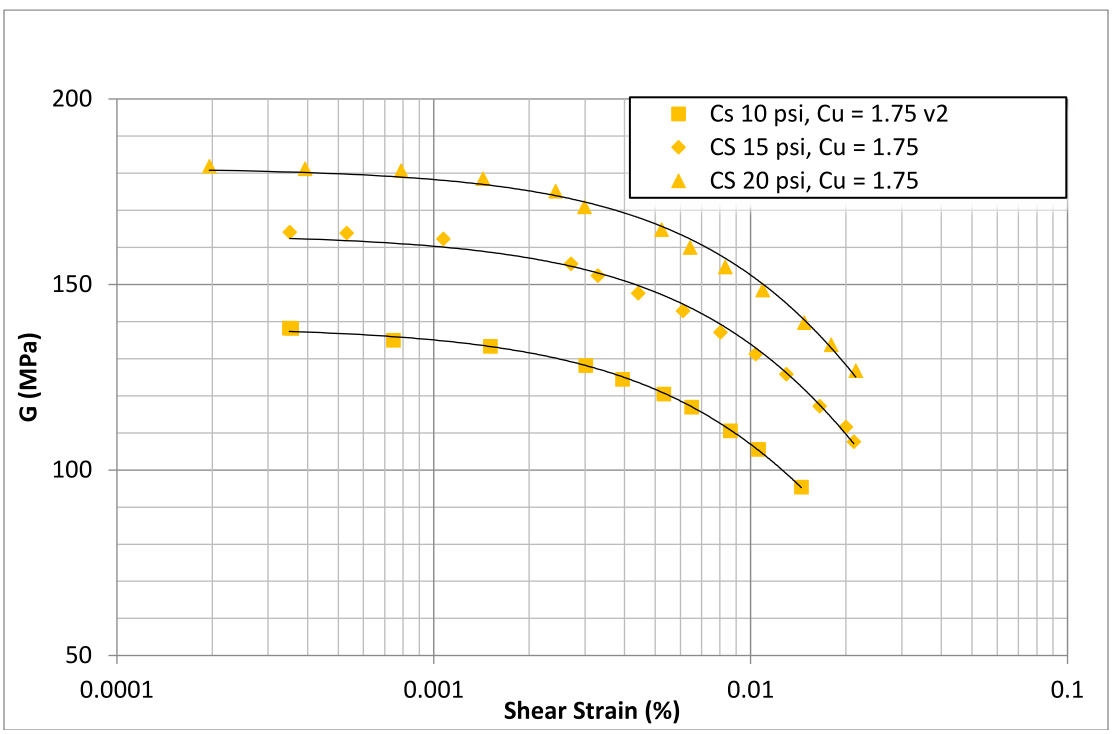

Figure 6.6 Effects of Confinement on Shear Modulus (G) on Carbonate Sand

As seen in Figure 6.6, the carbonate sands tested had higher shear modulus values when compared to the other sands. Carbonate sands have a large void ratio due to the intra-granular voids within the particles and are well known for being more compressible than silica-based sands. Some researchers have found that sands that have greater tendency for contraction, like carbonate sands, can produce lower values of shear modulus (Catano Arango, 2006). Therefore, it was initially thought that the compressive nature of carbonate sands would result in a less stiff soil when compared to the other sands. This research has found that the carbonate sand results are consistent with other researchers such as LaVielle, T.H. et al. (2008). In all cases, studies that have compared the cyclic strength of carbonate sands to silica or quarzitic sands have found these sands to be stronger (Hyodo et al. 1996; Hyodo et al. 1998; Kaggwa et al. 1988; Morioka and Nicholson 1999). Authors have attributed this to the highly angular nature of calcareous sand particles. This angularity can create a more stable interlocking soil fabric, that can create a stiffer soil skeleton at low strains (LaVielle, T.H. et al (2008).

6.4.2 Effects of the Mineral Composition on Shear Modulus Results

Figures 6.7 through 6.9 compares the shear modulus results for all sands tested per confinement pressure. It is clearly seen that as the confinement pressure is increased, the shear modulus increases proportionally.

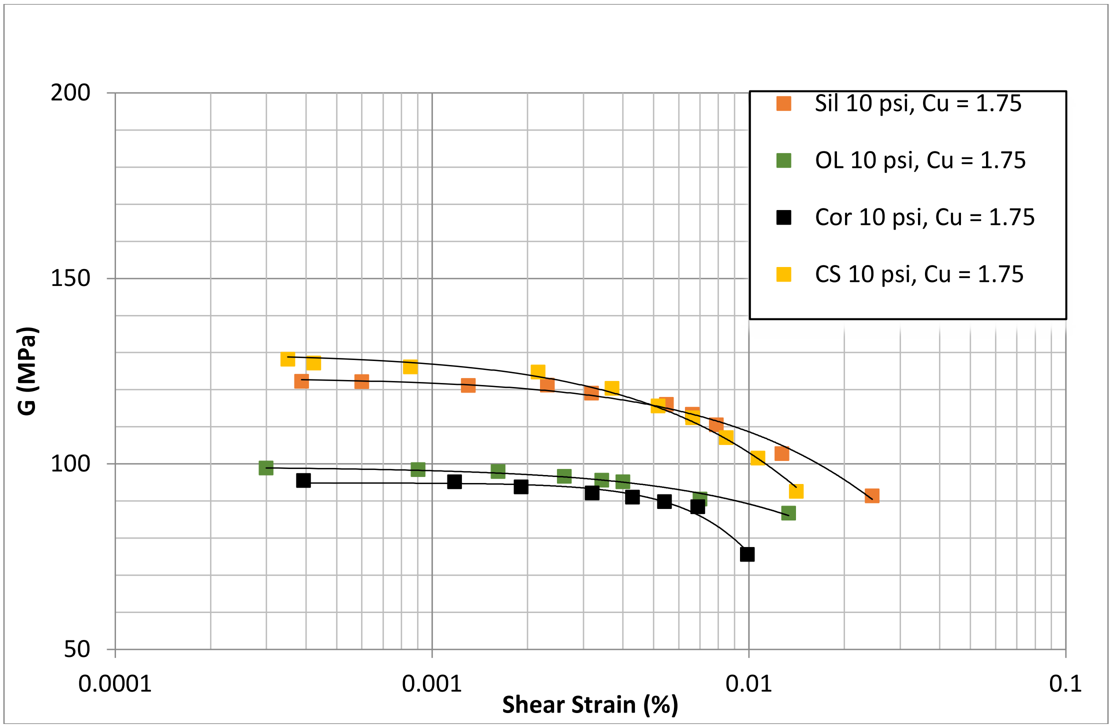

Figure 6. 7 Effects of Mineral Composition on G at Confinement Pressure of 10 psi (69 kPa)

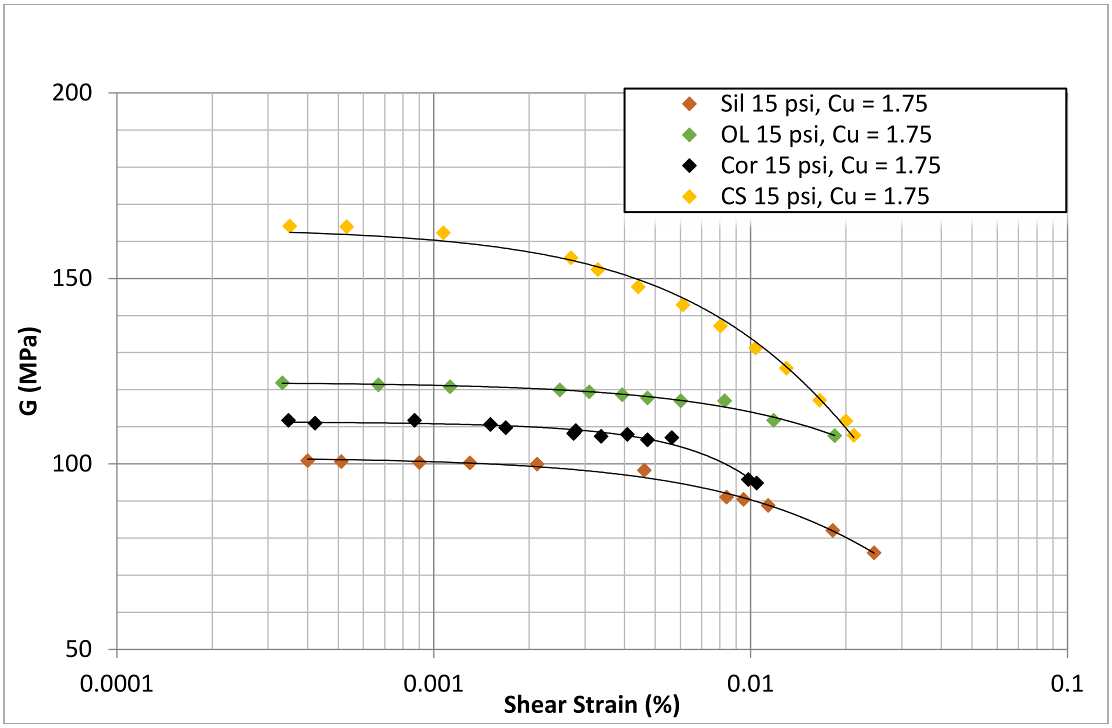

Figure 6.8 Effects of the Mineral Composition on G at a Confinement Pressure of 15 psi (103.4 kPa)

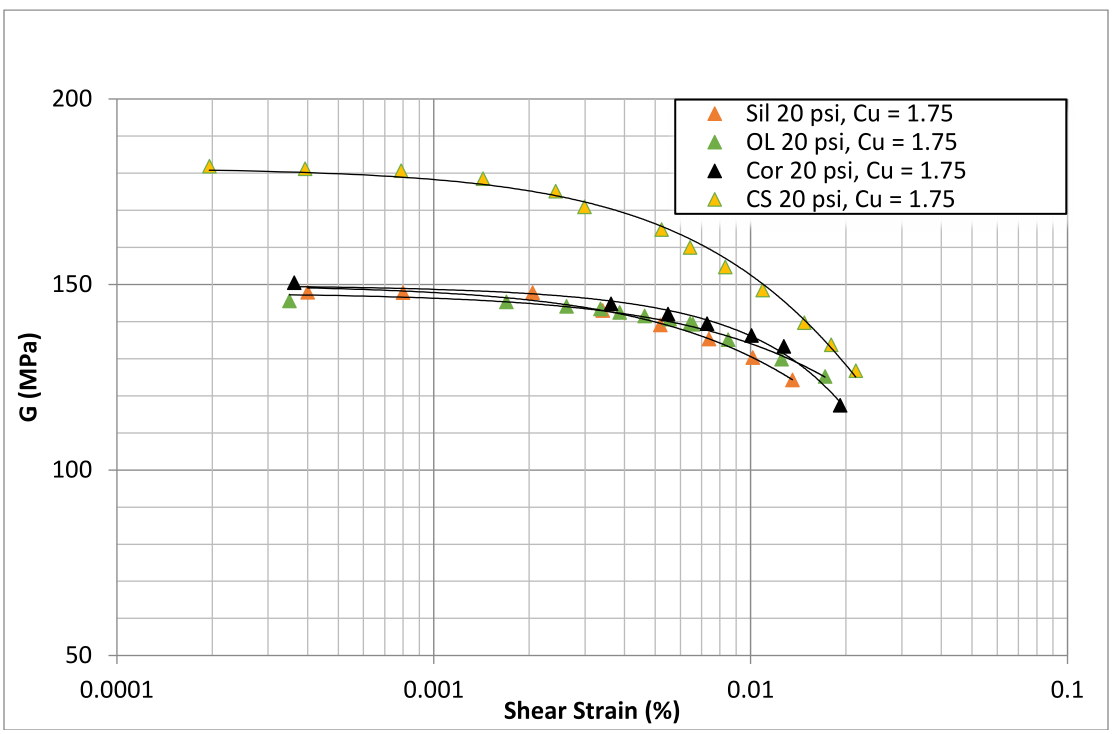

Figure 6.9 Effects of the Mineral Composition on Shear Modulus at Confinement Pressure of 20 psi (137.0 kPa)

In addition, it can be appreciated the range of shear modulus values among all sands tested. In order to quantify this difference, Figure 6.10 shows the maximum shear modulus (G_{max}) for the case related to a confining pressure of 20 psi (137.0 kPa). G_{max} was calculated at a cyclic strain (γ) corresponding to approximately 0.0003 %.

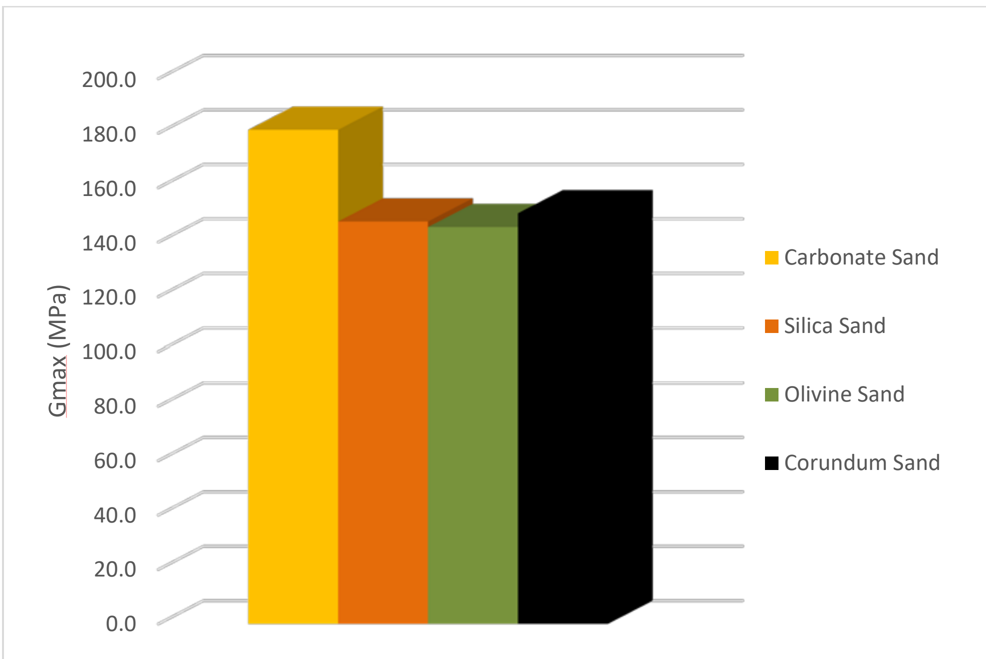

Figure 6.10 Maximum Shear Modulus (G_{max}) for Sands Tested at a Confinement Pressure of 20 psi (137.0 kPa)

Table 6.5 shows that the percentage of difference between the sands tested when compared to silica sand. Silica Sand was used as the basis for reference because researchers such as Seed et al. (1966), Iwasaki, T., and Tatsuoka, F. (1977), among others, have used silica-based sands in numerous experiments. Of note, Ottawa sand, a natural silica sand, has been popularly used in geotechnical engineering applications for a very long time. It can be shown that, as discussed in section 6.4.1, the carbonate sands tested produced the highest G_{max} value with a percentage of difference of 22.8 %.

Table 6.5 Percentage of Difference Against Silica Sand

	G_{max} (MPa)	**% diff**
Carbonate Sand	**181.2**	**22.8%**
Silica Sand	**147.6**	**0.0%**
Olivine Sand	**145.6**	**-1.4%**
Corundum Sand	**150.6**	**2.0%**

6.4.3 <u>*Effects of Mineral Composition in Natural Frequency*</u>

In order to better understand the importance of shear modulus, G, in real life scenarios, an analysis was made to ascertain its effects on site characterization parameters, mainly on the natural frequency of a soil deposit. Consider a typical structure overlying a soil deposit of depth, H (see figure

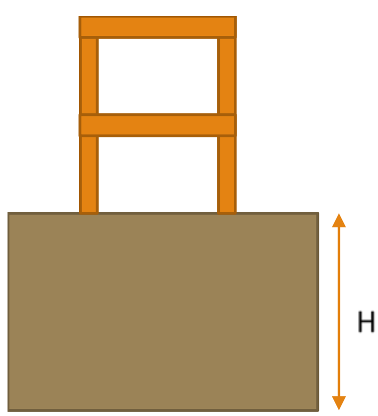

Figure 6.11 Schematic of Typical Structure Overlying a Soil Deposit

The natural frequency, f_n, of a soil deposit can be calculated as follows:

$$f_n = \frac{V_s}{4H} \qquad (32)$$

Where:

Vs = $\sqrt{\frac{G}{p}}$ = Shear Wave Velocity

G = Shear Modulus

ρ = soil density

H = Thickness of Soil Deposit

In general practice, the average seismic shear-wave velocity, V_s, from the surface to a depth of 30 meters (100 feet) is defined as V_{s30} (Borcherdt, 2012). This is commonly used as a parameter to characterize site response for simplified earthquake resistant design. It was initially introduced by Borcherdt (1992) to provide unambiguous definitions of site classes and site coefficients for the estimation of site-dependent response spectra for use in the 1994 edition of the "Recommended National (US) Earthquake Hazard Reduction Program (NEHRP) Building Code Provisions". It is based on correlations derived from extensive borehole logging and comparative ground-motion measurement programs in California. This parameter is commonly used in simplified building codes, ground motion predicting equations (GMPE), ShakeMap, and seismic hazard mapping.

Based on the maximum shear modulus values calculated in Table 6.5 and Equation 34, natural frequencies were calculated for hypothetical soil deposits of 10 m and 30 m, respectively. Figure 6.12 shows the natural frequency results for all sands tested.

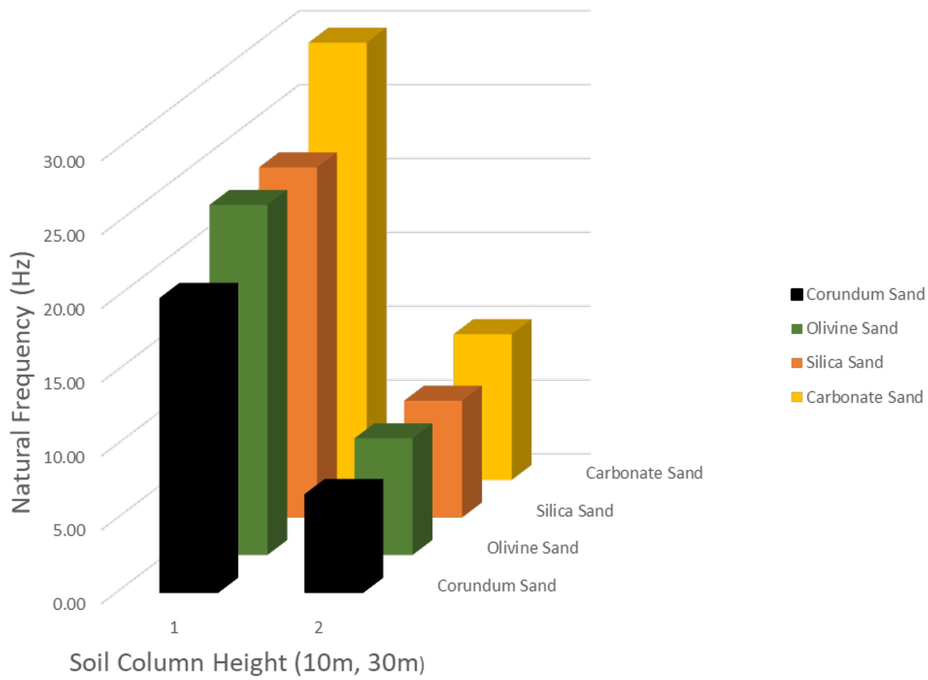

Figure 6.12 Natural Frequencies for All Sands Tested at 10 m and 30 m, respectively

As previously discussed, that natural frequency values can vary among different sands with the same gradation. It can be noted that the results follow similar trends already discussed in previous section, mainly carbonate sand produce higher results. This is because, as stated in Equation 34, the natural frequency, f_n, is directly proportional to shear modulus, G.

Table 6.6 Percentage of Difference for Natural Frequencies

	Fn (Hz)	**% diff**
Silica Sand	21.4	0.0%
Olivine Sand	23.7	10.8%
Corundum Sand	19.9	6.8%
Carbonate Sand	29.6	38.4%

Table 6.6 shows that the percentage of difference between the sands tested when compared to silica sand. Silica Sand was also used as the basis for reference. It can be shown that, as discussed in section 6.4.1, the carbonate sands tested produced the highest natural frequency value with a percentage of difference of 38.4 %.

6.4.4 Normalized Shear Modulus Comparison with Current Design Curve.

As discussed in subsection 2.5, the modulus degradation curves created by Vucetic and Dobry (1991) are commonly used as design curves in typical geotechnical applications. In order to better understand how the results, correlate with the typical design curve, normalized shear modulus values, G/G_{max}, were calculated for all sands. When the G values are normalized, the effects of confining pressure are considerably reduced, and the effects of degradation can be better observed. The reference value of G_{max} was obtained at approximately 0.0003 for all sands. Figures 6.13 show the G/G_{max} values for all sands plotted against the design curve.

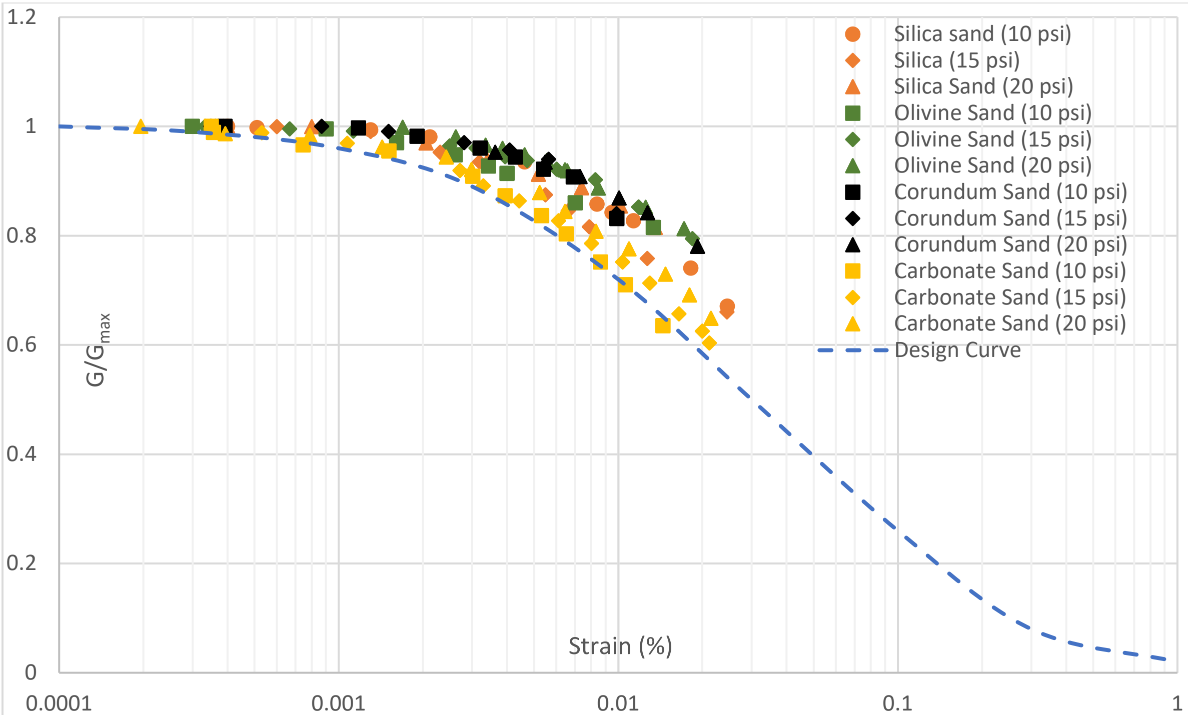

Figure 6.13 Normalized Shear Modulus Comparison with Design Curve

Figure 6.13 shows that all sands follow typical degradation trends. As strains increase, G/ G_{max} decrease. In addition, it can be shown that non-linearity increases as strain increases for all sands. This is consistent with Vucetic and Dobry (1991) who stated that cohesionless nonplastic soils, like gravels and sands are the most nonlinear, as they start to behave nonlinearly at the smallest strain levels. Figure 6.13 also shows the difference between the design curve and results obtained. This shows the importance of assessing the dynamic properties of soil samples as they can be higher than the design curve values. Figure 6.14 and Table 6.7 provides quantifiable data related to the difference between the values obtained and the design curve.

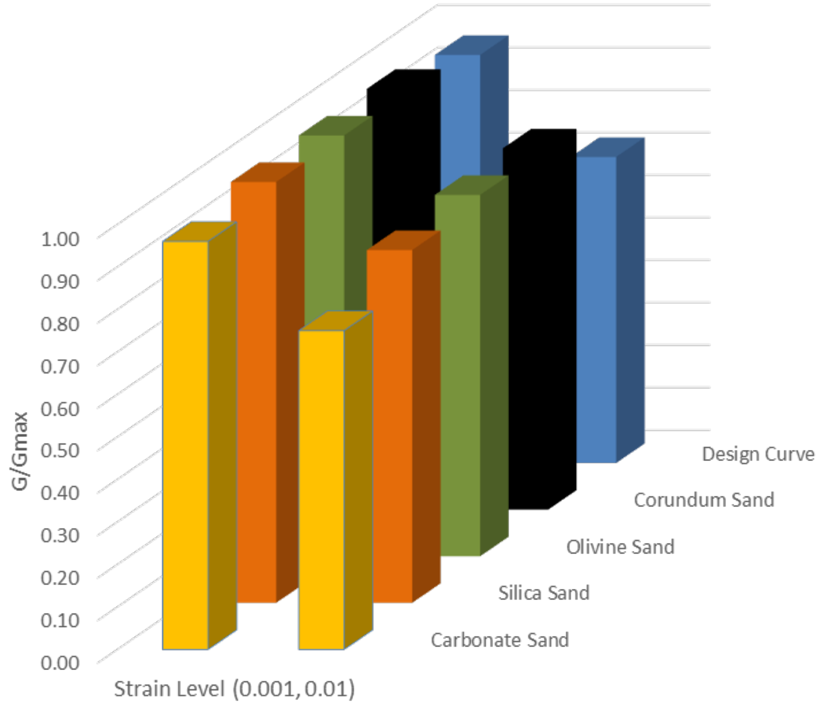

Figure 6.14 G/ G_{max} Values at Different Strain Levels

Table 6.7 Percentage of Difference Between Sands and Design Curve

	Strain = 0.001%		**Strain = 0.01%**	
	G/G_{max}	**% diff**	**G/G_{max}**	**% diff**
Design Curve	0.96	N/A	0.72	N/A
Carbonate Sand	0.96	0.00%	0.75	4.17%
Silica Sand	0.99	3.13%	0.83	15.28%
Olivine Sand	0.99	3.13%	0.88	22.22%
Corundum Sand	0.99	3.13%	0.85	18.06%

Table 6.7 shows the G/ G_{max} values for all sands at strains of 0.001% and 001%, respectively and compares it to the design curve values. At low strains, 0.001%, the difference is minimal, less than 3.13%, for all cases. This is expected

behavior because at low strain values the normalized shear modulus tends to behave more linearly, and the effects of strain are well established. At higher strains, 0.01%, the differences are more pronounced. The difference can vary as high as 22.22%.

6.5 Damping Results

The following sections will discuss the damping results of sand gradations corresponding to a uniformity coefficient, C_u , of 1.75. The results for sands corresponding to C_u of 2 and 3 follow the same trends. Appendix A shows applicable graphs and charts.

The effects of confinement, mineral composition, and its effects on site response are further discussed.

6.5.1 Effects of Confinement on Damping Results

As discussed in Section 5.3, all sands were tested under three confinement pressures, 10 psi (69 kPa), 15 psi (103.4 kPa), and 20 psi (137.0 kPa). Figures 6.15 through 6.18 show the damping results for all sands tested. As the confinement pressure is increased, the damping tends to decrease. Contrary to the shear modulus, the effects of confinement on damping are not as apparent. In fact, in some of the sands tested, the effects of confinement are minimal. This behavior is consistent with the conclusions arrived by Hardin and Richart (1963) and Vucetic and Dobry (1991) that damping can decrease or stay constant with increased confinement pressure.

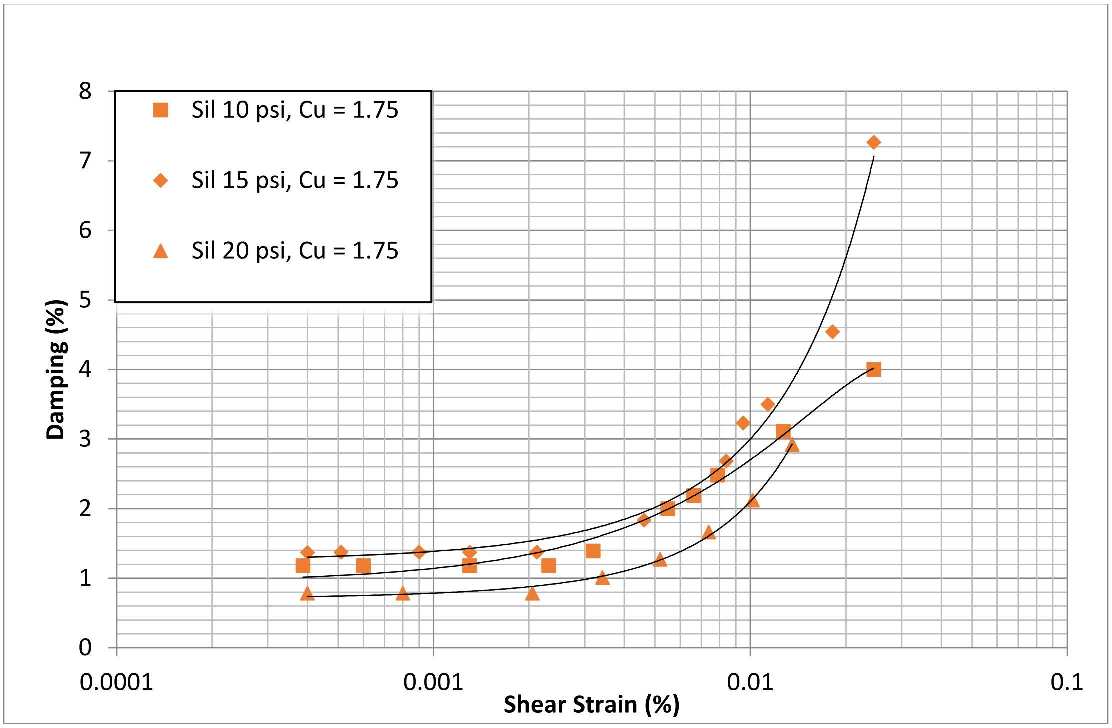

Figure 6.15 Effects of Confinement on Damping - Silica Sand

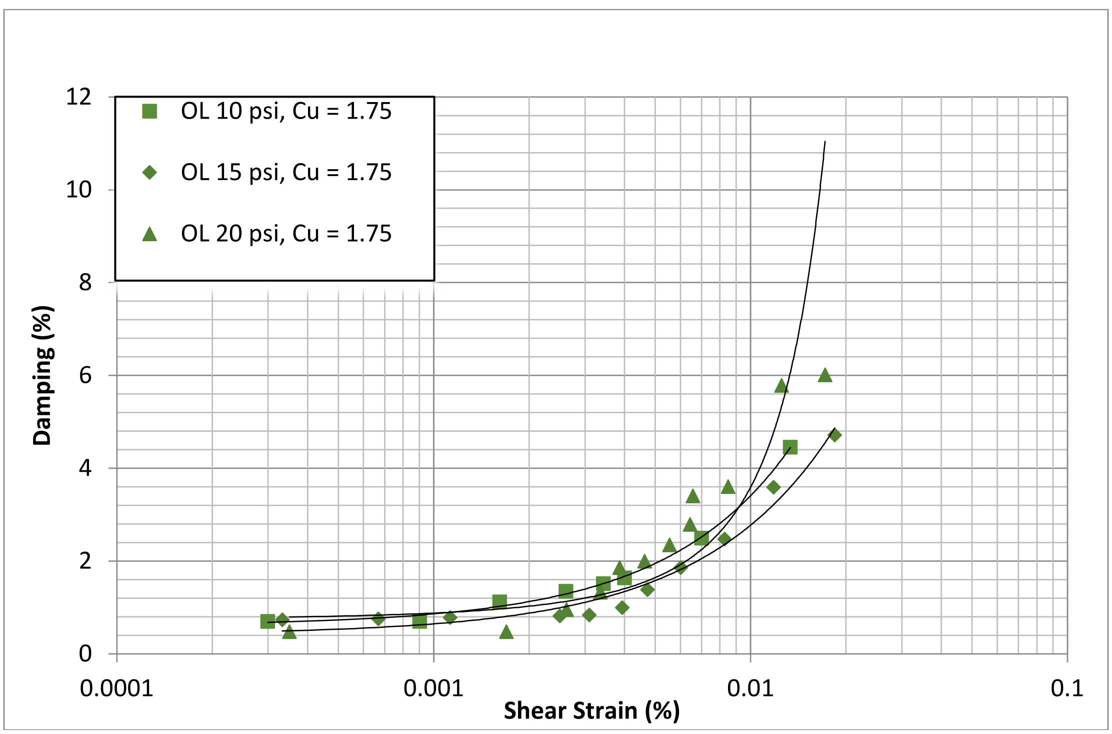

Figure 6.16 Effects of Confinement on Damping - Olivine Sand

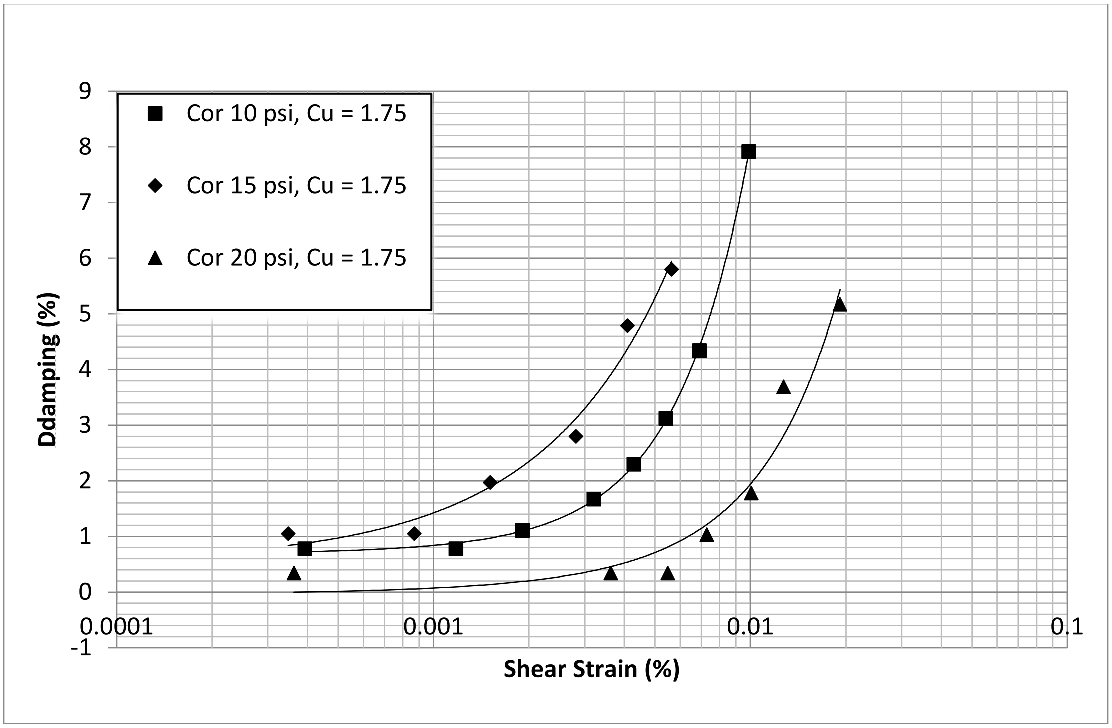

Figure 6.17 Effects of Confinement on Damping - Corundum Sand

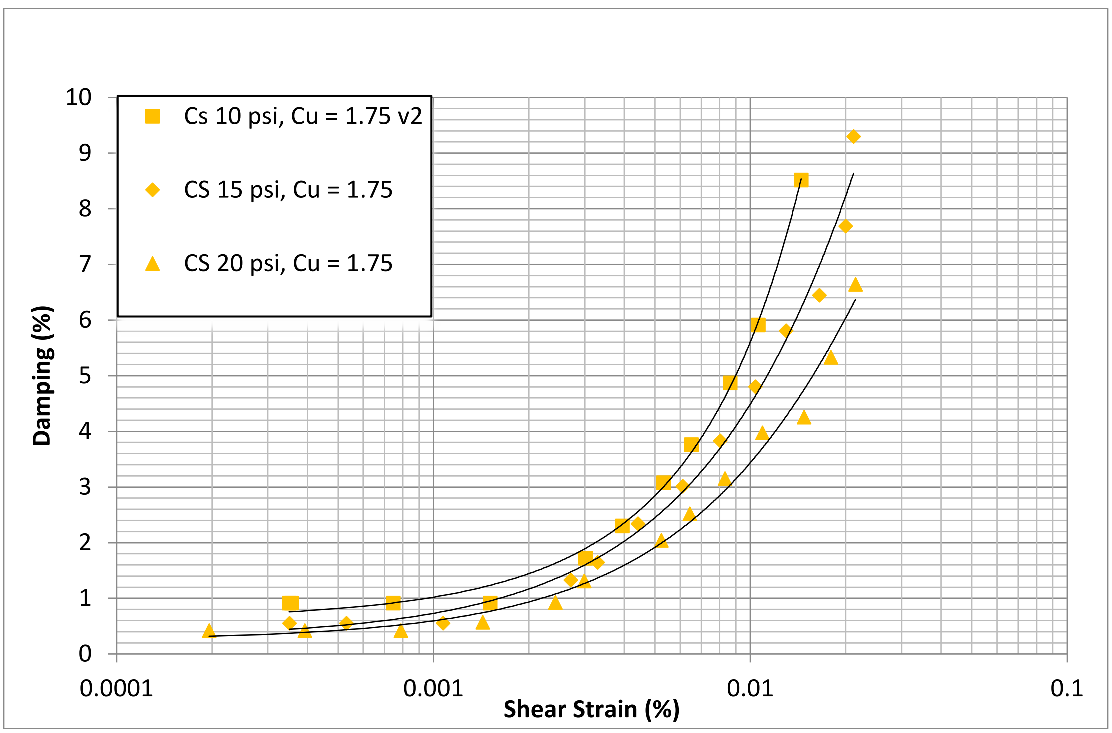

Figure 6.18 Effects of Confinement on Damping - Carbonate Sand

6.5.2 *Effects of Mineral Composition on Damping Results*

Figures 6.19 through 6.21 compares the damping ratio results for all sands tested at each confinement pressure. There is no evident trend that can be attained from the results as no sand stands out. As expected, as strains increase damping ratio increases and the response increases in nonlinearity. This is consistent with results arrived by Hardin and Richart (1963) and Vucetic and Dobry (1991) that damping can decrease or stay constant with increased confinement pressure.

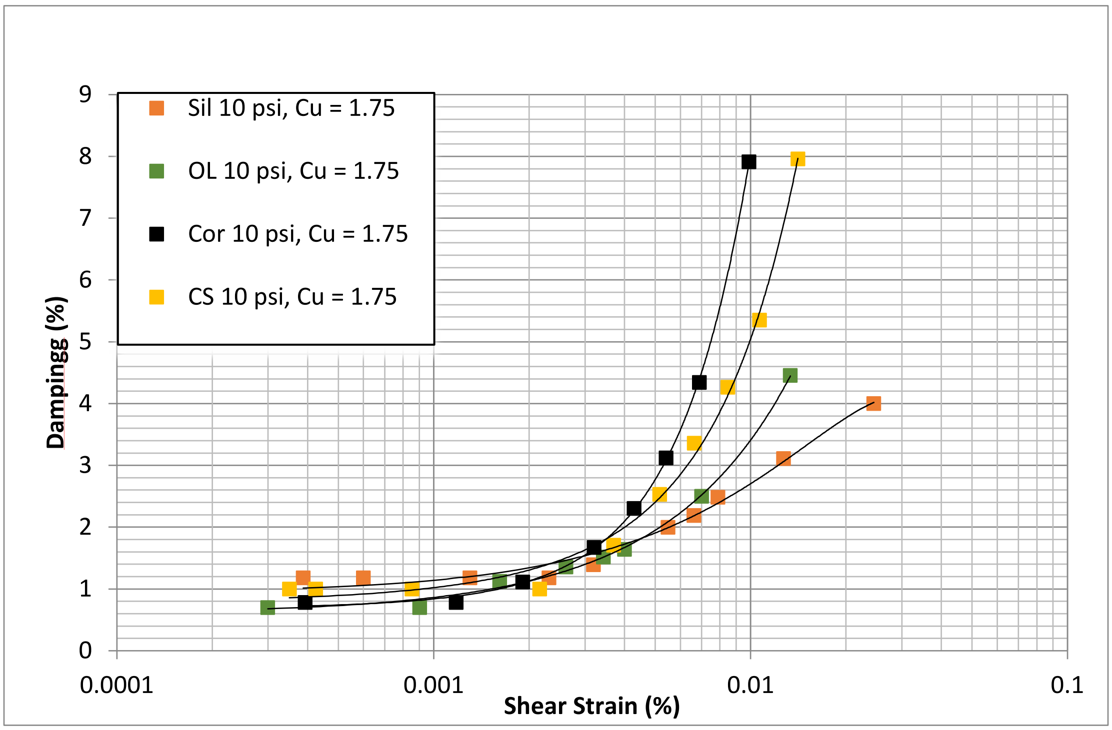

Figure 6.19 Effect of the mineral composition on Damping at Confinement Pressure of 10 psi (69 kPa)

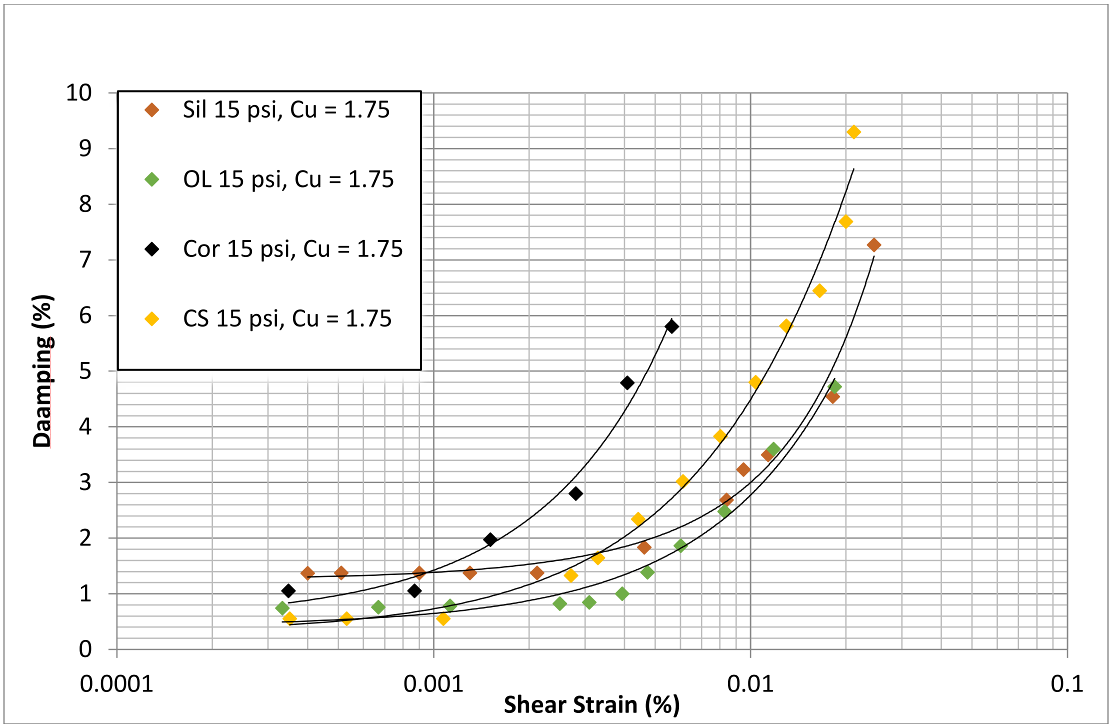

Figure 6.20 Effect of Mineral Composition on Damping at Confinement Pressure of 15 psi (103.4 kPa)

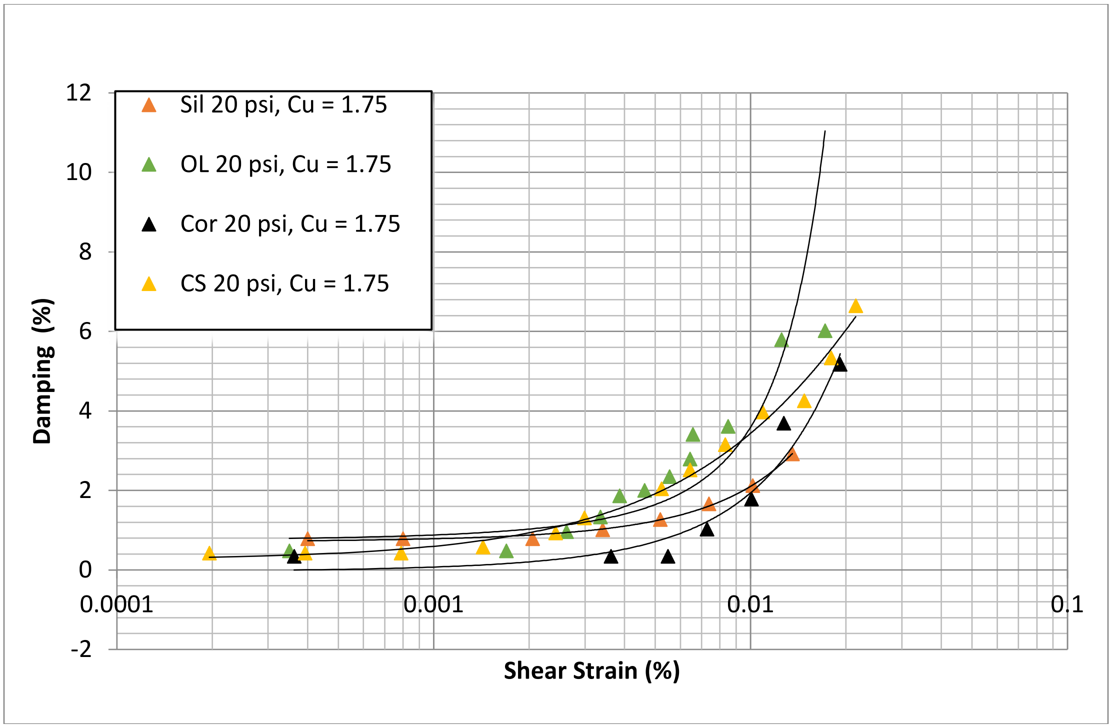

Figure 6.21 Effects of the Mineral Composition on Damping at Confinement Pressure of 20 psi (137.0 kPa)

6.5.3 <u>*Effects of Strain Level on D in Comparison with the Design Curve*</u>

As discussed in subsection 2.5, the damping curves created by Vucetic and Dobry (1991) are commonly used as design curves in typical geotechnical applications. In order to better understand how the results, correlate with the typical design curve, damping ratios for all sands were plotted against the design curve (see Figure 6.22. For the sands tested, most values plotted below the design curve. In addition, all sands tend to behave in the same fashion. As expected, as strains increase, damping increases proportionally. This behavior is consistent with conclusions arrived by many researchers including Vucetic and Dobry (1991, In order to quantify the difference between the design curve and the plotted values, a comparison was made between all sands at two strain levels, 0.001% and 0.01%, respectively. This was performed for all confinement stresses. Figures 6.23 through 6.25 show graphical representations of the damping values for all sands tested. Tables 6.8 through 6.10 quantify the differences between the sands tested and the damping design curve.

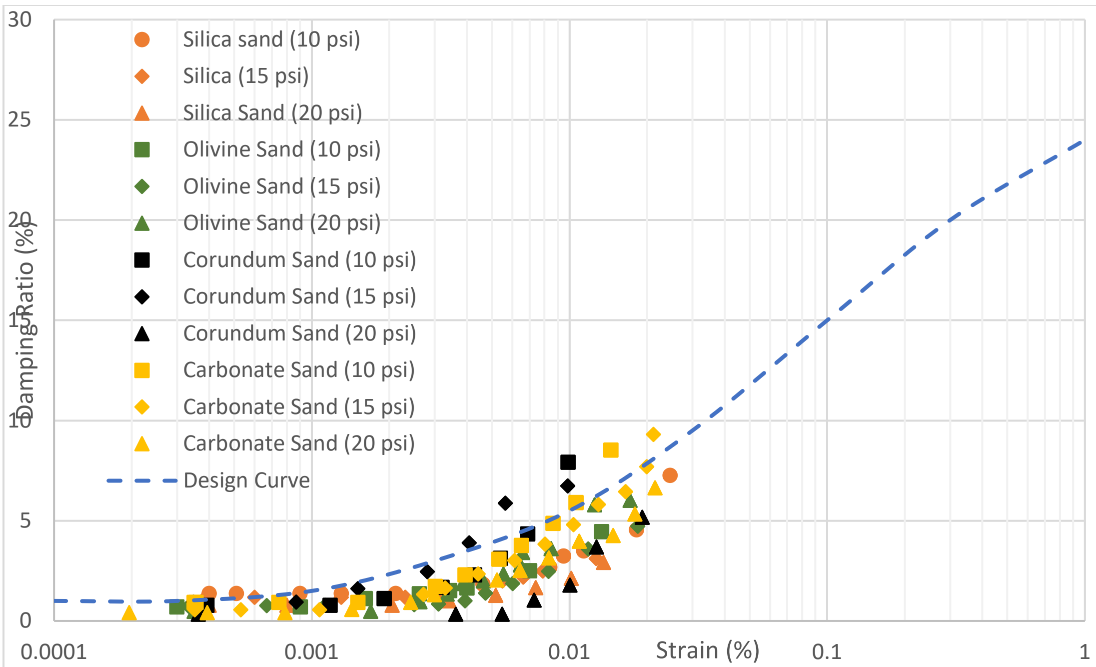

Figure 6.22 Damping for all Soils Tested in Comparison with the Design Curve

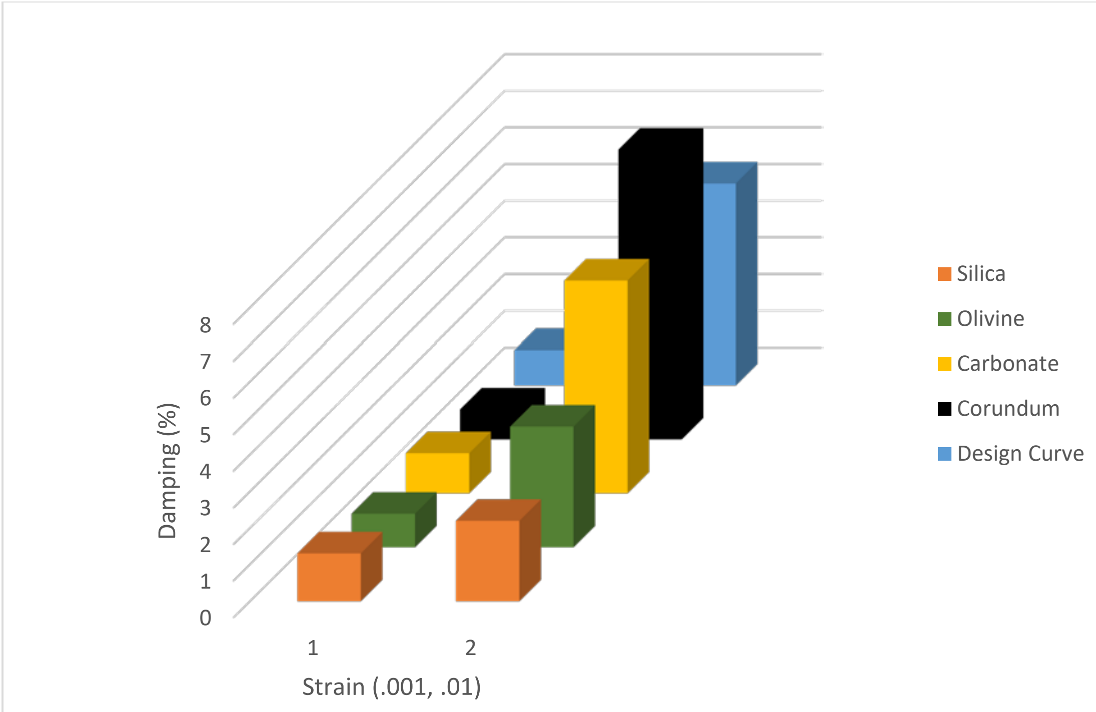

Figure 6.23 Effects of Strain Level on D in Comparison with the Design Curve - Confinement Pressure of 10 psi (69 kPa)

Table 6.8 Difference in Damping Between Sands Tested and Design Curve - Confinement Pressure of 10 psi (69 kPa)

Confinement stress	**10 psi (69 kPa)**			
Strain level (%)	**0.001**		**0.01**	
	D (%)	**% diff**	**D (%)**	**% diff**
Design Curve	0.96	N/A	5.5	N/A
Silica	1.31	36.5%	2.2	-60.0%
Olivine	0.92	-4.2%	3.3	-40.0%
Corundum	0.82	-14.6%	7.9	43.6%
Carbonate	1.1	14.6%	5.8	5.5%

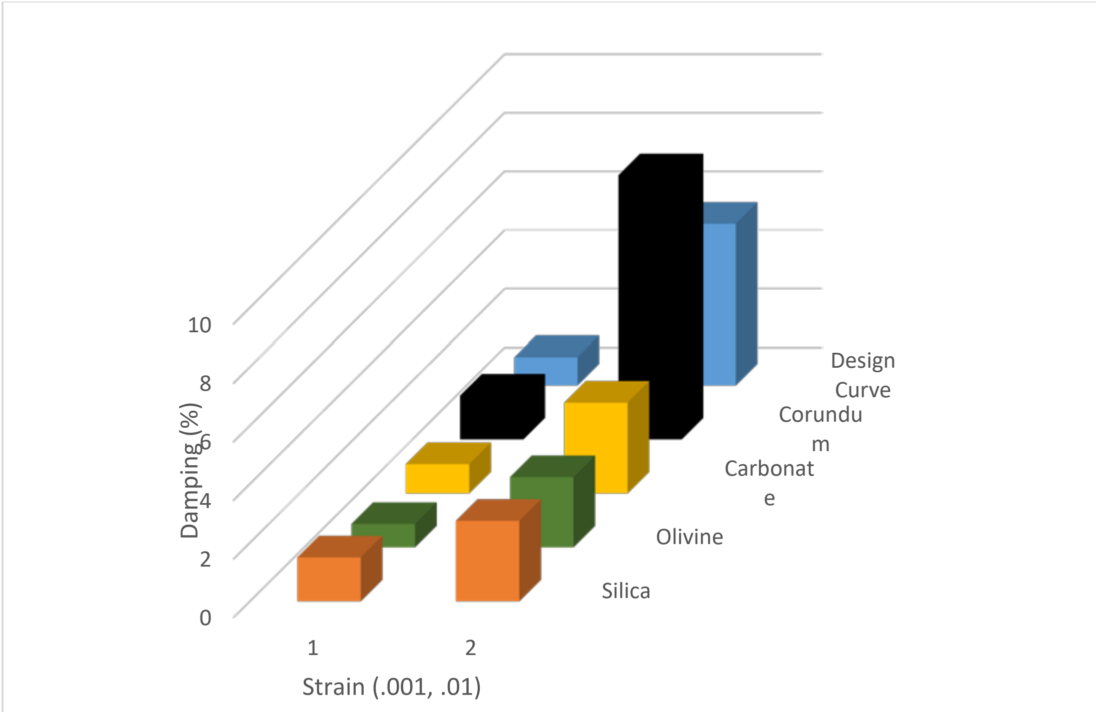

Figure 6.24 Effects of Strain Level on D in Comparison with the Design Curve - Confinement Pressure of 15 psi (103.7 kPa)

Table 6.9 Difference in Damping Between Sands Tested and Design Curve - Confinement Pressure of 15 psi (103.7 kPa)

Confinement stress	**15 psi (103.7 kPa)**			
Strain level (%)	**0.001**		**0.01**	
	Actual (%)	**% diff**	**Actual (%)**	**% diff**
Design Curve	0.96	N/A	5.5	N/A
Silica	1.5	56.3%	2.75	-50.0%
Olivine	0.8	-16.7%	2.4	-56.4%
Corundum	1.5	56.3%	9	63.6%
Carbonate	1	4.2%	3.1	-43.6%

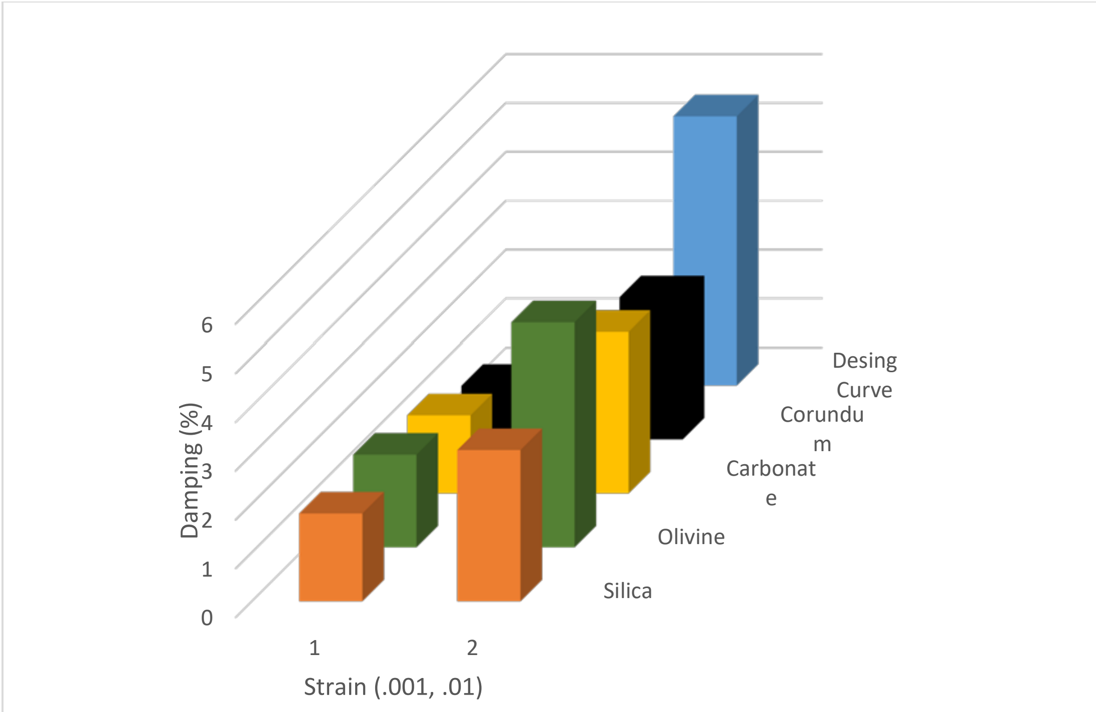

Figure 6.25 Effects of Strain Level on D in Comparison with the Design Curve - Confinement Pressure of 20 psi (137 kPa)

Table 6.10 Difference in Damping Between Sands Tested and Design Curve - Confinement Pressure of 20 psi (137 kPa)

Confinement stress (psi) (kPa)	**20 psi (137 kPa)**			
Strain level (%)	**0.001**		**0.01**	
	Actual (%)	**% diff**	**Actual (%)**	**% diff**
Design Curve	0.96	N/A	5.5	N/A
Silica	1.8	87.5%	3.1	-43.6%
Olivine	1.9	97.9%	4.6	-16.4%
Corundum	1.1	14.6%	2.9	-47.3%
Carbonate	1.6	66.7%	3.3	-40.0%

The data shows that there is a lot of variability between sands tested and the design curve at all levels of strain.

CHAPTER 7

CONCLUSIONS AND RECOMMENDATIONS

7.1 Conclusions

A series of resonant column tests were performed on various sand samples with different mineral compositions. Sands were selected based on their respective mineral hardiness or Mohs number in order to encompass a wide range of hardnesses. The following sands were selected for this purpose: Carbonate Sand (Mohs = 3), Silica Sand (Mohs = 7), Olivine Sand (Mohs = 7) and Corundum Sand (Mohs = 9). Sands were engineered to have the same uniformity coefficient (C_u) and mean particle size (D_{50}). Resonant column tests were performed at various confining stresses in order to assess each sand's shear modulus (G) and damping ratio (D). The following shear modulus results were observed:

1. Shear modulus curves for all sands follow the classical shape characteristics
2. Sands with similar gradation (C_u) and mean particle size (D_{50}), but different mineral compositions; were tested under the same confinement pressures and strains. The G values varied among them with a maximum of 23%.
3. This wide spectrum of G values has real world effects as it is demonstrated in the natural frequency calculation. Natural frequency calculations can vary as much as 38.4% percent in some cases.

4. a Carbonate Sand (Mohs = 3) degrades faster and has a sharper downturn than the Corundum sand (Mohs = 9). This behavior is indicative of the effect of mineralogy in shear modulus degradation. Possible causes for this difference in behavior:
    - Higher susceptibility of carbonate grains to crush when stressed
    - Cementation and fabric related to its carbonate materials

In a similar fashion, the following results for damping ratio were observed:

1. Curves for all sands follow classical shape characteristics
2. Sands with similar gradation (C_u) and mean particle size (D_{50}) but with different mineral components were tested under the same confinement pressures and strains; damping values vary among them.
3. Under the same confinement stresses, the effects of mineral composition were not evident as opposed to the shear modulus trends.
4. Differences in Damping can vary greatly at larger strains.
5. Currently the design curve can produce higher damping values, as high as 60% at high strains and about as high as 90% in small strains, than the sands tested.

7.2 Recommendations

This research has shown that the mineral composition can have a large effect on the behavior of shear modulus and damping.

It shows that the when the mineral composition of the soil under review is not known a priori, solely relying on published design curves during the site characterization process can have significantly different effects in the expected behavior of said soil during dynamic events.

It emphasizes the importance of testing soils during the site characterization process in order to understand its mineral composition and dynamic properties

APPENDIX A

SHEAR MODULUS RESULTS

This Appendix encompasses all the shear modulus (G) results not discussed in the body of this work. For each sand tested in this research (Silica, Olivine, Carbonate and Corundum) a minimum of 18 resonant column tests were performed, including 2 series of tests to ensure repeatability and accountability of the results. In the following charts the "(2)" represents "Series 2" tests. In total, \over 72 tests were performed for this effort. The following table describes the testing approach.

Table A.1 Shear Modulus Tests Breakdown

Sand	C_u	**Series**	**σ' (psi)**
Silica Sand, Olivine Sand, Carbonate Sand, and Corundum Sand	1.75	1	10
			15
			20
		2	10
			15
			20
	2.00	1	10
			15
			20
		2	10
			15
			20
	3.00	1	10
			15
			20
		2	10
			15
			20

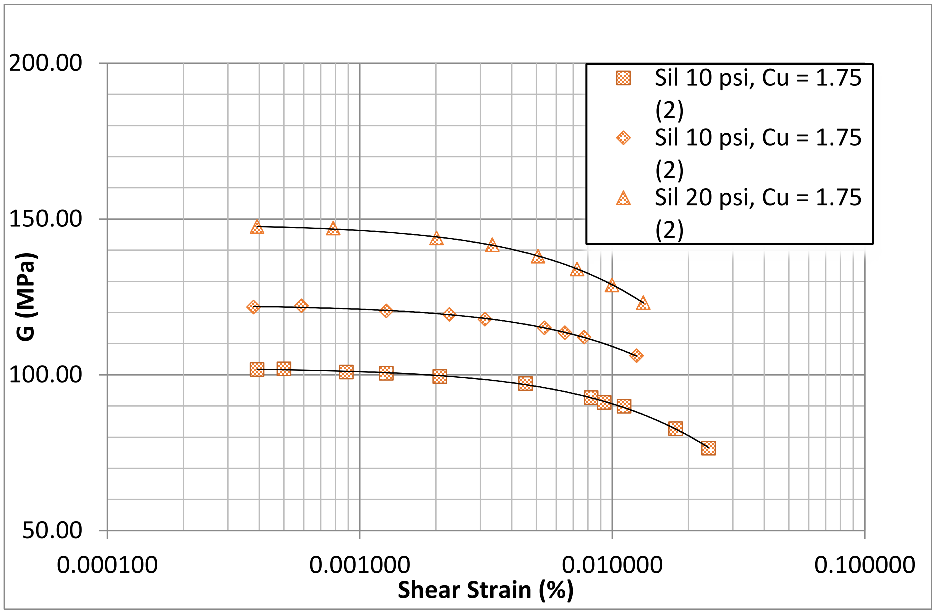

Figure A.1 Effects on Confinement on Shear Modulus (G) for Silica Sand for C_u =1.75, Series 2

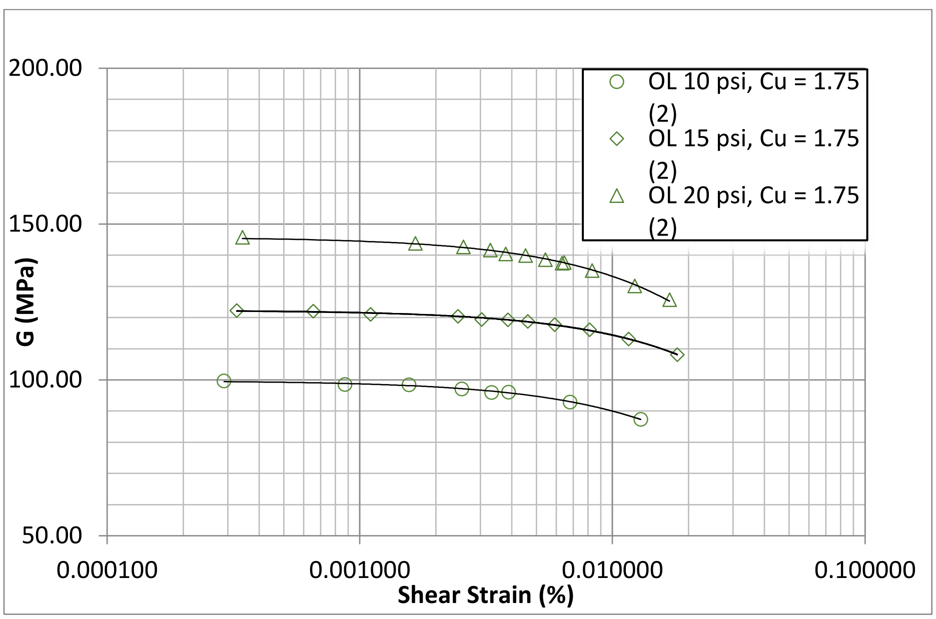

Figure A.2 Effects on Confinement on Shear Modulus (G) for Olivine Sand for Cu =1.75, Series 2

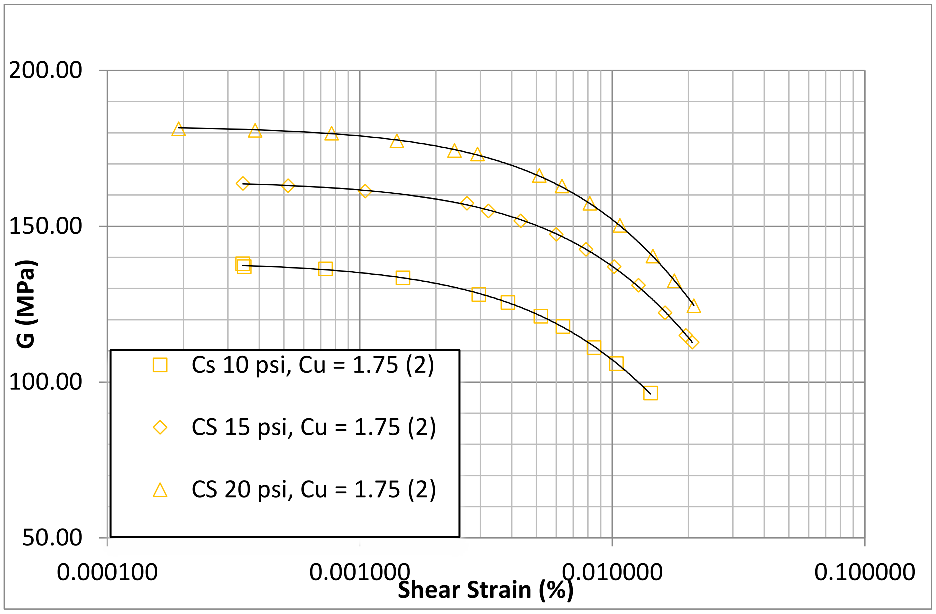

Figure A.3 Effects on Confinement on Shear Modulus (G) for Carbonate Sand for Cu =1.75, Series 2

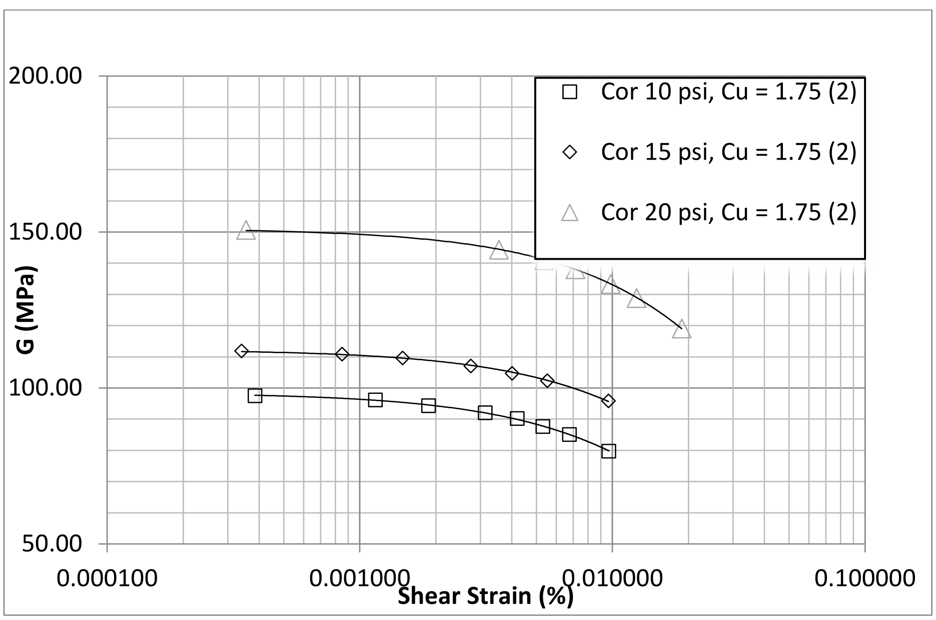

Figure A.4 Effects on Confinement on Shear Modulus (G) for Corundum Sand for Cu =1.75, Series 2

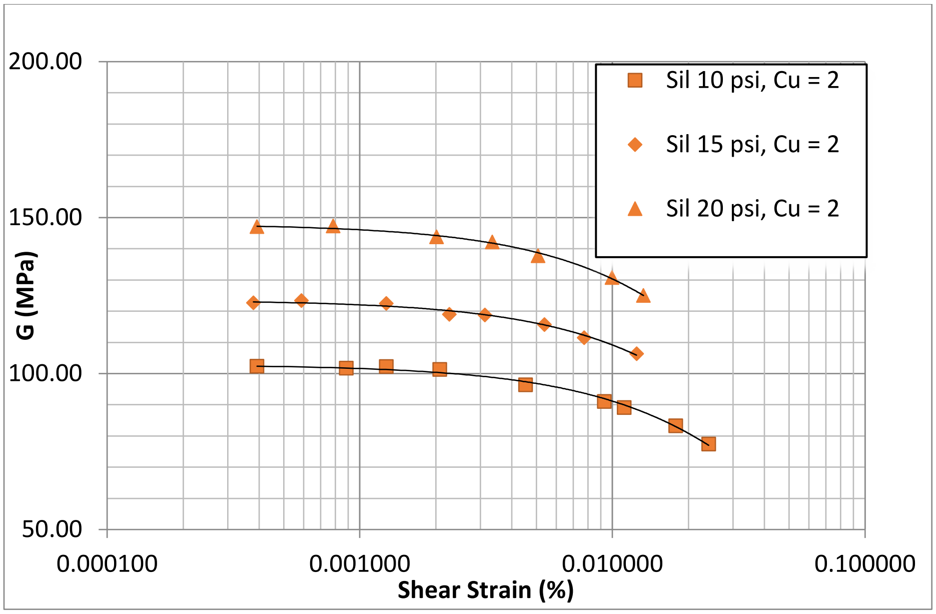

Figure A.5 Effects on Confinement on Shear Modulus (G) for Silica Sand for Cu =2, Series 1

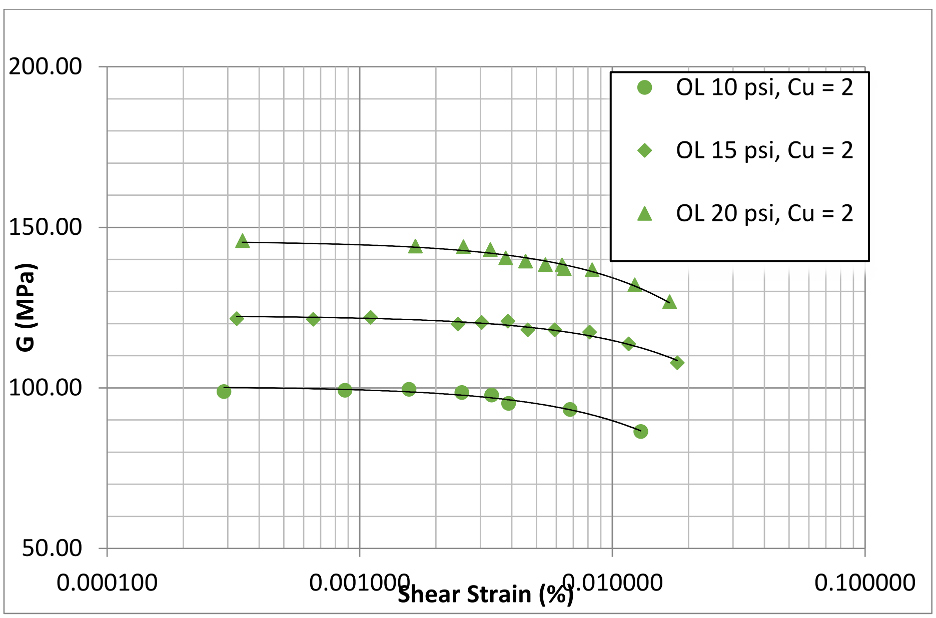

Figure A.6 Effects on Confinement on Shear Modulus (G) for Olivine Sand for Cu =2, Series 1

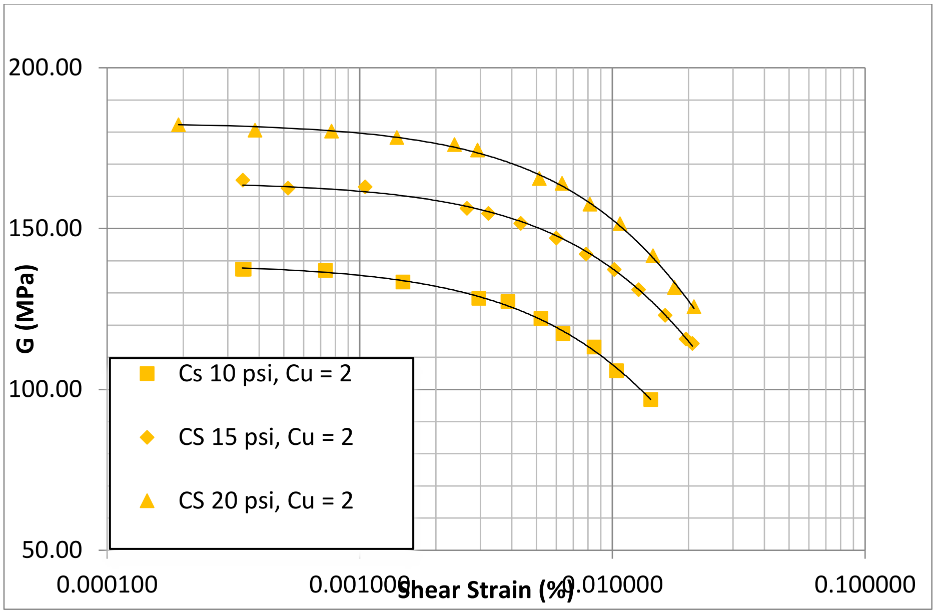

Figure A.7 Effects on Confinement on Shear Modulus (G) for Carbonate Sand for Cu =2, Series 1

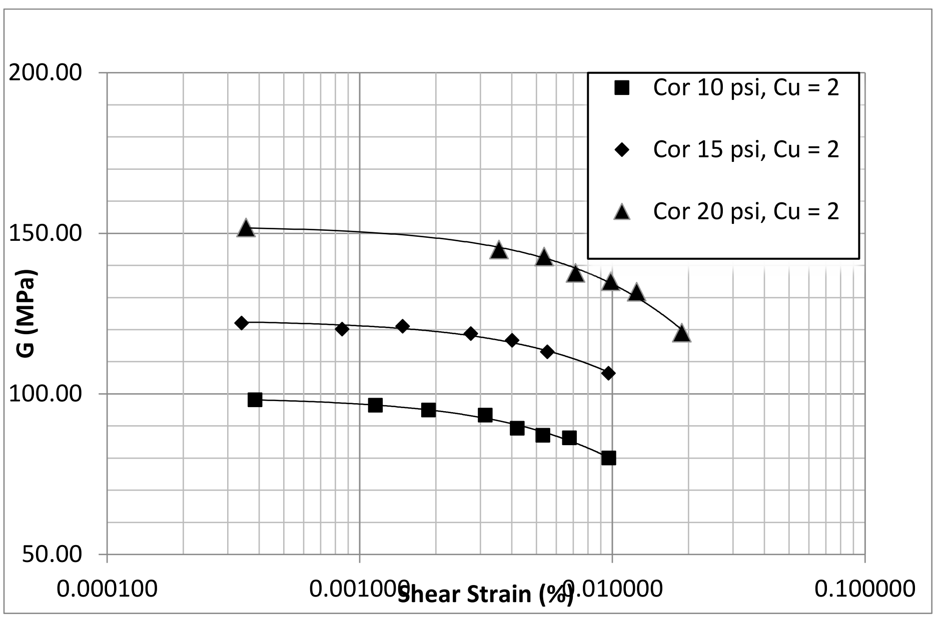

Figure A.8 Effects on Confinement on Shear Modulus (G) for Corundum Sand for Cu =2, Series 1

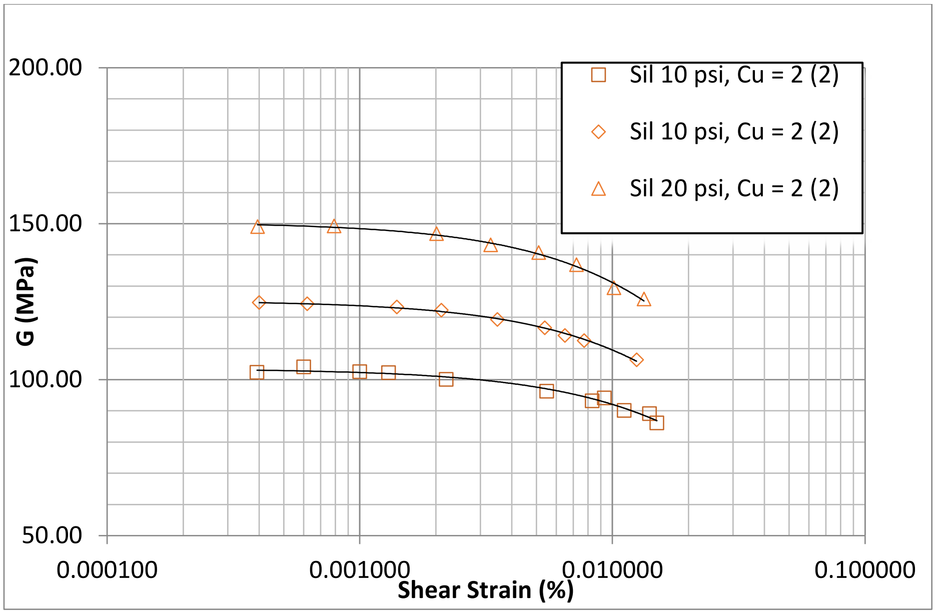

Figure A.9 Effects on Confinement on Shear Modulus (G) for Silica Sand for Cu =2, Series 2

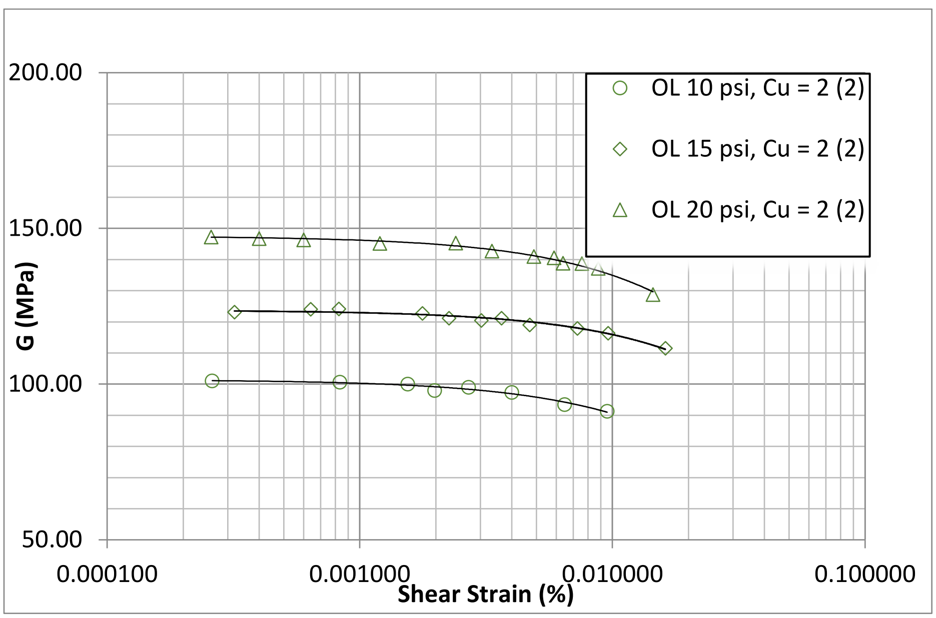

Figure A.10 Effects on Confinement on Shear Modulus (G) for Olivine Sand for Cu =2, Series 2

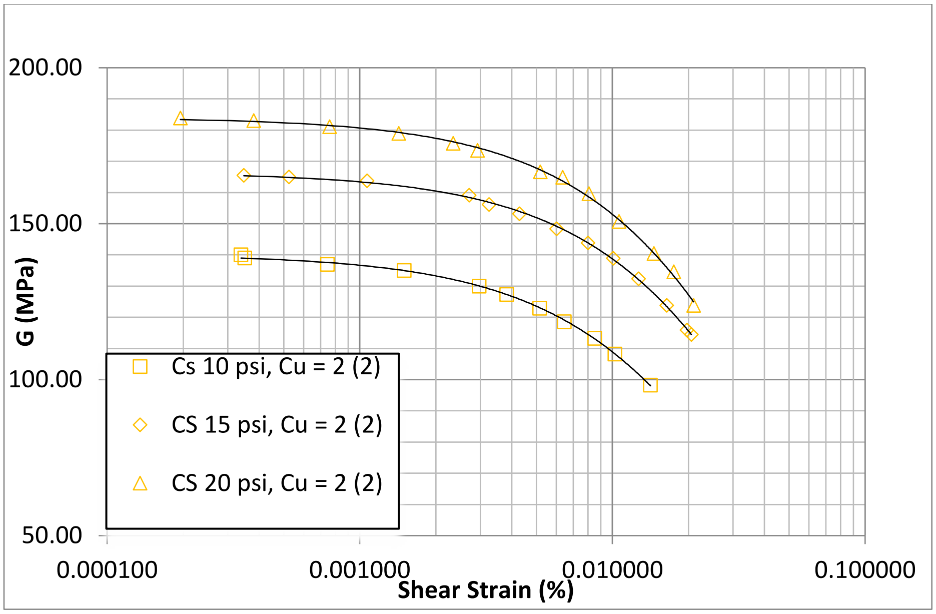

Figure A.11 Effects on Confinement on Shear Modulus (G) for Carbonate Sand for Cu =2, Series 2

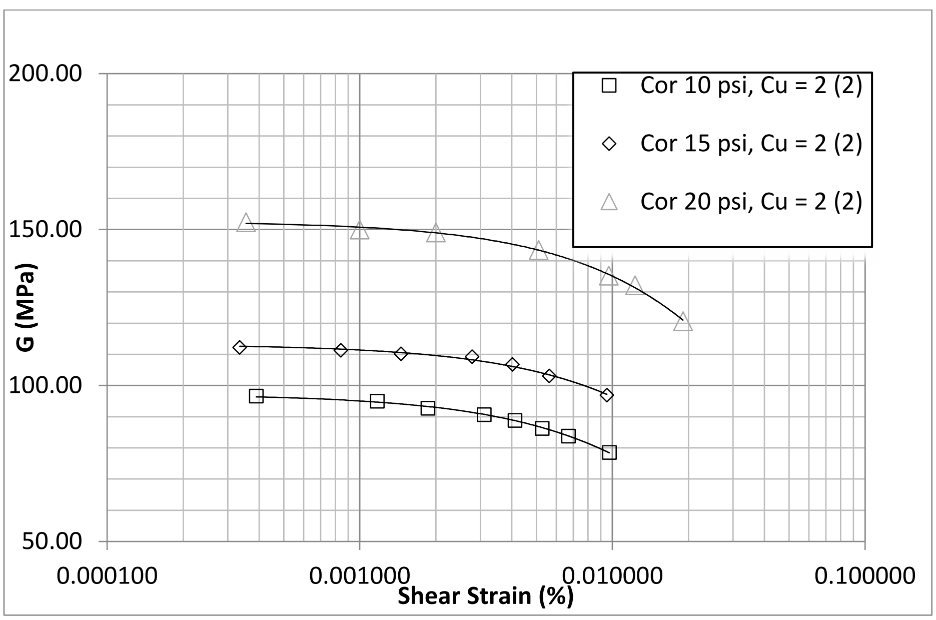

Figure A.12 Effects on Confinement on Shear Modulus (G) for Corundum Sand for Cu =2, Series 2

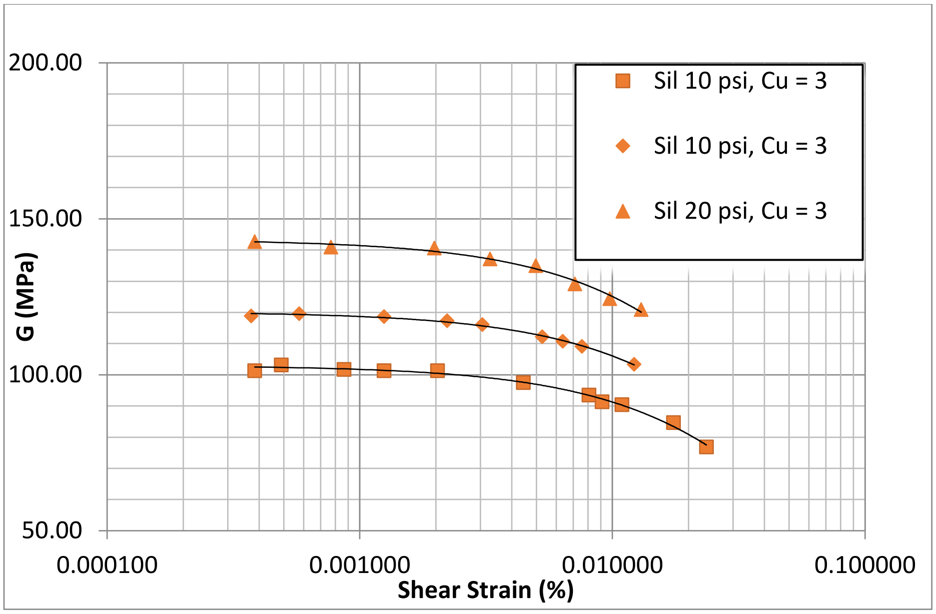

Figure A.13 Effects on Confinement on Shear Modulus (G) for Silica Sand for Cu =3, Series 1

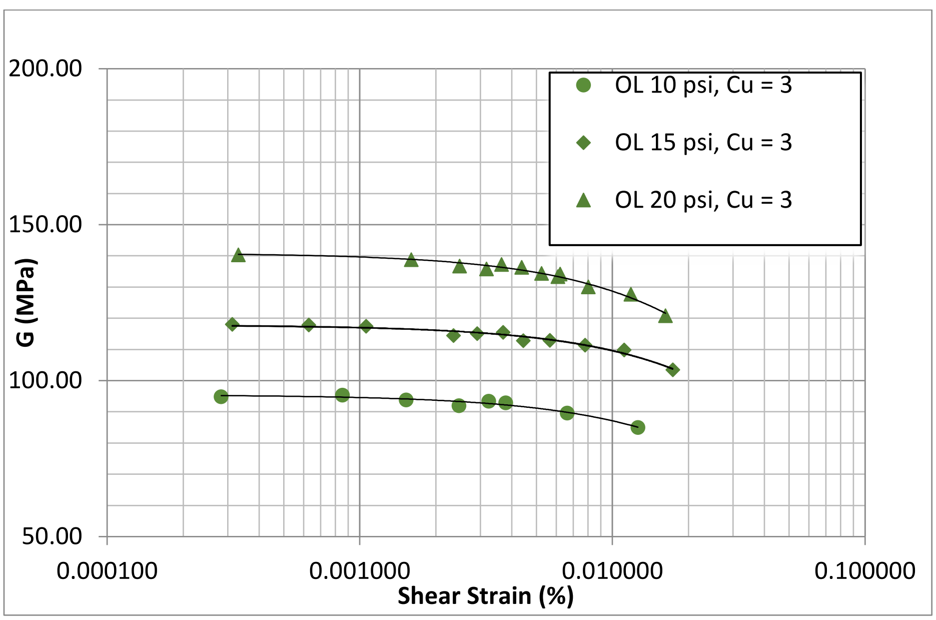

Figure A.14 Effects on Confinement on Shear Modulus (G) for Silica Sand for Cu =3, Series 1

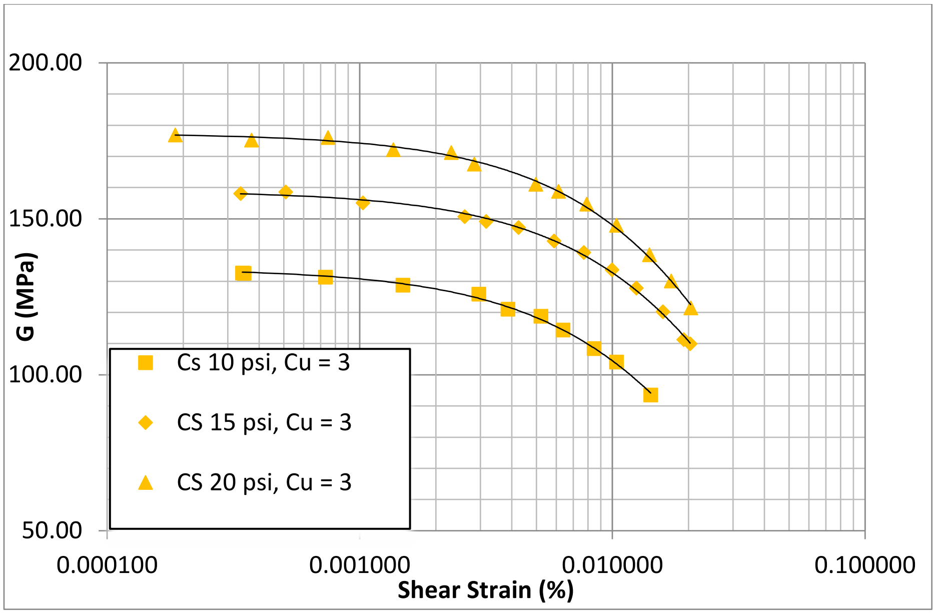

Figure A.15 Effects on Confinement on Shear Modulus (G) for Carbonate Sand for Cu =3, Series 1

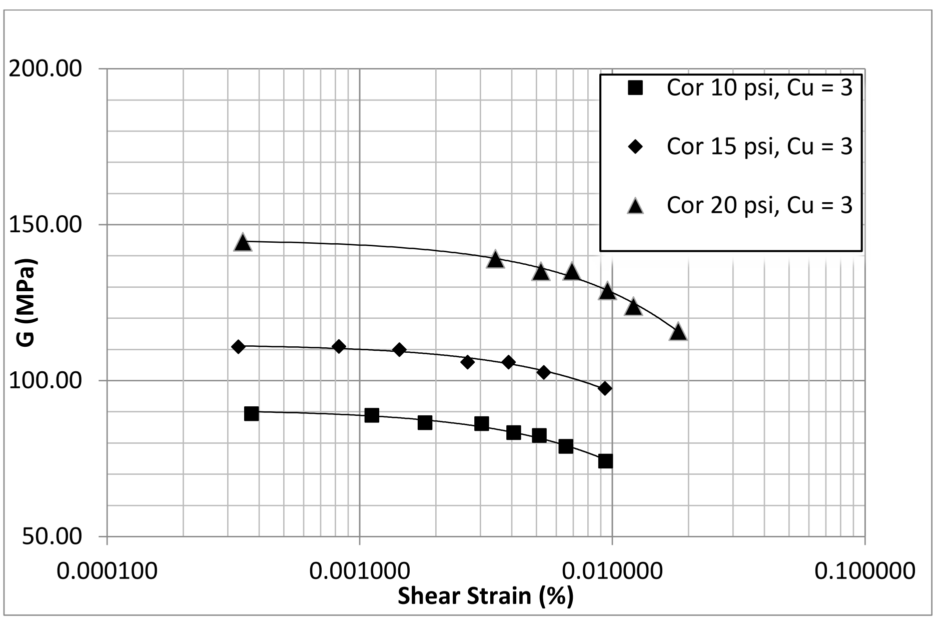

Figure A.16 Effects on Confinement on Shear Modulus (G) for Corundum Sand for Cu =3, Series 1

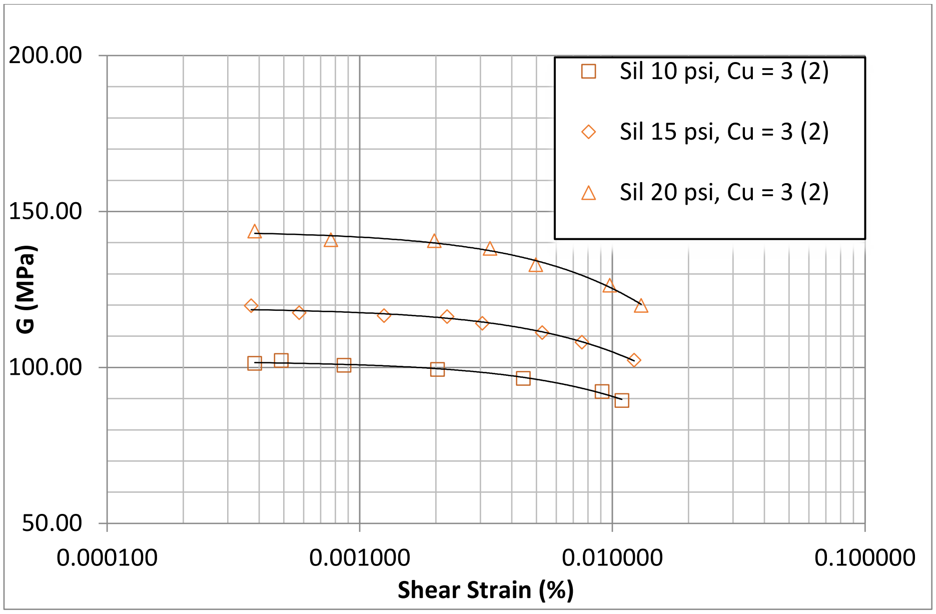

Figure A.17 Effects on Confinement on Shear Modulus (G) for Silica Sand for Cu =3, Series 2

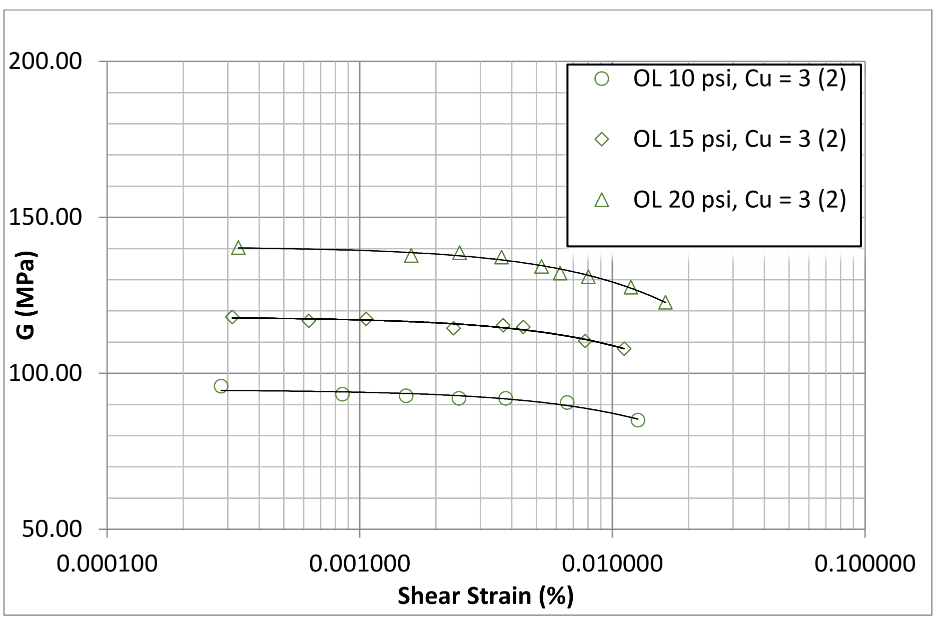

Figure A.18 Effects on Confinement on Shear Modulus (G) for Olivine Sand for Cu =3, Series 2

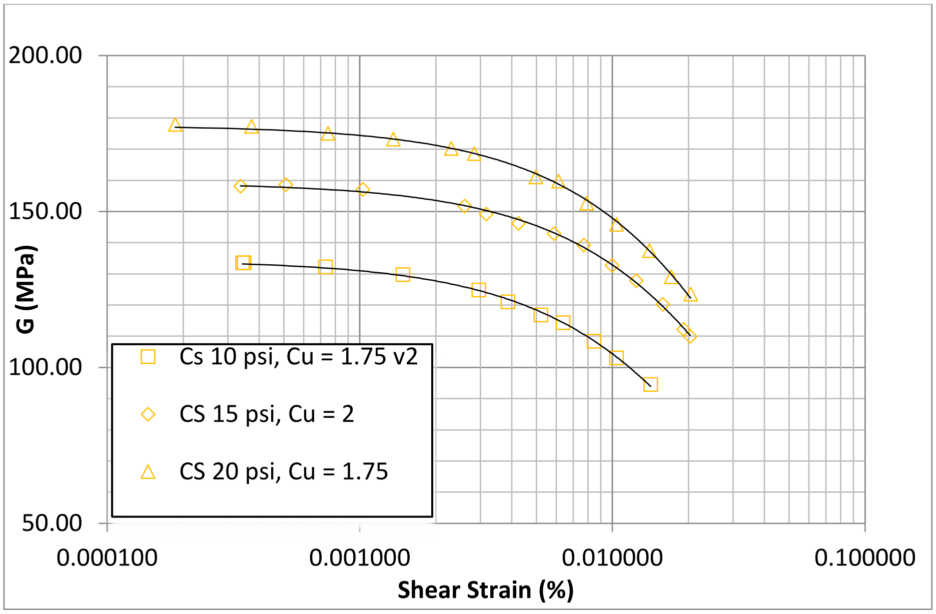

Figure A.19 Effects on Confinement on Shear Modulus (G) for Carbonate Sand for Cu =3, Series 2

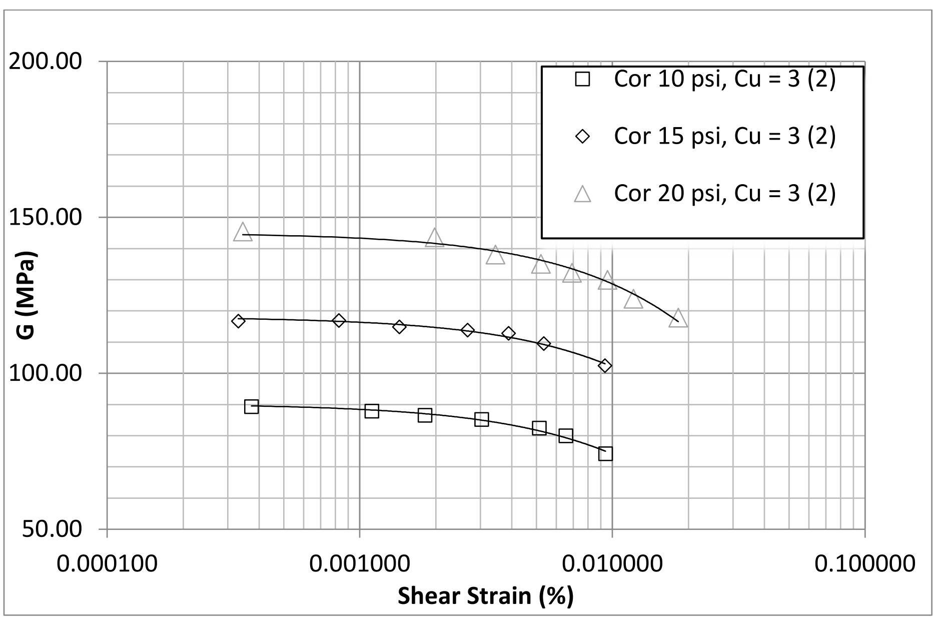

Figure A.20 Effects on Confinement on Shear Modulus (G) for Corundum Sand for Cu =3, Series 2

APPENDIX B

DAMPING RATIO RESULTS

This Appendix encompasses all the Damping Ratio (D) results not discussed in the body of this work. For each sand tested in this research (Silica, Olivine, Carbonate and Corundum) a minimum of 18 resonant column tests were performed, including 2 series of tests to ensure repeatability and accountability of the results. In the following charts the “(2)” represents “Series 2” tests. In total, over 72 tests were performed for this effort. The following table describes the testing approach.

Table B.1 Damping Ratio Tests Breakdown

Sand	C_u	**Series**	**σ' (psi)**
Silica Sand, Olivine Sand, Carbonate Sand, and Corundum Sand	1.75	1	10
			15
			20
		2	10
			15
			20
	2.00	1	10
			15
			20
		2	10
			15
			20
	3.00	1	10
			15
			20
		2	10
			15
			20

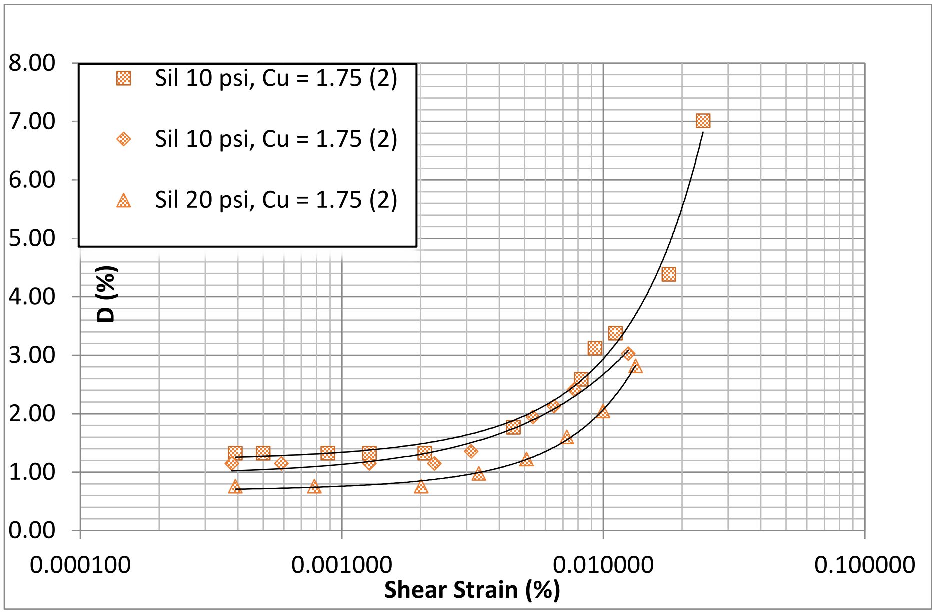

Figure B.1 Effects on Confinement on Damping Ratio (D) for Silica Sand for C_u =1.75, Series 2

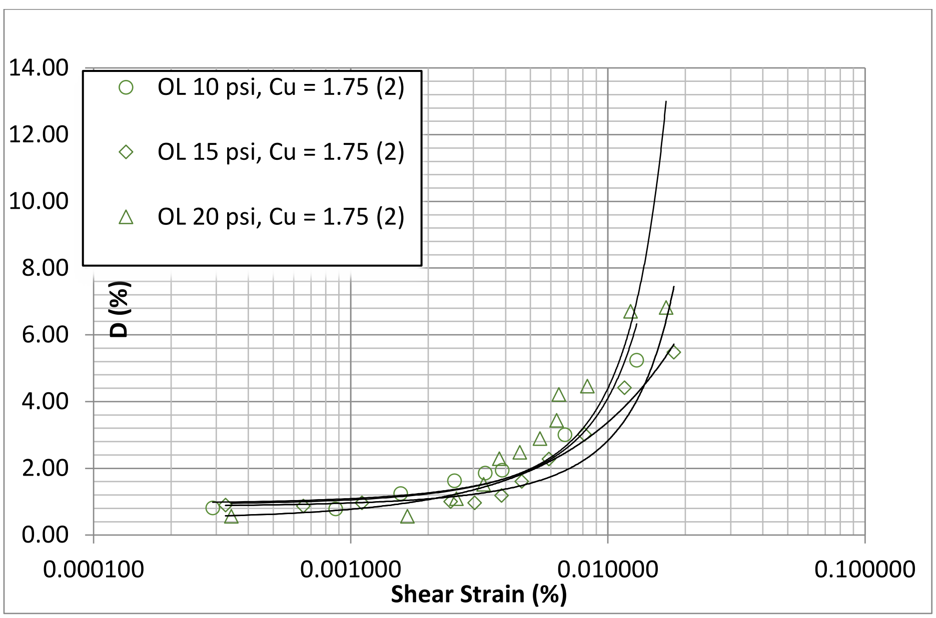

Figure B.2 Effects on Confinement on Damping Ratio (D)) for Olivine Sand for C_u =1.75, Series 2

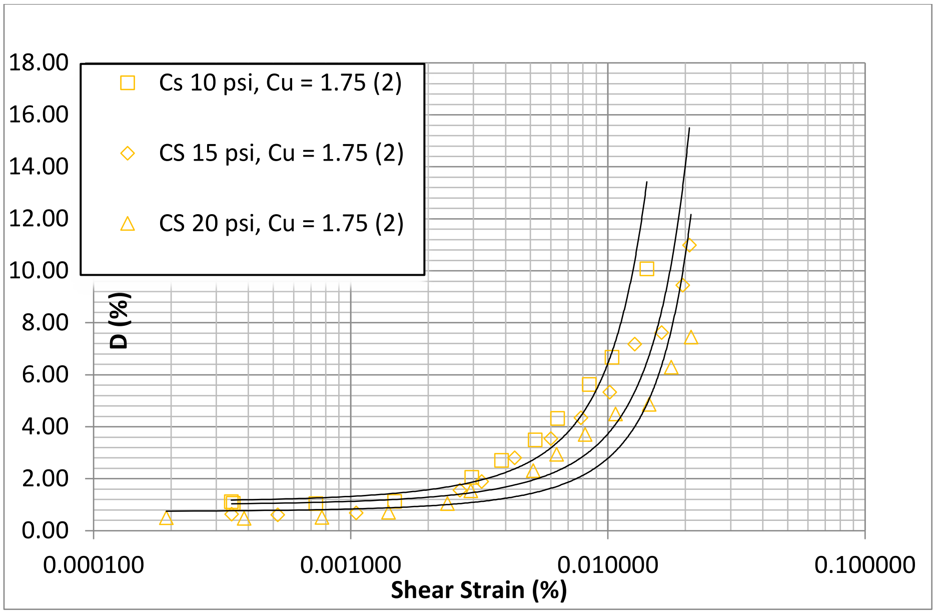

Figure B.3 Effects on Confinement on Damping Ratio (D)) for Carbonate Sand for C_u *=1.75, Series 2*

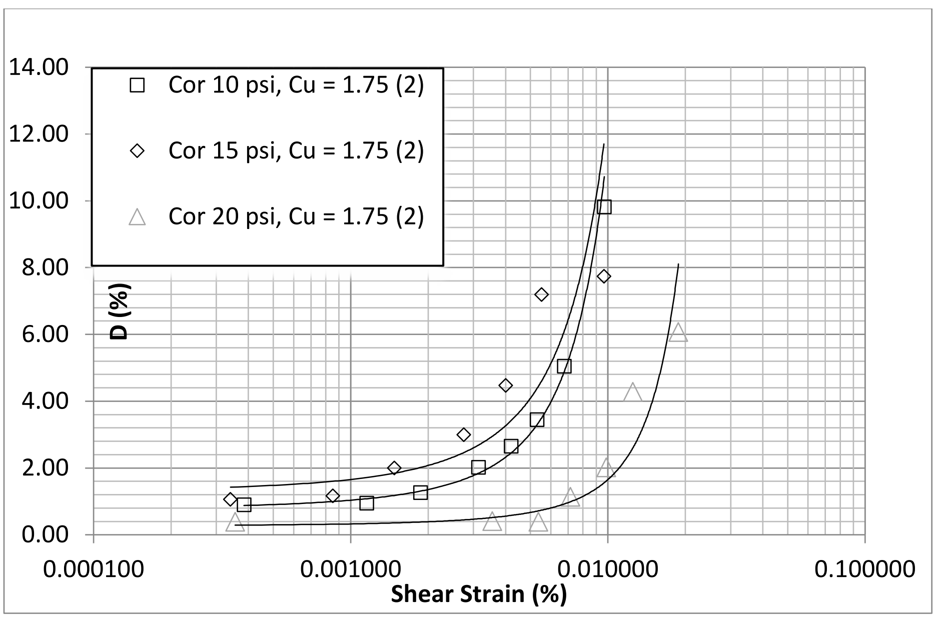

Figure B.4 Effects on Confinement on Damping Ratio (D) for Corundum Sand for C_u *=1.75, Series 2*

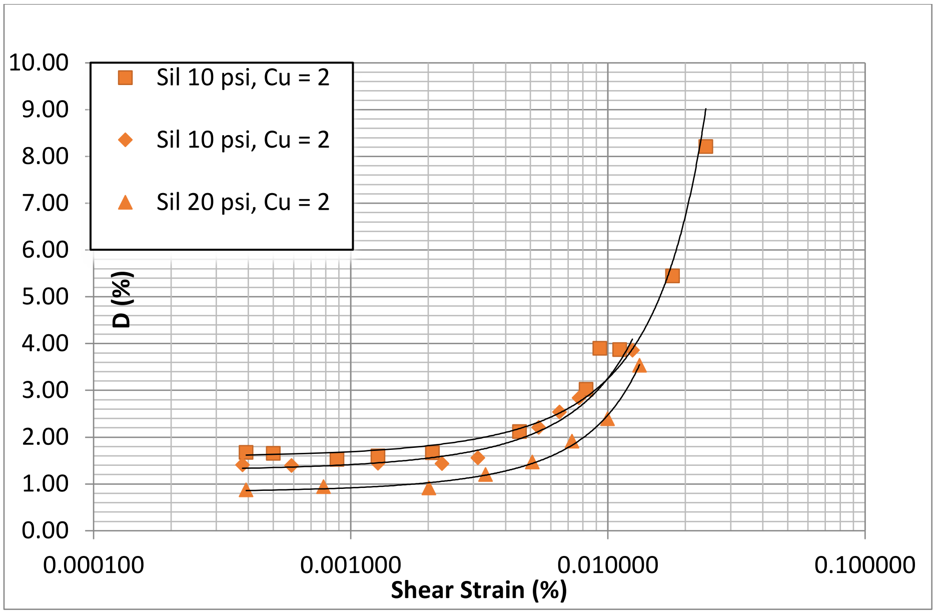

Figure B.5 Effects on Confinement on Damping Ratio (D) for Silica Sand for C_u =2, Series 1

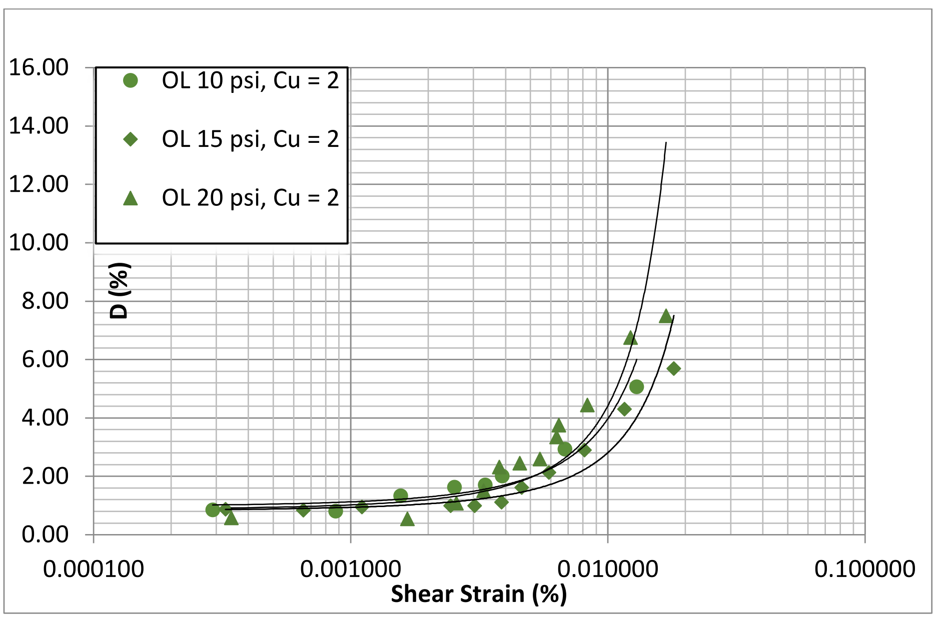

Figure B.6 Effects on Confinement on Damping Ratio (D) for Olivine Sand for C_u =2, Series 1

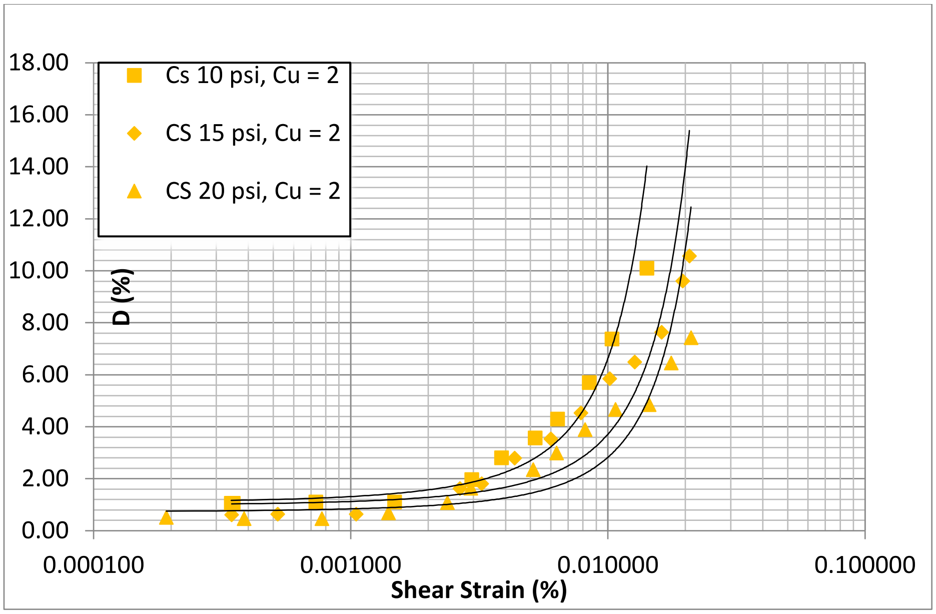

Figure B.7 Effects on Confinement on Damping Ratio (D) for Carbonate Sand for C_u =2, Series 1

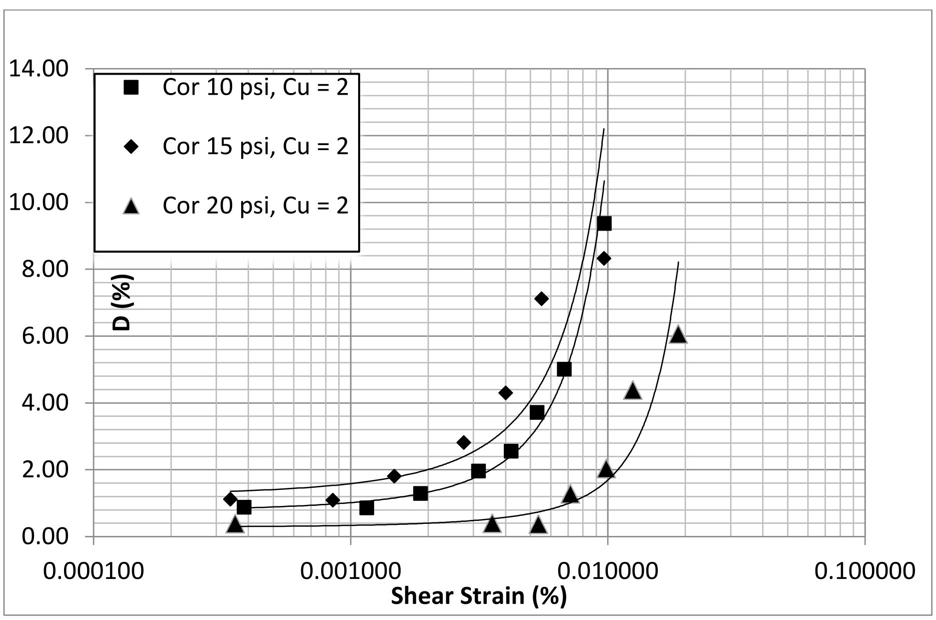

Figure B.8 Effects on Confinement on Damping Ratio (D) for Carbonate Sand for C_u =2, Series 1

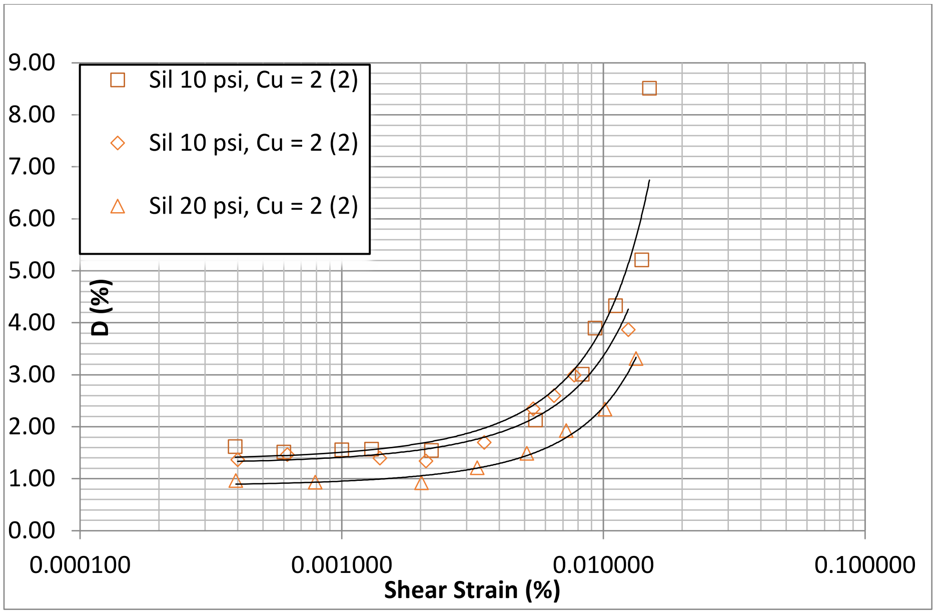

Figure B.9 Effects on Confinement on Damping Ratio (D) for Silica Sand for C_u =2, Series 2

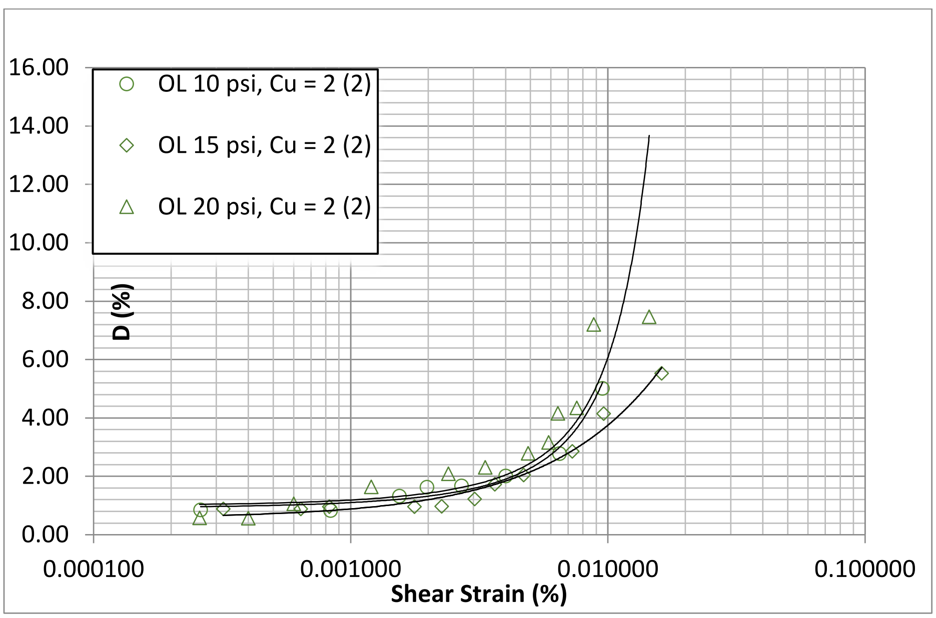

Figure B.10 Effects on Confinement on Damping Ratio (D) for Olivine Sand for C_u =2, Series 2

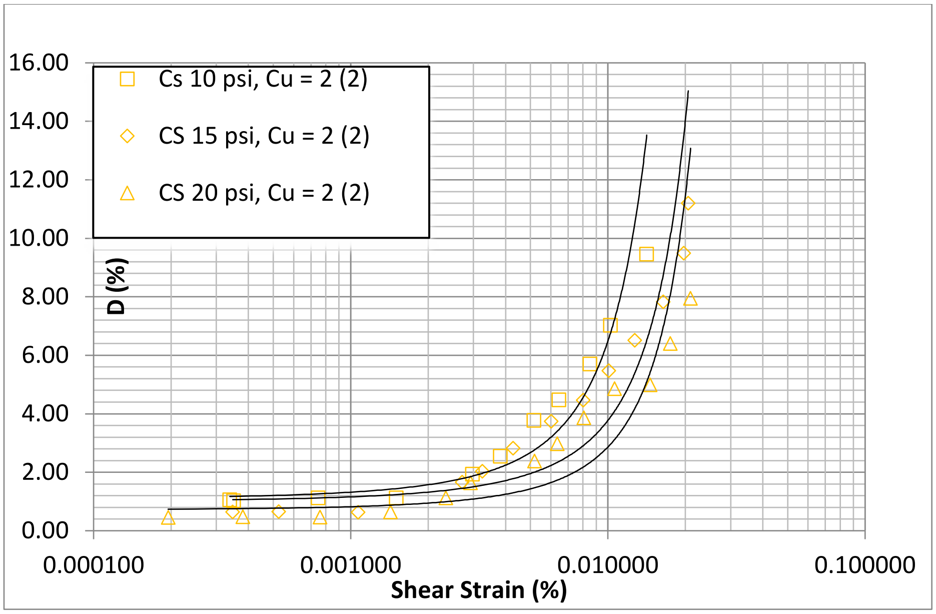

Figure B.11 Effects on Confinement on Damping Ratio (D) for Carbonate Sand for C_u =2, Series 2

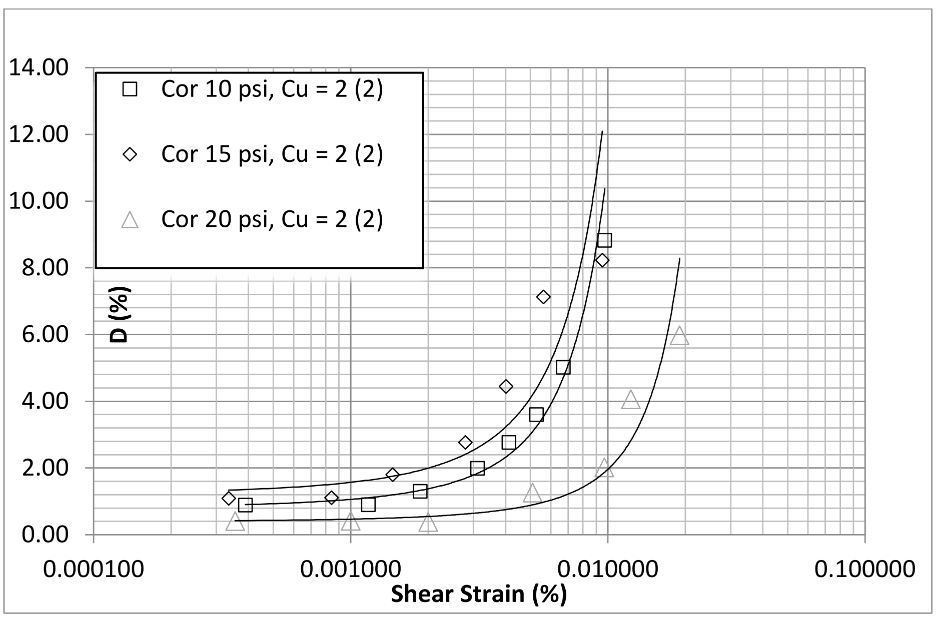

Figure B.12 Effects on Confinement on Damping Ratio (D) for Corundum Sand for C_u =2, Series 2

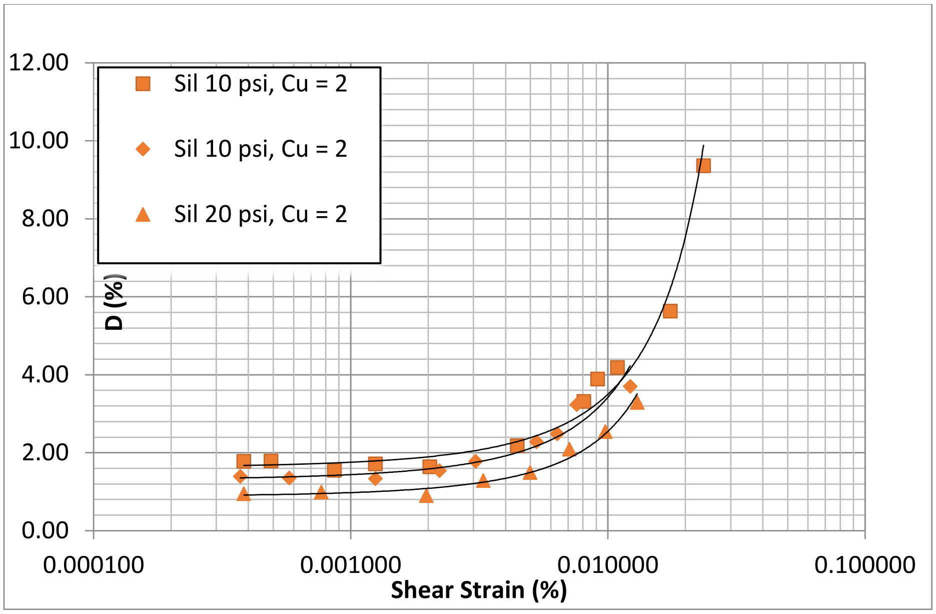

Figure B.13 Effects on Confinement on Damping Ratio (D) for Silica Sand for C_u =3, Series 1

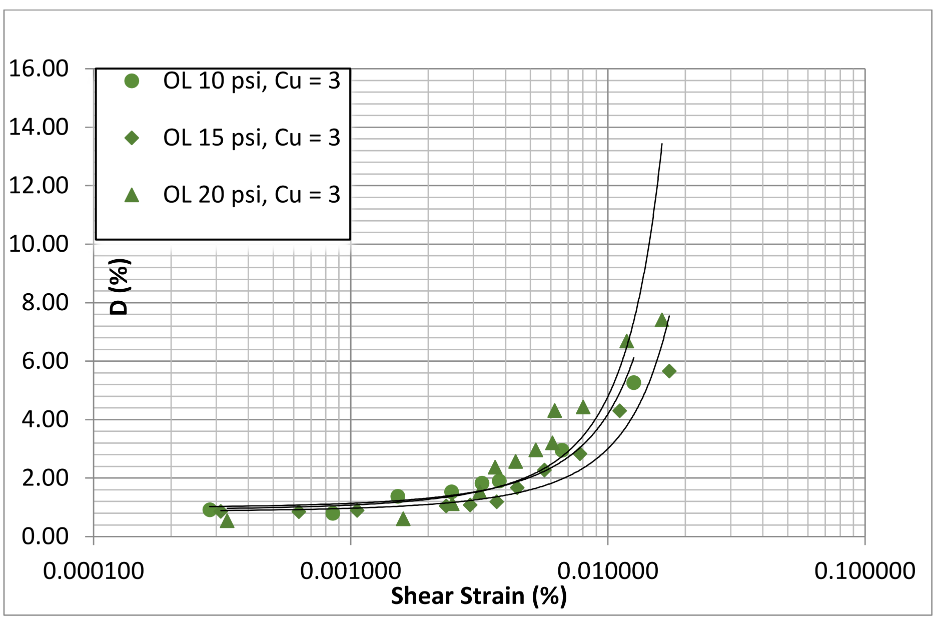

Figure B.14 Effects on Confinement on Damping Ratio (D) for Olivine Sand for C_u =3, Series 1

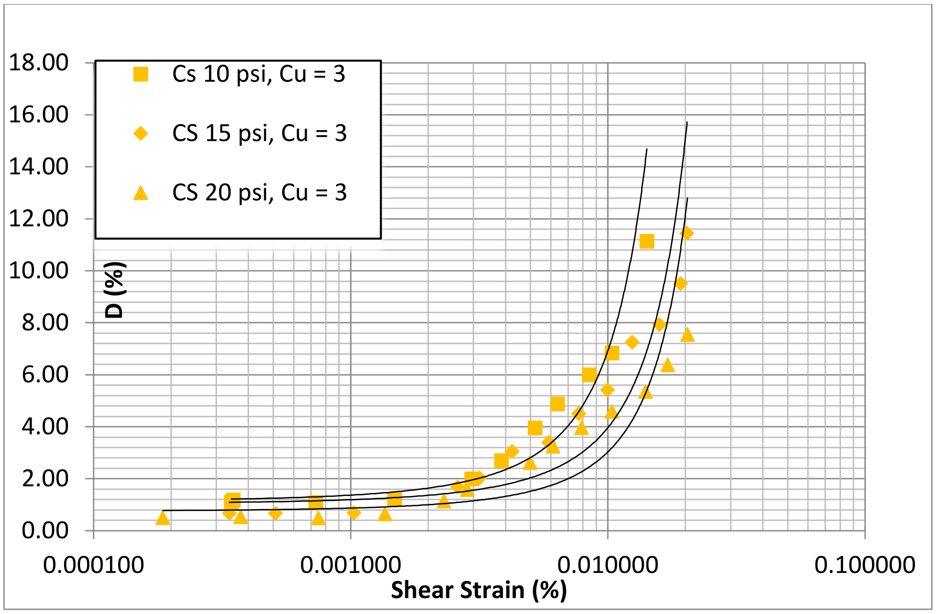

Figure B.15 Effects on Confinement on Damping Ratio (D) for Carbonate Sand for C_u =3, Series 1

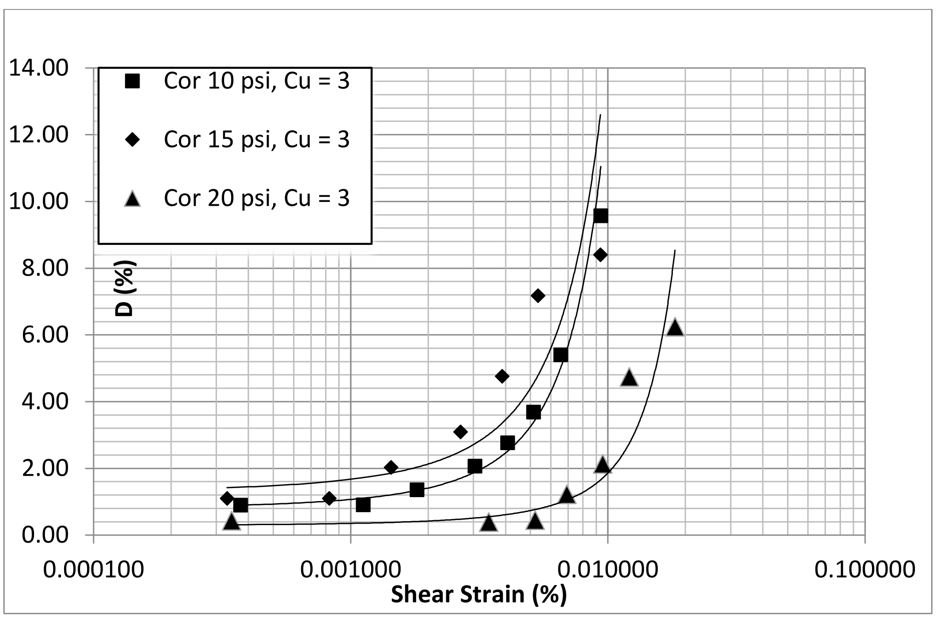

Figure B.16 Effects on Confinement on Damping Ratio (D) for Corundum Sand for C_u =3, Series 1

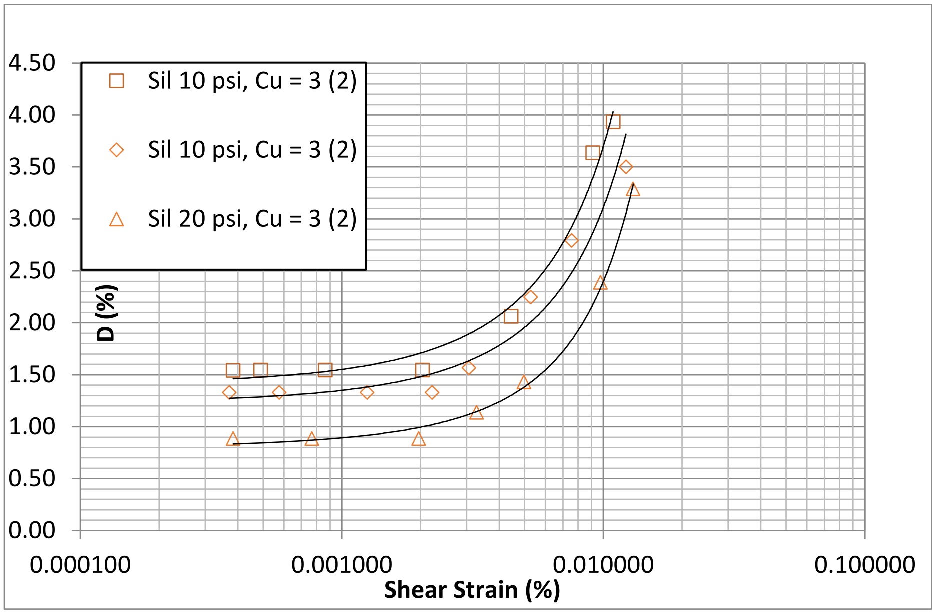

Figure B.17 Effects on Confinement on Damping Ratio (D) for Silica Sand for C_u =3, Series 2

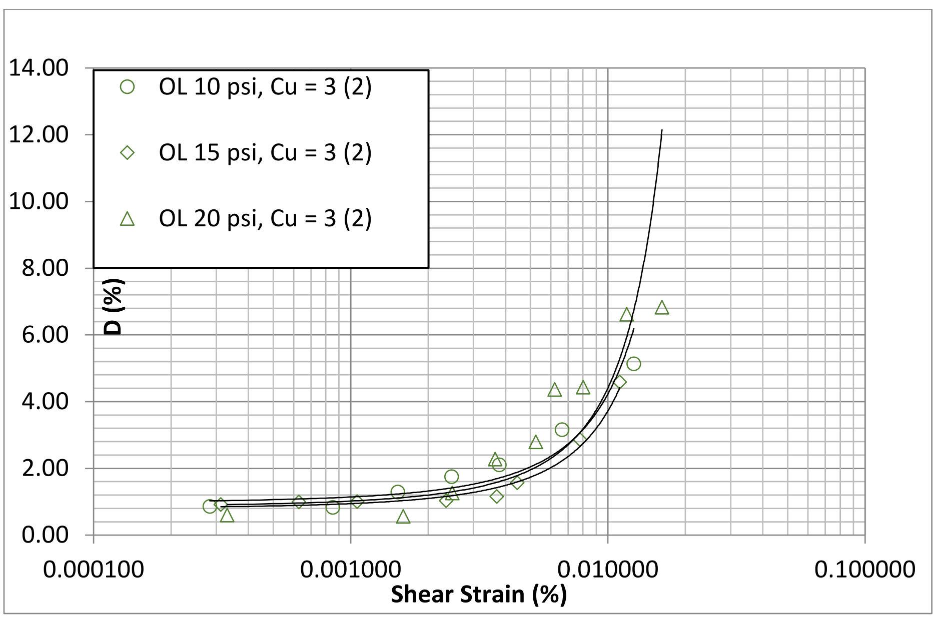

Figure B.18 Effects on Confinement on Damping Ratio (D) for Olivine Sand for C_u =3, Series 2

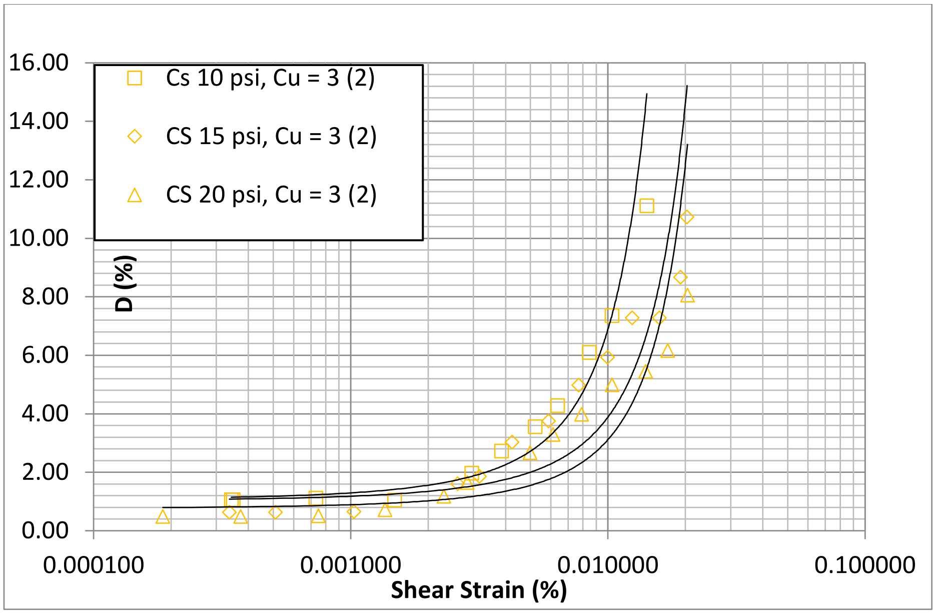

Figure B.19 Effects on Confinement on Damping Ratio (D) for Carbonate Sand for C_u =3, Series 2

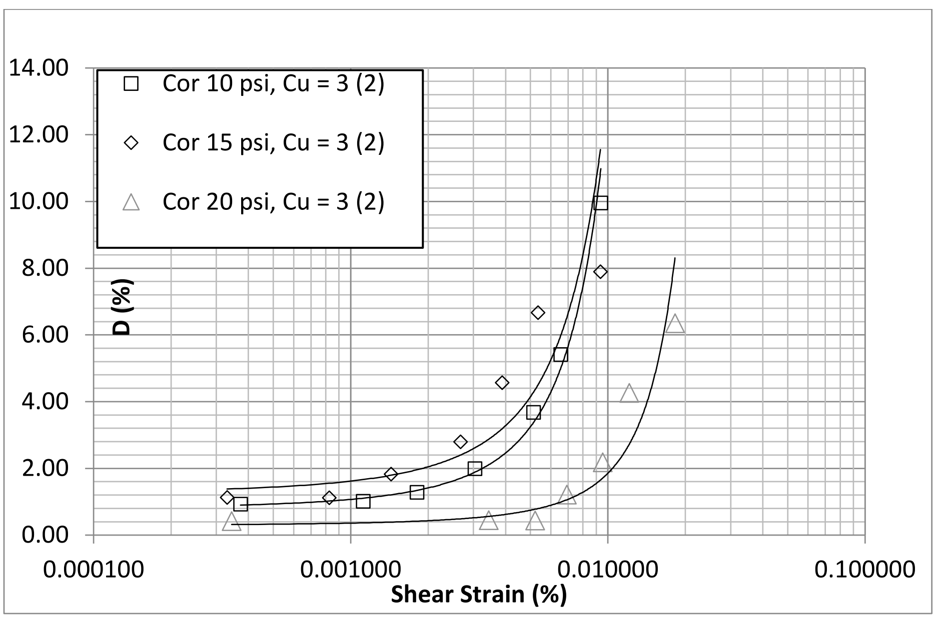

Figure B.20 Effects on Confinement on Damping Ratio (D) for Corundum Sand for C_u =3, Series 2

BIBLIOGRAPHY

Al-Sanad, H., & Aggour, M. S. (1984). Dynamic Soil Properties from Sinusoidal and Random Vibrations. *Proceedings, 8th World Conference on Earthquake Engineering*, *3*, 15-22. San Francisco, CA.

Al-Sanad, H., Aggour, M., S. & Yang, J. (1983). Dynamic Shear Modulus and Damping Ratio from Random Loading Tests. *ASTM Geotechnical Testing Journal*, *6*(3), 120-127.

Afifi, S. S., and Richart, F. E., Jr. (1973). "Stress-history effects on shear modulus of soils." Soils Found., 13(1), 77-95.

Amir Faryar, B. (2012). Improvement of Dynamic Properties and Seismic Response of Clay Using Fiber Reinforcement. College Park, MD. PhD Dissertation. University of Maryland.

Berslien E. (2012). *An Introduction to Forensic Geoscience*. Wiley & Sons.

Borcherdt, R.D. (1992). Simplified site classes and empirical amplification factors for site-dependent code provisions. NCEER, SEAOC, BSSC workshop on site response during earthquakes and seismic code provisions, Univ. Southern California, Los Angeles, California, Nov. 1992.

Borcherdt, R.D. (1994). Estimates of site-dependent response spectra for design (methodology and justification). Earthquake Spectra 10,617–654

Borcherdt, R.D. (2012). "V_{S30} – A Site-Characterization Parameter for Use in Building Codes, Simplified Earthquake Resistant Design, GMPEs, and ShakeMaps" 15 WCEE Lisboa.

Shannon, & Wilson. (1972). Soil Behavior Under Earthquake Loadings Conditions, "Evaluation of Soil Characteristics for Seismic Response Analysis". U.S. Atomic Energy Commission, IIDD-26444.

Darendeli, M. (2001). Development of a New Family of Normalized Modulus Reduction and Material Damping Curves. Austin. TX: PhD. Dissertation, University of Texas at Austin.

De Alba, P. Baldwin, K., Janoo, V., Roe, G. and Celikkel., B. (1984). "Elastic Waves velocities and liquefaction potential", Geotechnical Testing Journal, ASTM, Vol. 7, No. 2, pp. 77-88.

Demars, K. R., and Chaney, R. C. (1982). "Symposium Summary." Geotechnical Properties, Behavior and Performance of Calcareous Soils, ASTM Special Technical Publication 777, 395-404.

Drnevich, V. (1975). *Resonant Column Testing Apparatus Patent.* United States Patent Office (USPTO).

Drnevich, V. (1978). Resonant Column Testing Problems and Solutions. *ASTM Dynamic Geotechnical Testing, STP 654*, 384-398.

Drnevich, V., Hardin, B., & Shippy, D. (1978). Modulus and Damping of Soils by the Resonant Column Method. *Dynamic Geotechnical Testing*, 91-117.

Dobry, R., and Vucetic, M. (1987). "State-of-the-art report: Dynamic properties and response of soft clay deposits." Proc. Int. Symp. on Geotechnical Engineering of Soft Soils, Vol. 2, 51-87.

Farndon, J (2006). "The Complete Guide to Rock and Minerals" Blackfriars Road, London. Hermes House.

Florke O.W., Graetsch H.A., Brunk F., et al. (2008). "Silica" Ullmann's Encyclopedia of Industrial Chemistry. Weinheim. Wiley.

Hardin, B., & Drnevich, V. (1972a). Shear Modulus and Damping in Soils: Measurements and Parameter Effect. *ASCE Journal of the Soil Mechanics and Foundation, 98*(SM6), 603-624.

Hardin, B., & Drnevich, V. (1972b). Shear Modulus and Damping in Soils: Design Equations and Curves. *ASCE Journal of the Soil Mechanics and Foundations, 98*(SM7), 667-692.

Hyodo, M., Aramaki, N., Itoh, M., and Hyde, A. F. L. (1996). "Cyclic strength and deformation of crushable carbonate sand." Soil Dynamics and Earthquake Engineering, 15(5), 331-336.

Hyodo, M., Hyde, A. F. L., and Aramaki, N. (1998). "Liquefaction of crushable soils." *Geotechnique*, 48(4), 527-543.

Idriss, I., & Seed, H. (1968). *ASCE Journal of the Soil Mechanics and Foundations Division, 94*(SM4), 1003-1031.

Iler, R.K. (1979). *The Chemistry of Silica*. New York. Wiley

Ishibashi, I., & Zhang, X. (1993). Unified Dynamic Shear Moduli and Damping Ratios of Sand and Clay. *Soils and Foundations, 33*(1), 182-191.

Ishihara, K. (1996). *Soil Behavior in Earthquake Geotechnics.* Walton Street, Oxford, UK: Oxford University Press.

Iwasaki, T., and Tatsuoka, F. (1977). “Effects of grain size and grading on dynamic shear moduli of sands.” Soils Found., 17(3), 19–35.

Kaggwa, W. S., and Poulos, H. G. (1990). "Comparison of the behaviour of dense carbonate sediments and silica sand in cyclic triaxial tests." University of Sydney, School of Civil and Mining Engineering.

Kaggwa, W. S., Poulos, H. G., and Carter, J. P. (1988). "Response of carbonate sediments under cyclic triaxial test conditions." Engineering for Calcareous Sediments, Proc. Int. Conf. on Calcareous Sediments, Jewell and Andrews, eds., Balkema, Rotterdam, Perth, Australia, 97-107.

Kim, D., & Stokoe, I. K. (1992). *Characterization of Resilient Modulus of Compacted Subgrade Soils Using Resonant Column and Torsional Shear Tests.* TRB.

Klein, C., & Hurlbut Jr., C. (1985). *Manual of Mineralogy* (20th ed.). John Wiley & Sons.

Kramer, S. (1996). *Geotechnical Earthquake Engineering.* Upper Saddle River, NJ: Prentice Hall.

Kokusho, T., Hara, T., and Hiraoka, R. (2004). “Undrained shear strength of granular soils with different particle gradations.” J. Geotech. Geoenviron. Eng., 130(6), 621–629.

Lanzo, G., Vucetic, M., & Doroudian, M. (1997). Reduction of Shear Modulus at Small Strains in Simple Shear. *ASCE Journal of Geotechnical and Geoenvironmental Engineering, 123*(11), 1035-1042.

LaVielle, T.H. (2008). *Liquefaction Susceptibility of Uncemented Calcareous Sands from Puerto Rico by Cyclic Triaxial Testing*. MSc Thesis. Virginia Polytechnic Institute and State University.

LoPresti, D.C.F., Pallara, O., Lancellotta, R., and Maniscalco, R. (1993). "Monotonic and cyclic loading behavior of two sands at small strains." Geotechnical Testing Journal, 16(4), 409-424.

Luna, Ronaldo & Jadi, Houda. (2001). Determination of dynamic soil properties using geophysical methods.

Meng, J. (2007). Earthquake Ground Motion Simulation with Frequency-Dependent Soil Properties. *Journal of Soil Dynamics and Earthquake Engineering, 27*(3), 234– 241.

Menq, F.Y. (2003). *Dynamic Properties of Sandy and Gravelly Soils.* PhD Dissertation. University of Texas at Austin

Morioka, B. T. (1999). “Evaluation of the Static and Cyclic strength properties of calcareous sand using cone penetrometer tests”, Ph.D. Dissertation, University of Hawaii, Manoa, HI.

Olgun, G.C., Martin II, J.R., LaVielle, T.H. (2009). “Liquefaction Susceptibility of Calcareous Sediments Along the Coastal Plains of Puerto Rico”. Research Supported by the U.S. Geological Survey (USGS) under award number 07HQGR0043

Richart, F. (1960). Foundation Vibrations. *Proceedings JSMFD. 86*, 1-34. ASCE.

Schnabel, P., Lysmer, J., & Seed, H. (1972). *SHAKE: A Computer Program for Earthquake Response Analysis of Horizontally Layered Sites, Report No. EERC 72-12*. Berkeley, CA: Earthquake Engineering Research Center, University of California.

Seed, H. B., and Lee, K. L. (1966). "Liquefaction of saturated sands during cyclic loading." Journal of the Soil Mechanics and Foundations Division, ASCE, 92(SM6), 105-134.

Seed, H., & Idriss, I. (1970). *Soil Moduli and Damping Factors for Dynamic Response Analyses, Report No. EERC 70-10.* Berkeley, CA: Earthquake Engineering Research Center, University of California.

Seed, H., Mori, K., & Chan, C. (1977). Influence of Seismic History on

Liquefaction of Sands. *Proceeding ASCE, JGED*, *103*, 257-270.

Seed, H.B., Wong, R.T., Idriss, I.M. and Tokimatsu, K. (1986). “Moduli and Damping Factors for Dynamic Analyses of Cohesionless Soils,” Journal of the Soil Mechanics and Foundations Division, ASCE, Vol. 112, No. SM11, pp. 1016-1032.

Shirley, D.J., Anderson, A.L. (1975). “Acoustic and engineering properties of sediments”. Report ARL-TR-75-58, Applied Research Laboratory, University of Texas, Austin

Stokoe, K. H., Darendeli, M. B., Gilbert, R., Menq, F. Y., & Choi, W. K. (2004). Development of a New Family of Normalized Modulus Reduction and Material Damping Curves. *Proceedings, NSF/PEER Int. Workshop on Uncertanitites in Nonlinear Soil Properties and Their Impact on Modeling Dynamic Soil Response.* Berkeley, CA: University of California at Berkeley.

Stokoe, K. H., Hwang, S. K., Roesset, J. M., & and Sun, C. (1994). Laboratory Measurement of Small-Strain Material Damping of Soil Using a Free-Free Resonant Column. *Earthquake Resistant Construction and Design, S. A. Savidis, Ed., Balkema, Rotterdam*, 195–202.

Sykora, DW (1987). Examination of existing shear wave velocity and shear modulus correlations in soils, Department of the Army, Waterways Experiment Station, Corps of Engineers, Miscellaneous Paper GL-87-22.

Tawfiq, K., Aggour, M., & Al-Sanad, H. (1988). Dynamic Properties of Cohesive Soils from Impulse Testing. *Proceedings, 9th World Conference on Earthquake Engineering, 3*, 11-16. Tokyo, Japan.

Towhata, I. (2008). *Geotechnical Earthquake Engineering.* Berlin, Germany: Springer series in Geomechanics and Geoengineering.

Varde, A., Sandford, T., & Dagher, H. (1996). Model Uncertainty in Anchorage Design for Anchored Bulkheads. Proceedings, Uncertainty in the Geologic Environment: From Theory to Practice, Geotechnical Special Publication No 58, 727-745. Madison, WI: ASCE Geotechnical Engineering Division, Vol. 2.

Vucetic, M., & Dobry, R. (1991). Effect of Soil Plasticity on Cyclic Response. *Journal of Geotechnical Engineering, ASCE, 117*(1), 89-107.

Vucetic, M., Lanzo, G., & Doroudian, M. (1998). Damping at Small Strains in Cyclic Simple Shear Test. *Journal of Geotechnical and Geoenvironmental Engineering, 124*(7), 585-594.

Wilson, S. &., & Associates, A.-J. (1972). *"Soil Behavior Under Earthquake Loading Conditions" Evaluation of Soil Characteristics for Seismic Response Analysis.* US Atomic Energy Commission, IID-26444.